SEPTEMBER 2017

Ph.D in Electrical and Electronics Engineering

NOOR BAHA ALDIN

UNIVERSITY OF GAZİANTEP
GRADUATE SCHOOL OF
NATURAL & APPLIED SCIENCES

DEVELOPMENT OF POSITIONING SYSTEMS: SATELLITE-BASED POSITIONING AND TERRESTRIAL-BASED POSITIONING

Ph.D THESIS

IN

ELECTRICAL AND ELECTRONICS ENGINEERING

BY

NOOR BAHA ALDIN

SEPTEMBER 2017

Development of Positioning Systems: Satellite-Based Positioning and Terrestrial-Based Positioning

Ph.D Thesis

in

Electrical and Electronics Engineering

University of Gaziantep

Supervisor

Prof. Dr. Ergun ERÇELEBİ

by

Noor BAHA ALDIN

September 2017

REPUBLIC OF TURKEY
UNIVERSITY OF GAZİANTEP
GRADUATE SCHOOL OF NATURAL & APPLIED SCIENCES
ELECTRICAL AND ELECTRONICS ENGINEERING

Name of the thesis: Development of Positioning Systems: Satellite-Based Positioning and Terrestrial-Based Positioning

Name of the student: Noor BAHA ALDIN

Exam date: 13/09/2017

Approval of the Graduate School of Natural and Applied Sciences

Prof. Dr. Ahmet Necmeddin YAZICI
Director

I certify that this thesis satisfies all the requirements as a thesis for the degree of Doctor of Philosophy.

Prof. Dr. Ergun ERÇELEBİ
Head of Department

This is to certify that we have read this thesis and that in our consensus opinion it is fully adequate, in scope and quality, as a thesis for the degree of Doctor of Philosophy.

Prof. Dr. Ergun ERÇELEBİ
Supervisor

Examining Committee Members	Signature
Prof. Dr. Ergun ERÇELEBİ	.....
Prof. Dr. İlyas EKER	.....
Assoc. Prof. Dr. Sema KOÇ KAYHAN	.....
Asst. Prof. Dr. Serkan ÖZBAY	.....
Asst. Prof. Dr. Murat FURAT	.....

I hereby declare that all information in this document has been obtained and presented in accordance with academic rules and ethical conduct. I also declare that, as required by these rules and conduct, I have fully cited and referenced all material and results that are not original to this work.

Noor BAHA ALDIN

ABSTRACT

DEVELOPMENT OF POSITIONING SYSTEMS: SATELLITE-BASED POSITIONING AND TERRESTRIAL-BASED POSITIONING

BAHA ALDIN, Noor
Ph.D. in Electrical and Electronics Engineering
Supervisor: Prof. Dr. Ergun ERÇELEBİ
September 2017
160 pages

Nowadays, global positioning system (GPS) is utilized broadly in the world, but performance can be substantially degraded in a multipath and non-line of sight (NLOS) environments. Since the multipath can present indecorous errors of the received signal with deformation of the phase and delay that preclude the accurate approximation of the receiver position. The power of the GPS signal will be weakened, and its reliability and position accuracy will be degraded much in the low signal to noise ratio (SNR) environment that gives restrictions in terms of tracking performance. In this thesis, the receiver's structure of a GPS has been modified using GPS repeaters to ameliorate the indoor positioning performance and the quality of the GPS signal reception. Also, we suggested a modified particle filter (MPF) that can approximate the entire parameters and produces preferable model fit which is compared to alternative estimation procedures. Based on adaptive particle filter (PF), a filtering algorithm has been proposed to improve the positioning accuracy of GPS receiver and to solve the error of GPS positioning. The experimental results show that for long periods of time, the system is capable to give an accurate outdoor and indoor positioning. Also, indoor location based on active RFID technologies has been studied. Due to the multipath propagation and random noise interference of complex indoor environment, for the pursuit of higher localization accuracy, an optimized algorithm has been suggested to negotiate some insufficiency in LANDMARC and VIRE algorithms. The boundary virtual reference (BVIRE) tag that relates to the overall system precision is ameliorated and a new error correction model is established. In the experiments, it is seen that the proposed algorithm is effective and precise compared with other algorithms.

Key Words: GPS, RFID, multipath, particle filter, repeaters, BVIRE, Indoor positioning system, non-Gaussian.

ÖZET

KONUMLAMA SİSTEMLERİ GELİŞTİRİLMESİ: UYDU TABANLI KONUMLAMA ve KARASAL TABANLI KONUMLAMA

BAHA ALDIN, Noor
Doktora Tezi, Elektrik-Elektronik Mühendisliği Bölümü
Tez Yöneticisi: Prof. Dr. Ergun ERÇELEBİ
Eylül 2017
160 sayfa

Şu günlerde, küresel konumlama sistemi (GPS) dünyada yaygın olarak kullanılmaktadır, ancak performans çokluyol ve görüş hattında olmayan (NLOS) ortamlarda oldukça bozulabilir. Çünkü çokluyol, alınan faz bozulmalı ve alıcı konumunun doğru şekilde saptanmasını engelleyen gecikmeli işaretin uygun olmayan hatalarını gösterebilir. Takip performansı açısından sınırlamalar getiren düşük işaret/gürültü (SNR) oranı ortamında, GPS işaretinin gücü zayıflayacak, güvenilirliği ve konum doğruluğu çok düşecektir. Bu tezde, iç ortam konumlama performansı ve GPS işareti alımının kalitesinin geliştirilmesi için, GPS tekrarlayıcılar kullanarak alıcının yapısı yenilendi. Ayrıca, tüm parametreleri yaklaştıran ve alternatif tahmin prosedürlerine kıyasla tercih edilen model uygunluğu üreten yenilenmiş parçacık süzgeci (MPF) önerdik. GPS alıcısının konumlama doğruluğunu iyileştirmek ve GPS konumlama hatasını çözmek için adaptif parçacık süzgeci (PF) temelli bir süzme algoritması önerilmiştir. Deneysel sonuçlar, uzun süreler boyunca sistemin doğru bir açık ve kapalı alan konumu vermeye muktedir olduğunu göstermektedir. Ayrıca, aktif RFID teknolojilerine dayanan iç ortam konumlama da çalışıldı. Karmaşık iç ortamın çokluyol yayılımı ve rasgele parazit etkileşimi nedeniyle, daha yüksek yer belirleme doğruluğu yakalamak için, LANDMARC ve VIRE algoritmalarındaki bazı yetersizliklikleri tartışmak için en iyi duruma getirilmiş bir algoritma önerildi. Bütün sistemin hassasiyetiyle ilgili sınır sanal referans etiketi iyileştirildi ve yeni bir hata düzeltme modeli oluşturuldu. Deneylerde, önerilen algoritmanın diğer algoritmalara kıyasla etkili ve hassas olduğu görülmektedir.

Anahtar Kelimeler: GPS, RFID, parçacık süzgeci, BVIRE, İç ortam konumlama sistemi, Gaussian olmayan.

DEDICATION

First of all, I would like to thank Almighty **Allah** for everything in my life who has given me strength, without his guidance I would never be able to accomplish anything in my whole life.

Every challenging work needs self-efforts as well as guidance of elders, especially those who were very close to my heart. I dedicate my modest effort to my sweet and loving **Parents** whose, love, encouragement and prayers of day and night make me able to get such success and honour, without their patience, understanding, support, and most of all their love, as well as their best dedication the completion of this work would not have been possible. I am eternally grateful for your love and sacrifice. Through my life, my loving parents were the best teachers I have ever had. You taught me to respect others and helped me build what has brought me this far. I know that I can never pay back what they have done for me. Thank you for earning an honest living for me and for supporting and encouraging me to believe in myself.

Also, special thanks to my wonderful and beloved sister **Shaima** for always being there on my side whenever I was in need & for helping me in close infinite ways. Thank you for your advice and your comforting words when I most need them as well as for the unforgettable moments. Thank you for all you have done, for being a shoulder to support, for wiping my tears.

I would like to express my greatest thanks to **Mahmut Aykaç**. This work would not have been possible without the help, support, advice and participation of him; I am impressed by his kindness. I owe you all much more than words can express.Thank you for standing by my side when times get hard.

Thanks my dear and best **sisters**, I'm really lucky to have a loving, caring sisters like you, thank you for always standing by my side and supporting me, but even more than that, trusting & believing in me.

ACKNOWLEDGEMENTS

I wish to express my deep sense of appreciation and many thanks to my supervisor **Prof. Dr. Ergun Erçelebi** for his continued guidance throughout my PhD. He always gave me very good suggestions when something blocked my way. I am extremely grateful for his friendship, supervision and advice. Especially for his confidence in me, he had been the one to give me the proper direction all along in my studies. Without you, I would not have been able to finish this work at all.

TABLE OF CONTENTS

ABSTRACT ..... **v**

ÖZET ..... **vi**

DEDICATION ..... **vii**

ACKNOWLEDGEMENTS ..... **viii**

TABLE OF CONTENTS ..... **ix**

LIST OF TABLES ..... **xiii**

LIST OF FIGURES ..... **xiv**

LIST OF ABBRIVATIONS ..... **xvii**

CHAPTER 1 INTRODUCTION **1**

1.1. Overview 1

1.2. Navigation and Locating Schemes 2

1.3. Terrestrial Systems 6

1.3.1. Locating of Radio Frequency Identification 7

1.4. Global Navigation Satellite Systems 7

1.4.1. Global Positioning System 7

1.4.1.1. Frequency Schedule 8

1.5. L1 of GPS 11

1.6. L2 of GPS 13

CHAPTER 2 SATELLITE BASED POSITIONING TECHNOLOGY **14**

2.1. Basic Concepts 14

2.1.1. GPS Overview 15

2.1.2. Overall Structure 16

2.2. General Description of GPS and How Does It Work 18

2.2.1. Space Segment 19

2.2.2. Control Segment 20

2.2.3. User Segment 21

2.3. Processing of Navigation……..……..……..……21
2.3.1. Criterion of the GPS Time 23
2.3.2. Comparative Pseudo Range Measurements 26
2.3.3. Numerical Formation of the Signals 27
2.4. Principles of Pseudo Range Error 28
2.5. Reference of Coordinate Systems 30
2.6. Coordinate Earth-Fixed/Centred System 31
2.6.1. Calculations of Longitude, Latitude, and Height 32
2.7. PRN Codes Utilizing Position Calculation 33
2.7.1. Computation of User Location 37
CHAPTER 3 TERRESTRIAL BASED LOCALIZATION SYSTEM 41
3.1. Basic Concept of Indoor Localization System 41
3.1.1. Basic of RFID Indoor Localization Algorithms 42
3.2. RFID System 43
3.2.1. The Background of Indoor Localization Technologies 44
3.2.1.1. Infrared Radiation Technology (IR) 44
3.2.1.2. Wireless LANs Technology 46
3.2.1.3. Ultra Wide Band Technology (UWB) 48
3.2.1.4. Radio Frequency Identification Technology 49
3.3. Typical RFID Technology Applications 51
3.3.1. RFID and Asset Tracking 52
3.3.2. RSSI Positioning Systems 52
CHAPTER 4 BOUNDARY VIRTUAL LABEL ALGORITHM 54
4.1. The Idea of BVIRE Algorithm 54
4.1.1. The Procedure of Algorithm 54
4.2. Adding the Boundary Virtual Reference Label 57
4.2.1. Appending Grid Virtual Reference Labels 60
4.2.2. Choosing of the Neighbouring Reference Tags 61
4.3. The Calculation of Weighting Factor 61
4.4. Circular Error Probability 62
4.5. The Evaluation of Positioning Accuracy 63
4.5.1. The MSE and RMSE 63
4.5.2. GDOP 64
4.5.3. Cumulative Distribution Function 65

4.5.4. Relative Positioning Error 65
CHAPTER 5 GPS REPEATER AND FILTERS 67
5.1. GPS Repeater 67
5.2. Theoretic Sides 72
5.3. Tracking and Positioning of Bayesian Filtering 76
5.3.1. The Derivate of Kalman Filter 77
5.3.1.1. Tracking of the Bias NLOS with Extended Kalman Filter 78
5.3.1.2. Adaptive EKF 79
5.3.2. Particle Filter 80
5.4. New Resampling of MPF Sequential 84
5.5. A Brief Introduction to some Nonlinear Filters 86
5.5.1. Unscented Kalman Filter 87
5.5.2. Gentric Difference of Kalman Filter 88
5.6. Ameliorating Reliability of Modified Particle Filter Depending on GPS 89
5.6.1. Characterization of the Motion Case 89
5.6.2. Incorporation of the System State Equation 89
5.7. An Approximation of Modified Particle Filtering 92
5.7.1. The Procedure of Resampling Method 92
5.7.2. Establishment of the Observance Equation 93
5.7.3. Data Filtering of MPF for GPS Locating 95
5.8. The Algorithm of Resampling 97
5.8.1. Regularized Resampling 97
5.8.2. Low Variance Resampling 98
CHAPTER 6 EXPERIMENTAL RESULTS 100
6.1. GPS L1 Repeater 100
6.2. Comparison of Performance Results 103
6.3. Influence of the Modified Particle Filter 106
6.4. Coping with NLOS Computations 108
6.5. Defining a Developed Model 110
6.6. Real-Life Experiment 115
6.6.1. Experiments Test and Results Analysis 115
6.7. Results of Improved BVIRE System Algorithm 120
6.8. Conclusions and Future Plans 126

REFERENCES……...129

APPENDIX……..134

VITA……...……..……..…..140

LIST OF TABLES

TABLES Page

Table1.1. Comparison of the present locating systems……...……...…...…..4

Table 1.2. Base features of GPS signals……...……...…..…10

Table 2.1. Pseudo range mensuration depending on relative receipt times……...…26

Table 2.2. Measurement of pseudo range depending on the time differences ....….26

Table 2.3. Error schedule of GPS PPS pseudo range…….…….……..29

Table 2.4. Error structure of GPS SPS pseudo range……..……..….29

Table 2.5. Calculation of ECEF parameters……..……...33

Table 3.1. Infrared positioning…….…..…....46

Table 3.2. RFID positioning……...…....50

Table 4.1. Standard deviations and coordinate variance of algorithms…….…....63

Table 5.1. Repeater specifications……75

Table 6.1. Produced signal parameters……104

Table 6.2. Azimuth and highness values of the apparent satellites…….105

Table 6.3. MPF RMSE & positioning output probability…….……...108

Table 6.4. Comparison of trajectory RMSE of the four approaches……118

Table 6.5. The CDF and percentage error comparison…….……122

Table 6.6. The estimation errors with sample tags……...124

LIST OF FIGURES

FIGURES Page

Figure 1.1. Service of management structure……...……...……..2

Figure 1.2. Representation of the basic locating technologies……..……..…..3

Figure 1.3. Basic GPS architecture……..…….……...5

Figure 1.4. GPS frequency plan……..…….……9

Figure 1.5. Interfaces of the space part GPS to the user part……..…….……..10

Figure 1.6. Data structure of the GPS navigation……..…….…...12

Figure 2.1. Structure of the common GNSS receiver……..…..……16

Figure 2.2. GPS segments……..…….……...19

Figure 2.3. Inclination of GPS orbit……..…….……....20

Figure 2.4. Segment of the GPS control…….……..……..…21

Figure 2.5. Logical steps of the receiver signal process……..….…….22

Figure 2.6. Fragmentation of the navigation message……..…….……23

Figure 2.7. Z-count exemplification……..…….…...24

Figure 2.8. Messages information……..…….……..….24

Figure 2.9. Transmission and reception with regard to time……..…….…..27

Figure 2.10. Ellipsoid representation……..…….…..……..……30

Figure 2.11. Fragmentation of the navigation message……...……...31

Figure 2.12. Ellipsoidal sample of earth……...…….…….32

Figure 2.13. Ranging of PRN code……...……..…34

Figure 2.14. 2D positioning……...…….……....35

Figure 2.15. Clock error effect on positioning……...…….……....36

Figure 2.16. Dilution of precision effect……..…….....36

Figure 3.1. Active badges of indoor positioning system……...….45

Figure 3.2. Infrastructure network……...…….…..47

Figure 3.3. Ad hoc networks……...……..….…….47

Figure 3.4. UWB approach of positioning……...…….…..….49

Figure 3.5. RFID system……...…….……50

Figure 4.1. Flowchart of BVIRE algorithm……...…….....55

Figure 4.2. Real time locating system……...…….…….57

Figure 5.1. Installation of GPS antenna, repeater, and receiver…….....67

Figure 5.2. Repeater with antenna…….……68

Figure 5.3. The iteration of the incoming signals using three repeaters…….…....69

Figure 5.4. The iteration of the incoming signals using four repeaters…….…..…69

Figure 5.5. The cycling of pseud from one repeater to another…….…....71

Figure 5.6. The progression of pseudo range…….……72

Figure 5.7. SIR algorithm's flowchart…….……...85

Figure 5.8. New resampling algorithm of MPF…….….86

Figure 5.9. Particles index of weights……...……..98

Figure 5.10. Regularization of the Resampling algorihm……..…..…..98

Figure 5.11. Resampling algorithm of low variance…….……...…99

Figure 6.1. Distribution of the signal to repeaters……100

Figure 6.2. Observations of GPS signal to noise ratio…….……101

Figure 6.3. Observations of indoor GPS phase…….…102

Figure 6.4. Observations of indoor GPS pseudo range code……102

Figure 6.5. RMSE form measurement of four filters……...103

Figure 6.6. TOA RMSE measures of four filters…….….104

Figure 6.7. Position RMSE with Lc=6 correlation samples…….……105

Figure 6.8. Position RMSE with Lc=10 correlation samples…….…..106

Figure 6.9. Position error of MPF/CDF with fixed speed case……..…107

Figure 6.10. Position error of MPF/CDF with unfixed speed case……...107

Figure 6.11. Evaluated trajectory using MPF of weight matrix……...109

Figure 6.12. Evaluated trajectory using MPF for moving target…….……110

Figure 6.13. Diagram of the receiver module…….……..111

Figure 6.14. PCB design of GPS-repeater…….…...111

Figure 6.15. The full design with antenna, repeater, and router…….……..112

Figure 6.16. Arrangement of the acquiring test…….……..113

Figure 6.17. The cases of acquiring test……...114

Figure 6.18. Comparison the error probability of filters…….…..116

Figure 6.19. Signal to noise ratio vs. RMSE of filters…….……116

Figure 6.20. Associated speed over time…….……117

Figure 6.21. MPF algorithm's errors in a range of 8 minutes…….……..118

Figure 6.22. Comparison of localization performance using different algorithms...120

Figure 6.23. The cumulative distribution function of several methods….……...121

Figure 6.24. Threshold effect on the positioning accuracy…….……..123

Figure 6.25. Geometric dilution of precision…….…….……..123

Figure 6.26. Localisation estimation error of tags…….……...124

Figure 6.27. Circular error probability…….……125

Figure 6.28. The correlation of height vs. estimation error…….….125

LIST OF ABBRIVATIONS

GPS	Global Positioning System
LBSs	Location-Based Services
ICSs	Intelligent Conveyance Systems
GNSS	Global Navigation Satellite System
WLANs	Wireless Local Area Networks
WMANs	Wireless metropolitan Area Networks
WSNs	Wireless Sensor Networks
RTLS	Real Transmitted Location System
RFID	Radio Frequency Identification
TOA	Time of Arrival
LOS	Line of Sight
ECEF	Earth-Centred, Earth-Fixed
SNR	Signal to Noise Ratio
AOA	Arrival of Assistance
RSS	Received Signal Strength
RF	Radio Frequency
RSSI	Received Signal Strength Induction
DOD	Department of Defense
SS	Space Segment
OCS	Operational Control Segment
US	User Segment
PVT	Position, Velocity, Time
SPS	Standard Position Service
PPS	Precise Position Service
CM	Civil Moderate
CL	Civil Long
NAV	Navigation

SBAs	Satellite Based Augmentation System
CDMA	Code Division Multiple Access
BPSK	Binary Phase Shift Keying
PRN	Pseudorandom Noise
SV	Satellite Vehicle
P	Precision
C/A	Coarse/Acquisition
NRZ	No Return to Zero
MSB	Most Significant Bit
IOC	Initial Operational Capability
HW	Hardware
SW	Software
DSP	Digital Signal Processor
ADC	Analog to Digital Convertor
LO	Local Oscillator
RHCP	Right Hand Circularly Polarized
LNA	Low Noise Amplifier
IF	Intermediate Frequency
MEO	Medium Earth Orbit
MCS	Master Control Satations
MS	Monitor Stations
HOW	Handover
TLM	Telemetry
TOW	Time of Week
UTC	Coordinated Universal Time
UERE	User Equivalent Range Error
SA	Selective Avialability
ECI	Inertial Coordinate System
WGS	World Geodetic System
NPA	Non Precision Approach
DSSS	Direct Sequence Spread Spectrum
DOP	Dilution of Precision
VIRE	Virtual Reference Elimination

KNN	K Nearest neighbours
LPM	Longest Prefix Match
TDOA	Time Difference of Arrival
IR	Infrared Radiation
WLAN	Wireless LANs Technology
LAN	Local Area Network
APs	Access Points
MSs	Master Stations
NIC	Networking Interface Card
UWB	Ultra Wideband Technology
FCC	Federal Communications Commission
IR-UWB	Impulse Radio UWB
BVIRE	Boundary virtual reference label positioning algorithm
CEP	Circular Error Probability
SEP	Sphere Error Probability
MSE	Mean Square Error
RMSE	Root Mean Square Error
CDF	Cumulative Distribution Function
PDF	Probability Density Function
RPE	Relative Positioning Error
SMA	Sub Miniature
LNA	Low Noise Amplifier
MAP	Maximum Posteriori
MMSE	Minimum Mean Square Error
KF	Kalman Filter
EKF	Extended Kalman Filter
NLOS	Non Line of Sight
AEKF	Adaptive Extended Kalman Filter
PV	Position Velocity
PVA	Position Velocity Acceleration
MCMC	Markov Chain Monte Carlo
PF	Particle Filter
SIS	Sequential Importance Sampling

SIR	Sequential Importance Resampling
LRM	Linear Regression Model
CDKF	Centric Difference of Kalman Filter
HGA	High Gain Antenna
PCB	Printed Circuit Board
AGPS	Assisted GPS
TTFF	Time to First Fix

CHAPTER 1

INTRODUCTION

1.1. Overview

The algorithm which is utilized related to other specified targets to calculate the location of one target is called locating. Ever since the human beings came into universe, it has been an essential need. Actually, with this matter in the pre technological era, many tools were progressed to transact based on observation of the stars. In the technical period and by utilizing radio transmissions, in real time to localize humans and targets it is conceivable. In this context, the great common sample of satellite positioning system is the global positioning system (GPS), which makes it achievable for objects with ground receivers to allocate their geographical position [1]. These days, for new location-based services (LBSs) and applications position acquaintance is turning to be a primordial matter. Especially, the wireless locating systems for many years have attracted significant attention [1, 2].

The fundamental applications of positioning techniques are intelligent conveyance systems (ICSs) in particular and conveyance in general, cargo tracking, routing of traffic, comprising incident administration, routing of traffic, and wayside service [3], which build the exploitation of the GPS. Safety latch for movable position location is one of the most important motifs, whose accomplishment is imposed for the contingency calls developed by dialling in Europe 112 or in the United State 911 numbers [1, 4]. Moreover, more and more attention and exploitations todays are enticing for LBSs, since based on personnel tracking, mobile local advertising, position-dependent billing, and navigation service, they cover the path for entirely recent opportunities and store managements. Figure 1.1 shows a graphical representation of the architecture of a context-aware service.

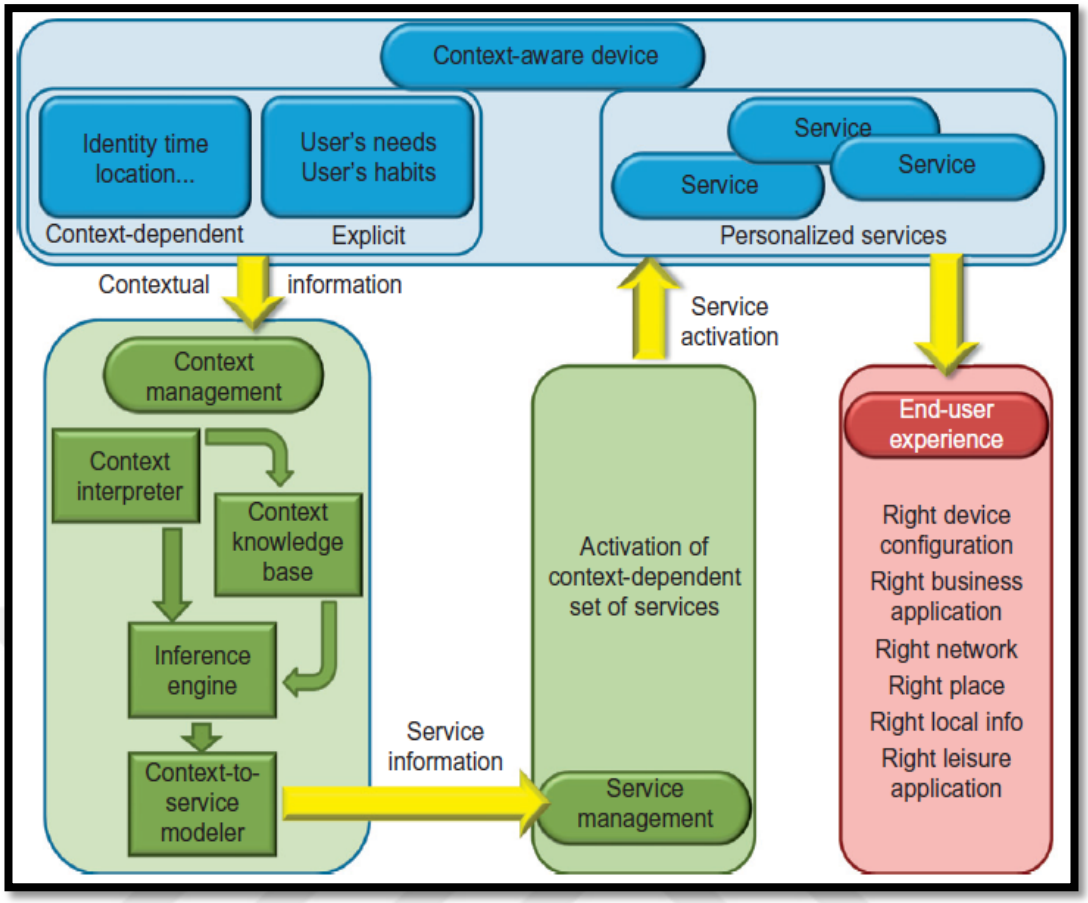

Figure 1.1 Service of management structure

1.2. Navigation and Locating Schemes

In this thesis, the navigation and locating schemes for which there occurs are analysed. The difference between terrestrial and satellite locating systems had been described. A picturesque sight of the primary locating technologies presently is obtainable and their uniform of accuracy and concealment are described in Figure 1.2. In familiar orbits, the satellite locating systems are utilized to accomplish rotating of the ranging measurements [5]. Inherently they are navigation systems, while many new terrestrial systems are proposed for just locating. Nowadays, the essential world-wide navigation satellite system (GNSS) is the well-known GPS.

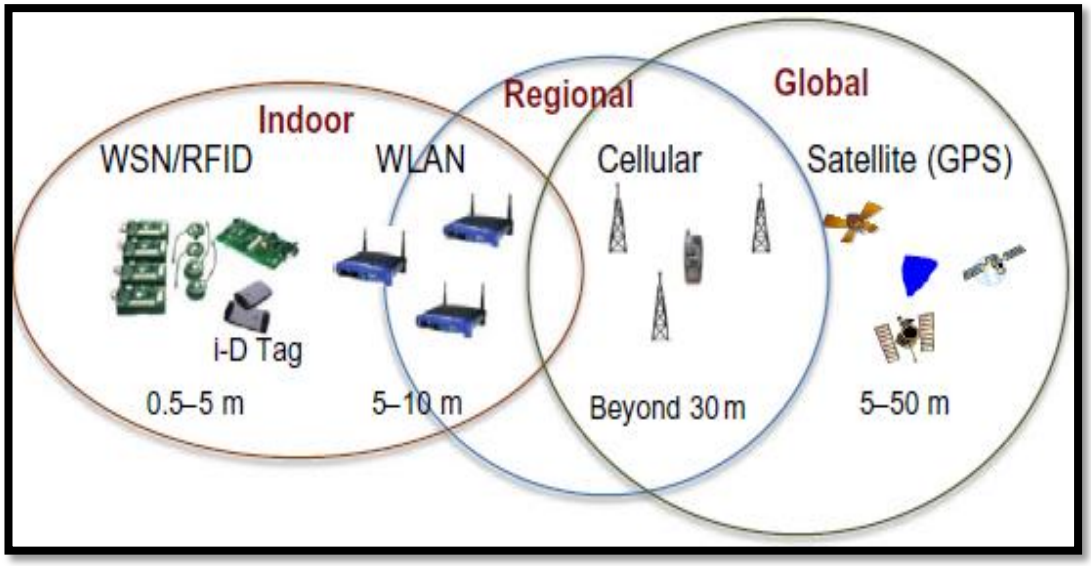

Figure 1.2 Representation of the basic locating technologies

As arrange of wireless communications systems, modern terrestrial location systems were originated. One of the basic divergences between present satellite and terrestrial locating systems for which the signal travelling from the transmitter to the receiver has been designed and considered is the quintessential aim: in the satellite state, the object is actually localization, whilst in the terrestrial state with respect to data communication, localization is overwhelmingly ancillary [1, 6]. For this basis, in the two states the challenges of the technological and extents are varied. This is the essential cause why the technology of the satellite navigation is observed frequently as an arrange of area varied from telecommunications, possibly near to the observation of earth and geographical sciences. Because of the diversity of implication initialises and terrestrial wireless systems, several varied approximations to activate locating in particular handsets and movable tools have been suggested [4]. These contain network and terminal-centred manners for cellular net, for more than fifteen years ago premature scheme were analysed, with processes oriented to the protocols and modulations for wireless metropolitan area networks (WMANs), wireless local area networks (WLANs), and wireless sensor networks (WSNs). For example, modern consecrated real transmitted location system (RTLS) depends on radio frequency identification (RFID). The primary features of a few pertinent existing systems are recapitulated in Table 1.1.

Table 1.1 Comparison of the present locating systems

Technology	Measurement Technique	Pros	Cons
GPS	TDOA	Earth scale coverage	Expensive infreatructure
Galileo	TDOA	Earth scale coverage	Expensive infrastructure
A-GNSS	TDOA	Country Coverage	Scarce indoor accuracy
Cellular	E-OTD/OTDOA	Country coverage	Requires synchronized base stations
Cellular	CelllD	Country coverage	Scarce accuracy
WLAN	RSS-fingerprinting	Indoor coverage, low cost	Database required for fingerprinting, low accuracy
WSN (ZigBee)	RSS	Indoor coverage, low power consumption, low cost	Low accuarcy
WSN (UWB)	TOA/TDOA/AOA	Indoor coverage, high accuracy	Short range (<20 m), problems in NLOS
RFID	Proximity	Indoor coverage, low power consumption, low cost	Low accuracy, one tag per location
NFR	E.M. near-field characteristics	Indoor coverage, low cost	Low frequency, large antenns
INS	Acceleration/angular rate/earth magnetic field	Works everywhere	Position/orientation drift, magnetic disturbance in indoor

The navigation system of the satellite radio that utilized to calculate dimensional positions and accurate time, anywhere on the earth is GPS. A clarification is given in Figure 1.3. By acquiring from a minimum of four GPS satellites at pseudo ranges or

time of arrival (TOA) signal measurements, GPS position solutions are achieved. Over the line of sight (LOS) the calculated distances of the signals promulgate by a piece of the N_{sat} satellites are clear pseudo ranges. The pseudo range ρ_k is for a piece satellite

$$\boldsymbol{\rho_k = \sqrt{(x_k - x_u)^2 + (y_k - y_u)^2 + (z_k - z_u)^2} + c.\Delta b_u, \quad k = 1, 2 \cdots, N_{sat}} \quad (1.1)$$

where x_k, y_k, and z_k are the coordinates for satellite k of Earth-centred, Earth-fixed (ECEF), and the c represents the speed of light. For the user the term u is standing and x_u, y_u, and z_u are the user's ECEF coordinates. The retrieve between the unknown time of the GPS and reference time of receiving and the unknown time of the GPS is the clock bias of user Δb_u [7].

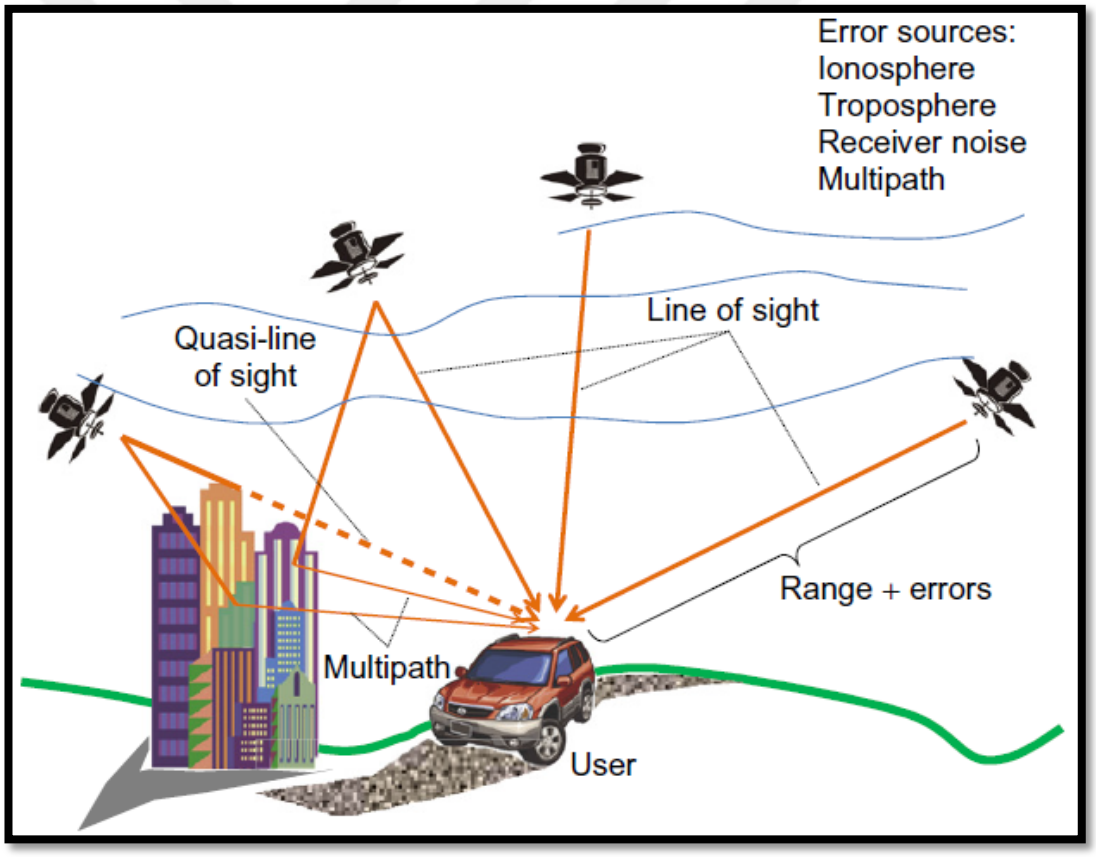

Figure 1.3 Basic GPS architecture

1.3. Terrestrial Systems

The way linked with LBSs of navigation systems by individual utilize needs that locating tools are capable to operate under several, changeable, and sensitive

circumstances, such as within storehouses, multi storied edifices, parking and underground, and indoor mercantile. Location detection of merchandise in a storehouse, location detection of preparation in a hospital or medical personnel, and discovering labelled conservation instruments and appointment littered all over a plant are examples of applications [4, 8]. Regrettably, by hard fading due to sheets and walls and by effect of multipath, the response of GNSS indoor is dramatically destroyed. Hence, for GNSS receiver design and signal proceeding the indoor environments start challenging matters. The signal response is represented by many reverberated or dispersed multipath elements and highly weakened immediate elements, when there is an indoor receiver. Depending on the nature of the concrete, the fading influencing the immediate way can extend from 10 to 25 dB, therefore the receiver by lowering the carrier power has to transact from about -160 dBW to even -190 dBW; anyways, in signal acquisition the nominal shakiness of present mercantile receivers is close to -178 dBW. In addition, sprinkling influences and multipath of indoor become far more prejudicial [2]. In such circumstances, the utilize of essential GPS receivers is actually refutable and extraordinarily varied schemes have to be assumed. Today, as a means of improving navigation and locating systems, many researches are focused on the utilize of technology of terrestrial wireless that operate where satellite systems fail. Recent LBSs to be met by the locating systems need a definite uniform of position reliability, regardless of wireless communication of all ideal proliferation issues, like a low signal to noise ratio (SNR), attenuation of channel, status of multipath, and multiuser conflict [3, 9, 10]. For indoor positioning, many wireless technologies have been analysed. Their characteristic elements are:

❖ There are many kinds of signal measurement which may use by positioning algorithm, like TOA, arrival of assistance (AOA), and received signal strength (RSS).

❖ We utilized the physical layer of the network base, to connect with the user's terminal.

In this thesis, the location systems that utilize wireless technologies completely extended on the ground point to the term of navigation and terrestrial based positioning systems. The most utilized wireless technology of this type is the RFID technology. Terrestrial based positioning systems local or short-range systems can

also be pointed, because their concealment field is limited to the area where they are propagated. Therefore, from GNSS they vary, whose concealment is universal [11].

1.3.1. Locating of Radio Frequency Identification

The technology of RFID has interested a portentous attract universal, since the early pioneering opinions dating back to 1948. A number of applications in many areas can now be found like logistics, automotive, automation systems, superintendence, and in common analogy of the real-time target [9]. An RFID system includes objects practised to their readers and targets. To receive the information hoarded on the reader interrogates the tags through a wireless link. Tag solutions are taken into regard when the price of tag, power, and size exhaustion needs become especially tight, passive or semi-passive.

Generally the relations relies on backscatter modulation, the logic of tag's control, and memory circuits to work from the radio frequency (RF) signal transmitted by the reader acquire the essential power. A tendency to demonstrate a new development of cross active RFID and received signal strength indication (RSSI) technologies [12]. In order to give extra functionalities, some RFID sellers are adjusting or assuming RSSI ideas for their products.

1.4. Global Navigation Satellite Systems

Presently for localisation of a radio-receiving station, GPS is utilized considered the most well-known and outstretched, in the 1970s designed and originated and since the 1990s totally operational. In several applications of modern life, GNSSs are assumed so strategic that after the GPS a number of distinct GNSSs were and are being originated and extended [8]. In this chapter, the basic features of the GNSSs obtainable and expected today in the near future are shown: the GPS of US, the GLONASS of Russian, Compass of Chinese, and the Galileo of European.

1.4.1. Global Positioning System

By the US department of defence (DoD), The NAVSTAR-GPS (NAVigation System for Timing And Ranging–Global Positioning System) scheme was formally introduced with the availability of uninterrupted -time availability and worldwide coverage to deploy and figure a locating service. The GPS was primarily germinated

only for military utilize, and in 1983 for civil users the posterity was released. Any GNSS system, the GPS in specific, is constructed in three segments: the constellation of satellite (the space segment (SS)), the operational control segment (OCS) which is network of the ground monitoring/control, and of all user receivers the associated equipment (the user segment (US)). Possesses the constellation of the orbits of the space segment, measures satellite signal propriety and health, and the OCS tracks and possesses the spacecraft. Additionally, the OCS adjusts satellite clock, and the updates of the constellation ephemeris [7, 13]. A definite equipment of user receiver that manages the signals of GPS is typically calculated the location of user, time, and speed.

Between 1990 and 1997, Block IIA introduced the present constellation of satellites, where the wholly Block IIR-M system was announced (2004-present), and Block IIR (1997-2004) functional. In May 2010, in Block IIF the first next reproduction satellite was initiated, while to be used in a post-2017 deployment, Block III satellites are designed. Around 11 h 58 minutes are the one half sidereal days of GPS of a nominal orbital interval. At a 60^0 separation of the equator with a formal tendency of 55^0 comparatively, the orbits are almost evenly spaced and rotated, while the radius of orbit is around 26,600 km. A 24-h time determination and global user navigation ability are given by the GPS constellation. To give two services, the GPS from its very origination was intended, matching to two dissimilar arranges of signal: the precise position service (PPS) and the standard position service (SPS). For civil group, the SPS is proposed, whilst proxy users of chosen government and the authorized military of the United States are slated for the PPS [14].

1.4.1.1. Frequency Schedule

The so-called GPS frequency aim is clarified in Figure 1.4. The aim for the various GPS sets consists of the determined bandwidth and the pertinent names. At varying transporter frequencies: L1, 1575.42 MHz, and L2, 1227.60 MHz, the present “interface” between the space segment and receiver of GPS compose of two RF links. For future services, namely L5, operating at1176.45 MHz an extra frequency is incarcerated. The dispensation of services on such frequencies is

recapitulated in Figure 1.5. With the essential frequency of GPS of precisely $f_0 = 10.23$ MHz, all of these frequencies are consistent. In reality, the above three mentioned frequencies can be associated with the essential frequency of clock as $f_{L1} = 1575.42$ MHz $= 154.f_0$, $f_{L2} = 1227.60\ MHz = 120.f_0$, and $f_{L5} = 1176.45\ MHz = 115.f_0$. The value $f_0 = 10.23\ MHz$ represents a formal frequency as it occurs on the ground to an beholder [15]. Due to satellite activity, to recover form relativistic influences, the real essential frequency of GPS of oscillators alongside the spacecraft is adjusted to before set to $f_0^{(act)} = 10.22999999543\ MHz$, so that on the ground a receiver of GPS would obtain a signal of the clock at precisely the required frequency f_0.

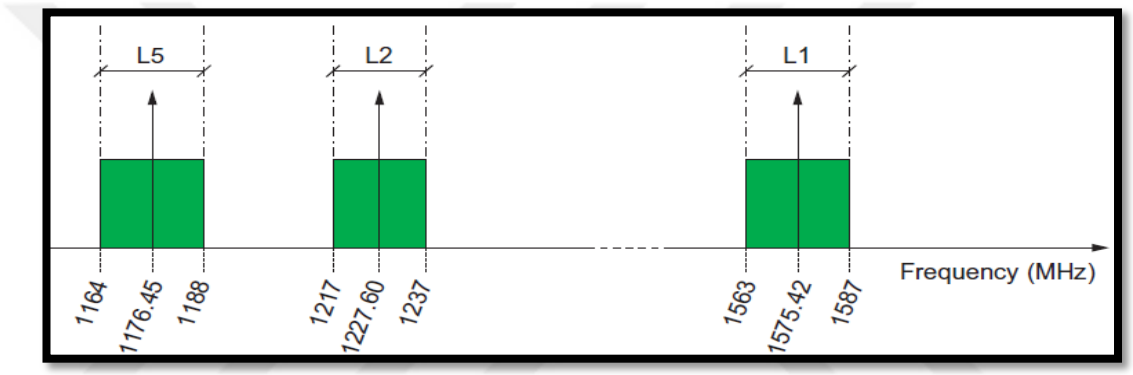

Figure 1.4 GPS frequency plan

However, the oscillation frequency differs in time owing to Doppler shift made by the relation movement of receiver and transmitter as obtained from the GPS user terminal of the carriers L1, L2, and L5. Such a shift of frequency is bested at least for terrestrial users in the range ± 5 kHz, and by the receiver has to be recompensed. In Table 1.2, Base features of GPS signals are described. Both the SPS and the PPS are given by the channel of L1, whereas the PPS presently supplies the only channel of L2. Two extra services will also give in block IIF, IIR-M by the satellites: The L2 civil-long (L2 CL) code and L2 civil-moderate (L2 CM) code [4]. Such extra characteristics contain a modern navigation (NAV) signal belong to the modernization program for civil use. GPS L1 frequency represents the frequency carrier of the satellite-based augmentation system (SBAS) signals [16].

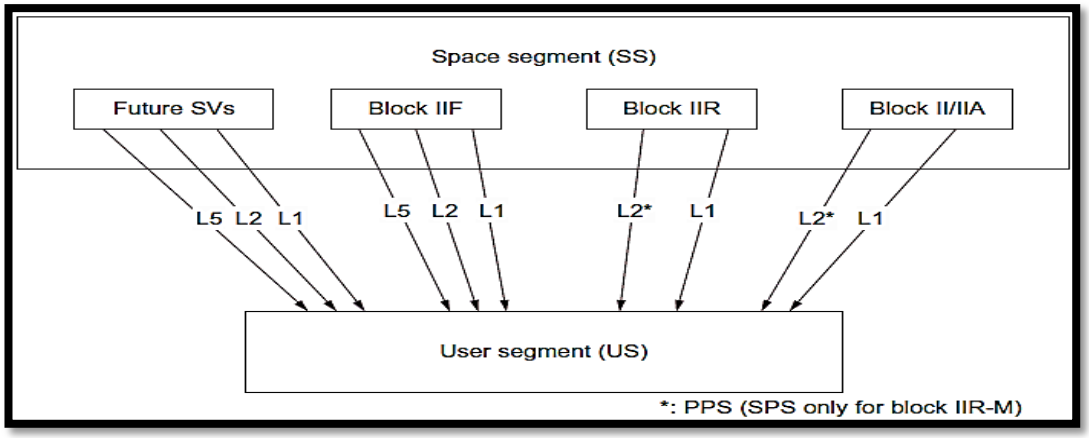

Figure 1.5 Interfaces of the space part GPS to the user part

Table 1.2 Base features of GPS signals

Frequency Band	**E1/L1**	**L2**	**E5/L5**
Signal name	GPS L1	GPS L2	GPS L5
Carrier frequency (MHz)	1575.42	1227.60	1176.45
Multiple-access technique	CDMA	CDMA	CDMA
Signal bandwidth (MHz)	20.46	20.46	24
Services	PPS, SPS	PPS, SPS	SPS
PRN code rate (Mcps)	1023 (C/A), 10.23 (P)	0.5115 (C/A), 10.23 (P)	10.23
PRN code length (c)	1023 (C/A), $2.35.10^{14}$ (P)	10230 (C/A), $2.35.10^{14}$ (P)	10230
NAV message data (bps)	50	50	25
NAV message symbols (sps)	50	50	50
Modulation	BPSK	BPSK	BPSK

By utilizing the code division multiple access (CDMA) technique, the same frequency bands involved. On each subbed the transferred signal that is utilized by the receiver is the low-rate binary phase shift keying (BPSK) that accomplish ranging which include the NAV data. A peerless PRN code is specified by each satellite vehicle (SV), and all of these sequences are interrelated approximately with one another, so that by just correlating the received signal all SV signals can be isolated and recognized with a satellite definite code of a fairly transferred municipal reproduction. By a GPS SV, different three codes of PRN rating are transferred [17]: (1) the code of precision (P), which is the code rating of essential NAV; (2) the code

of Y, utilized whenever anti-spoofing $(A-S)^2$ mode of operation is employed in the place of the code of P; and (3) for the procureation of the Y or P code the most used code is coarse/acquisition (C/A), is also the only one code that utilized in the applications of urban / mercantile.

1.5. L1 of GPS

The C/A and P are the two codes on the L1 carrier. A range chip is 10.23 Mcps for the P code. The composition of two PRN codes is originated by the special binary ranging sequence with the same chip rate. A restoration length of 15,345,000 chips is one of the two component periodic codes; the other one length is 15, 345,037 chips. The length of the code of these two codes created by their structure is $15{,}345{,}000 \times 15{,}345{,}037 = 2.35469592765E+14$ chips, or 23,017,555.5 seconds, since the two numbers 15,345,000 and 15,345,037 are a cognate prime which is partly longer than 38 weeks [2, 18]. Every satellite of the long P code with one week resumption interval uses a varied one-week-long segment. In reality, the 38-week-long part is partitioned into 37 varied parts, and each section is allocated to a varied SV. There are presently a whole of 32 satellite matching numbers, for other utilizes such with five more (33–37) restrained such as base transition. So precisely the infinite time of the week must be available, and it can be established in the signal of C/A code to accomplish procuration on it. Because of the chip average of the C/A code chip is 1.023 Mcps, The bandwidth of the spectrum of null to-null basic segment is 2.046 MHz. The code of C/A spectrum as well as many side lobes bears its own basic lobe to conciliate the P code. The duplication interval called 1023 chips of the code C/A is much less than that of the code P. The C/A code repetition time with a chip average of 1.023 Mcps is precisely 1 ms. The GPS receiver with a little carrier Doppler shift in the proper status of SNR in a reflection time as little as 1 ms can get the begin of the C/A code by a trialand- error step. In order to get the starting of a code C/A, just bounded information registered in the received signal is needed such as 1 ms. A varied PRN code is allocated by each satellite belonging to the group of identical Gold codes, as with the code P [13] along the carrier L1 with length bandwidth transferring of GPS satellites is around 20 MHz, so that the $1023 = 2^{10} - 1$. The C/A and P (Y) signals carried by the L1 frequency, while the frequency of L2 consisted just the signal of P (Y). The signals P (Y) and C/A are modulated on the L1

carrier for the *i*th satellite on the quadrature sets and in-phase of the bandpass signal, respectively:

$$\boldsymbol{s_{L1,i}(t) = A.P_i(t).D_i(t)\cos(2\pi f_{L1}t + \emptyset_1) + \sqrt{2}A.C_i(t).D_i(t)\sin(2\pi f_{L1}t + \emptyset_1)} \quad (1.2)$$

where $s_{L1,i}(t)$ represents the signal at frequency L1 of band-pass; A represents the amplitude of P code; $P_i(t) = \pm 1$ and $C_i(t) = \pm 1$ represent the binary code of P and C/A, respectively; $D_i(t) = \pm 1$ are the data of navigation; f_{L1} is the frequency of L1; and $\emptyset_1$ represents the first phase. The carrier frequencies of C/A, P (Y) are all phase closed; that is, they all carry phase and a constant frequency related to one another. A simple no return to zero (NRZ) design is carried by all data and/or code with rectangular pulses. 50 Hz is the range of bit. Each data bit includes 20 replicas of the code C/A and it is 20 ms long. As seen in Figure 1.6, the structure of a message is indicated along 25 frames. Every frame is divided into five sub frames, and each sub frame including 10 words. The most significant bit (MSB) of all words is transferred first. By considering 50 bps bit range, the entire message of GPS ultimate 12.5 min, by considering a 50 bps bit range.

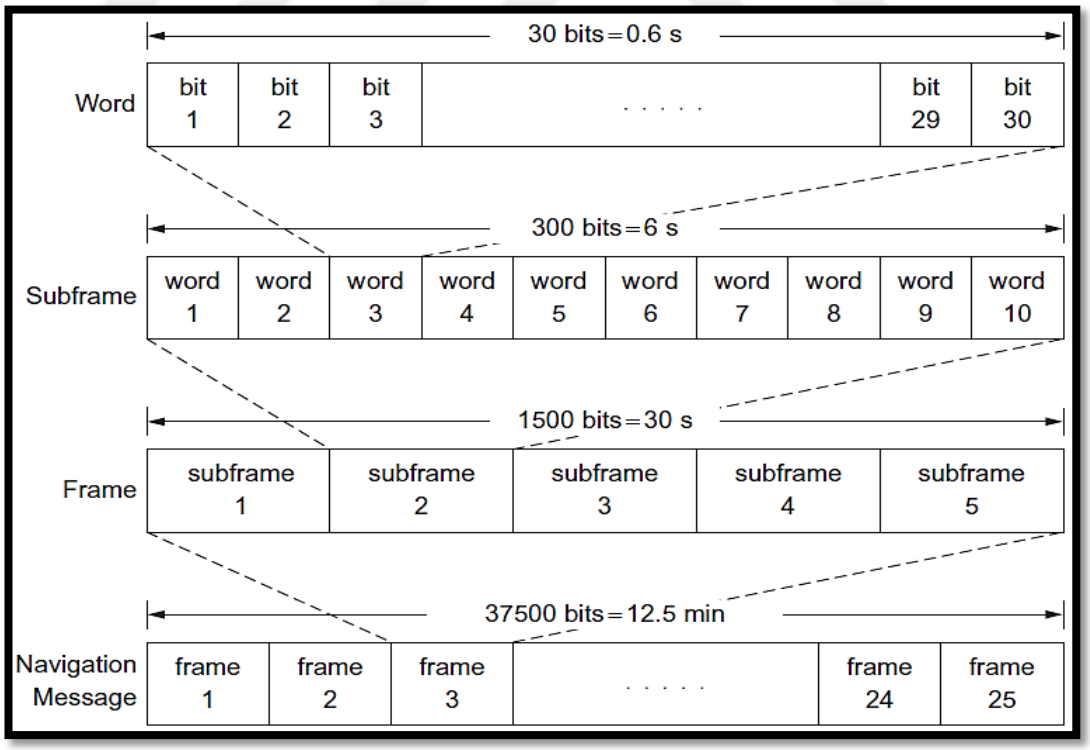

Figure 1.6 Data structure of the GPS navigation

1.6. L2 of GPS

The signal of L2 just consists of the Y or P code, and upon base command the data modulation can be changed on or off:

$$\boldsymbol{s_{L2,i}(t) = \frac{A}{\sqrt{2}} . P_i(t) . D_i(t) \cos(2\pi f_{L2} t + \emptyset_2)} \quad (1.3)$$

Where $s_{L2,i}(t)$ represents at frequency L2 the signal of band-pass; A is the P code amplitude onto the channel of GPS L1; $P_i(t) = \pm 1$ is the P code phase; $D_i(t) = \pm 1$ represents the signal of the information ($D_i(t) = 1$ if modulation of data is off); f_{L2} represents the frequency of $L2$ and $\emptyset_2$ represents the first phase. However, from SVs in block IIR-M from SVs, the signal of real navigation information can have varied structures: permanently the signal works at 50 sps, but to present best protection versus noise, it may have channel coding. The bit range are equalized to each other without any coding, while the bit range is 25 bps, and a convolutional code around range 1/2 with channel [19].

CHAPTER 2

SATELLITE BASED POSITIONING TECHNOLOGY

2.1. Basic Concepts

Nowadays, satellite locating technology is the most significant locating technology because of its important application in the military areas and has become a national security of important strategic resources. Currently, the representation of an active GPS satellite navigation industry has become the world's fastest growing information; and represents a nearly ideal dual-use technology between the civil and military communities. GPS systems provide continuous, precise time for users worldwide, position, velocity, and other navigation information, whether it is in the military field or in civilian areas. In recent years, the GPS receiver has entered ordinary families and has become our daily lives the most common consumer products [20]. In order to achieve the positioning function in the satellite signal precisely, the recovery requires accurate satellite signal of a PRN code phase and phase carrier. This requires the synchronization in the signal reception, including signal acquisition and tracking. In the outdoor environment, the ordinary radio navigation receiver can be able to complete the localization, since the power intensity of GPS signal is considered to be 160 dBW, under such signal strength, the existing receivers can easily complete capturing and tracking tasks of the signals. However, when the signal conditions are not ideal, such as indoors, forest, urban environments, and other under SNR environment, the existing of GPS technology cannot catch the weak GPS signal. The ordinary GPS receiver will be difficult to catch and track navigation satellite signals. The research showed that in indoor environment, the GPS signal power of Ll wave band probably within a range 160dBW ~ 200dBW scopes, its signal power is very weak [21]. A weak GPS signal generally refers to the signal strength within the range 180dBW~190dBW.

Therefore, in indoor and other environment, the GPS receiver must be able to capture -160dBW. As can be seen from the above discussion, in indoor environments and other under Low SNR environment, the first part of the GPS receiver work, then functional modules capture a higher performance requirement, must be able to capture the signal in low SNR environment, and must have a good detection sensitivity.

2.1.1. GPS Overview

Currently, the norm found in the 1960s meets totally the operational of GPS for an optimum positioning system. The current GPS system was declared with initial operational capability (IOC) on December 8, 1993, and it is virtually identical today as the system was proposed in 1973. Over three decades, this system has kept the same design and general accuracy. All GPS signals are systematically influenced by the physics of the environment due to the troposphere, ionosphere or relativity, which can be removed either by modelling or direct measurement [10]. Due to the noise in the code, the navigation solution is limited by inaccurate range determinations between each GPS satellite and the GPS receiver. The system gives precise, three-dimensional location, persistent, universal, and speed data to servants with the proper obtaining tools. Nominally the constellation of satellite consists of 24 satellites organized with four satellites per level in six orbital levels. The wellness and estate of the satellites are controlled by a universal base monitoring/control network. On two frequencies via a technique, namely Code Division Multiple Access (CDMA) the satellite announces codes and navigation information; these two frequencies namely L1 (1,575.42 MHz) and L2 (1,227.6 MHz) are utilized by the system, each satellite transfer on these frequencies. Because of these, the codes have a characteristic with regard to one another of low cross-correlation. A small code creates by each satellite pointed to as the (C/A) code and Precision or P(Y) code indicated as a long code. At the signal transmitting time, the navigation information supplied the means to calculate the position of the satellite for the receiver, while to calculate the signal's extension time, the rating code allows the user's receiver and herewith to calculate the rate of satellite-to-user. The user receiver for this technique needs to include a clock. The measurements of the TOA rating be made to four satellites to determine the three dimensional position of the receiver. If the clock of

the receiver were coincided with the clock of satellite, just three measurement ranges would be necessitated. However, a crystal clock is generally used to reduce the cost in navigation receivers, and size of the receiver. Therefore, from the interior system time, four measurements are necessitated to calculate user latitude, longitude, height, and receiver clock offsets.

2.1.2. Overall Structure

On the basis of the signals arriving from the satellite, the user position is calculated using GNSS receiver. This is established normally by an aggregation of suitable software (SW) and hardware (HW) techniques. The recent receivers are almost digital, because of the shift of the analog-to-digital transition have seen a released by GNSS receivers as near as achievable to the obtaining antenna. Thus, all of the subsequent processing is accomplished during digital signal processor (DSP) techniques after signal digitisation in the analog-to-digital converter (ADC). The essential operational structure of a GNSS receiver is illustrated in Figure 2.1, independent of the assumed digital/analog section.

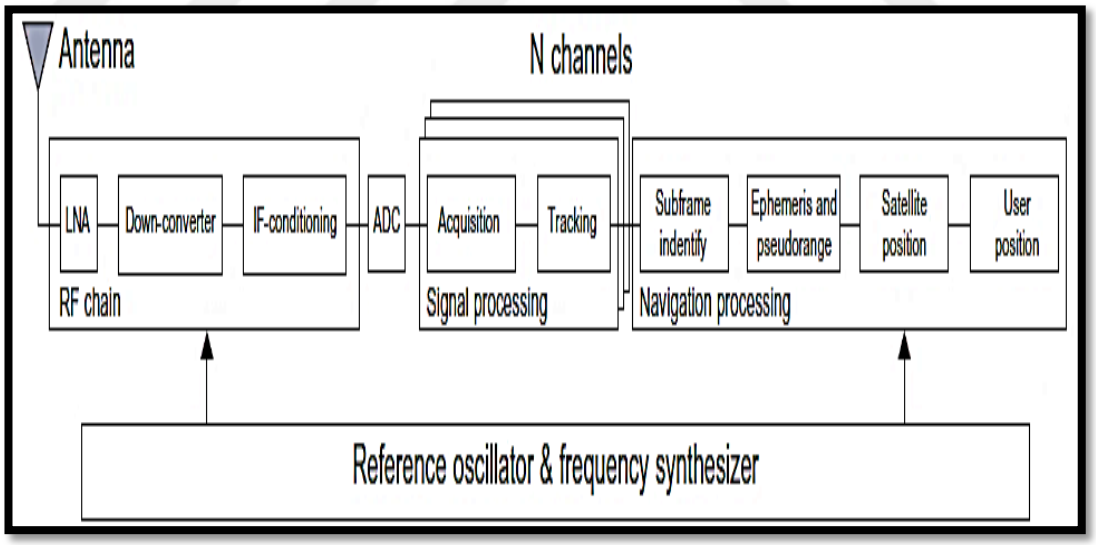

Figure 2.1 Structure of the common GNSS receiver

Six varied basic subsystems can be distinguished:

- Antenna
- RF chain

- Analog to digital convertor
- Processing of signal
- Processing of navigation
- Local oscillator (LO) or receiver carrier's dynamo

By an L-band antenna, the transferred right hand circularly polarized (RHCP) signals from the satellites are received, and have almost hemispherical concealment. Typically, to shorten discrepancy of the out band of RF chain, the antenna is directed by a passive band-pass prefilter. The input of the RF chain is the output of the antenna, wherein the forthcoming signal is aggrandized by a low-noise amplifier (LNA), and is down- transformed to a lower intermediate frequency (IF) f_{IF}. This is achieved in a super heterodyne receiver, during merging the received signal with a local RF oscillation at the frequency $(f_0 + f_{IF})$ of the carrier frequency f_c. In order to let the required signal pass unaltered, the bandwidth of such a filter must be big enough, regardless of diverges in the reference oscillator and a probable Doppler shift. Furthermore, the bandwidth must also be converted as small as probable to minimize interference and noise at the output of the RF-chain. After the chain of RF, an ADC is utilized to digitise the signal anterior on the resulting of the high-data-rate digital flow to executing signal process. For each satellite that is being processed, a distinct channel is required to achieve signal tracking, acquisition, and navigation processing. One of the basic characteristics of the receiver is the number of parallel channels that can cover the characteristics of the basic receivers simultaneously [23]. With the suitable transferring satellite in each channel, the arriving signal has to combine to be managed. Therefore, combined with one of the receiver's channels and at the instantaneous discrete time *n*, and from a definite satellite the IF digitized signal obtained which can be written as

$$\boldsymbol{y_{IF}[n] = \sqrt{2P_r c_{IF}(nT_c - \tau) D(nT_c - \tau) cos(2\pi(f_{IF} + f_D) nT_c + \emptyset_{IF}) + v[n]}} \quad (2.1)$$

where P_r is the received signal power at RF, $c_{IF}(nT_c - \tau)$ represents the rating code filtered over the front-end related to the satellite and by a sub carrier adjusted, $D(nT_c - \tau)$ is the information bit of navigation, T_c represents the code chip duration, τ is the code delay that calculates the distance of the receiver from the satellite, f_D represents the shift of doppler frequency, and $\emptyset_{IF}$ is the phase of IF carrier. The

expression of collective noise $v[n]$ with the thermic noise at the antenna includes influences of interference from both other satellites and extrinsic sources with the cross-correlation of nonzero code [22]. The acquisition phase is the procedure of bemoaning a channel to a special satellite, during the estimation of a coarse carrier frequency and delay of rating code of the satellite is achieved. The received signal of the reference rating code of the satellite is correlated with a local replica, once the acquisition is achieved. The input of the tracking loops for accurate approximation of the phase/ carrier frequency and code timing is the result of such correlation on a definite time window. The measurements of time delay from the user terminal to the pseudo ranges are interpreted into the values of the distances, and in the sky to get ephemeris and to calculate the satellite locations. The user location can be lastly computed from the pseudo ranges and satellite locations. The LOs in the receiver whose function to place the important reference frequency is an extra basic factor for the A/D, down-conversions, and propagation of code. The LOs are acquired by a frequency synthesizer from a reference oscillator.

2.2. General Description of GPS and How Does It Work

From immemorial times, people have travelled around the world looking for new lands, transporting, trading products with neighbouring communities, or simply travelling for fun. These are the origins of the navigation, the art of moving between two points following a known path. Recent progress in space technologies has prompted a revolution in the navigation methods. It is hoped that before 2020 the GNSS will replace the majority of the current navigation systems [8]. The GPS system was created and realized by the DoD and was initially designed to give service to the US army. But, since the first of May of 2000, civil users were allowed to access the error-free signal of GPS. Nowadays, GPS is the most important GNSS and the only one fully operational, providing different sorts of service to civilian and military users. At any place on the earth with all-weather situations, the users can calculate an accurate position, time, and velocity by allowing of the GPS.

The entire system can be divided into the following three parts as shown in Figure 2.2:

- Space segment: Formed by the satellites that provide the navigation messages within a defined signal format to the users.
- Control segment: Group of ground stations that follow and manage the satellites' orbital configuration, their health, and their signal integrity. Furthermore, they update the clock biases and the ephemeris or navigation messages (parameters needed to precisely calculate the position of the satellites).
- User segment: Formed by the users' receivers in charge of measuring time and calculate position from the satellites' signals [5, 24].

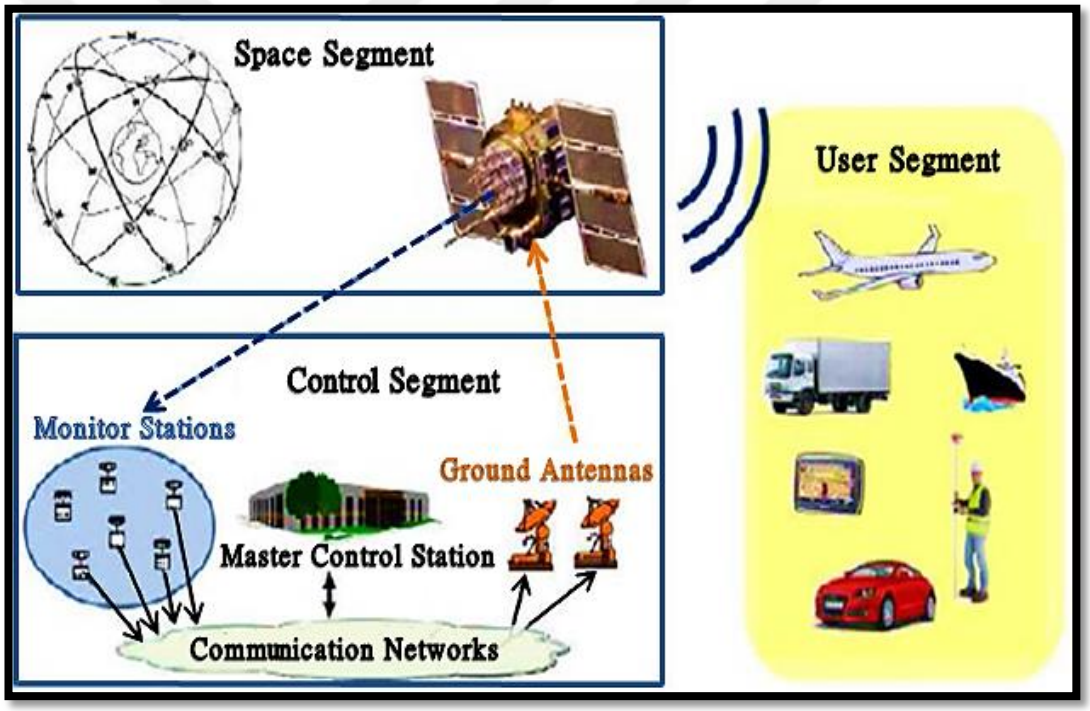

Figure 2.2 GPS segments

2.2.1. Space Segment

On a medium earth orbit (MEO) at an altitude of 20200 km, the space segment comprises in a constellation of at least 24 satellites in 6 orbital planes (four on each plane which is non-equally spaced). Each satellite circles the earth twice a day with periods of 11h 58' (half sidereal day). By 55º to the earth's equator, the orbits are inclined and the orbital planes are spaced 60° apart to give coverage to the whole

world. Ensuring a maximum number of satellites giving service under the polar regions, where there is more human activity as shown in Figure 2.3. The space segment is in charge of transmitting the navigation message provided by the ground segment to the user segment [25].

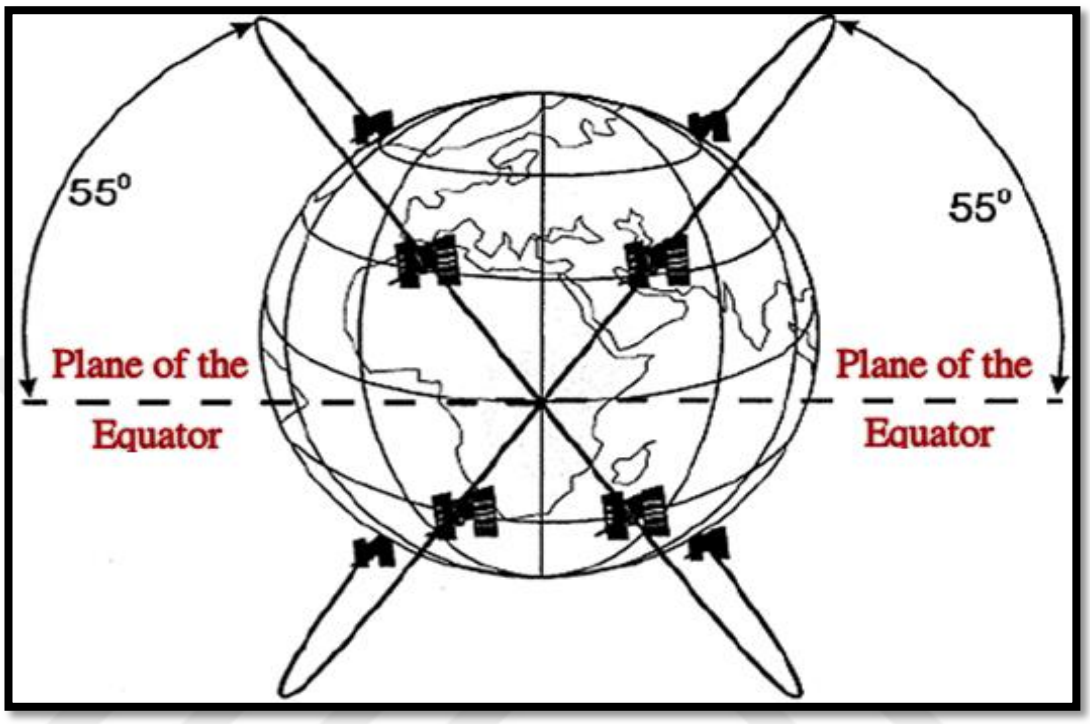

Figure 2.3 Inclination of GPS orbit

2.2.2. Control Segment

The new satellite generations are going to be able of exchanging data with each other and correct their orbit data on their own. In theory, the Block IIR satellites only need a contact to a ground station every 180 days. However, currently the control segment shown in Figure 2.4 is ground-based and formed by:

- Master control stations (MCS): Consist of a pair of ground stations; the main control station, located in Colorado (Falcon Air Force Base), and a backup station in Maryland. These stations represent the brain of the system. The whole administration of transmission places and remote monitoring are accountable by Colorado, such as controlling the satellite's health, predicting and correcting the clock and the orbital biases, monitoring satellite integrity, and generating the navigation messages (messages needed in the user segment to obtain a valid solution) [4, 26].

➢ Monitor stations (MS): Six monitoring stations are located all over the world to gather and up-link (transmit) information between the satellites and the MCS. MS are the link between MCS and satellites.

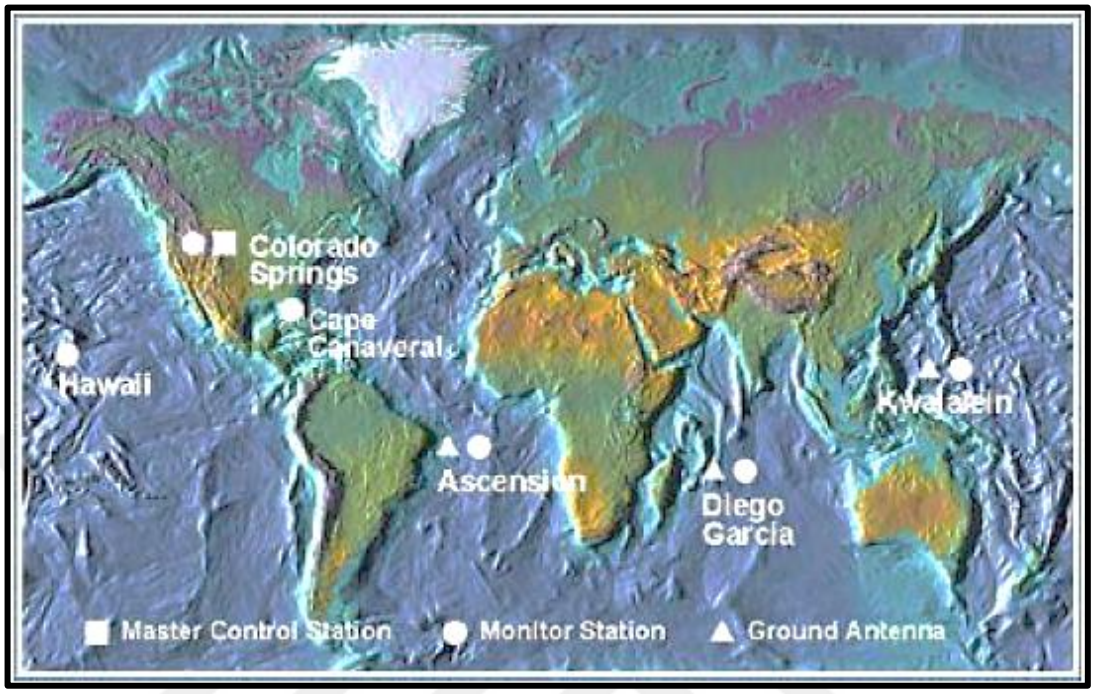

Figure 2.4 Segment of the GPS control

2.2.3. User Segment

The segment of user is simply all of the end users (military users included) who have purchased any of available GPS receivers [27].

2.3. Processing of Navigation

Processing of navigation, also namely processing of data, chooses usefulness of the transporter and code synchronization acquired once the tracking status is arrived, to calculate the PVT of the user. The varied processing levels within the receiver is described in Figure 2.5. The pseudo range value required to achieve the processing of navigation that acquired via pieces of data assembled from both the navigation message decoding and the processing of the signal level. The calculation with reference to the GPS systems of the pseudo range of a satellite are clarified by steps guiding. The same opinions also apply to other GNSSs. A timestamp in the global GPS time scale required by the computation of the pseudo range on the signals announce by the satellites. We demand that the message of GPS navigation is

organised in sub frames and pages, to realize how this is done, and with a sequence of two definite words. The first two words of each sub frame are the handover (HOW) word and the telemetry (TLM) word [11]. The 8-bit preamble with 16 confined bits and 6 equivalence bits are included by TLM, and it describes the sub frame starting: to coincide the message of navigation, it is utilized by the receiver. The HOW contains 4 parts and it is the second word of the sub frame:

- 1–17 bits: in 6 s units a counter demonstrating the time of GPS, incomplete version of the time of week (TOW) area
- 18–19 bits: event of system (mindful 18 bits, reliability indicator; bit 19: mode of anti-spoofing)
- 20–22 bits: designation of sub frame number
- 23–30 bits: valence of bits.

The fundamental for pseudo range computations is the purport of the HOW.

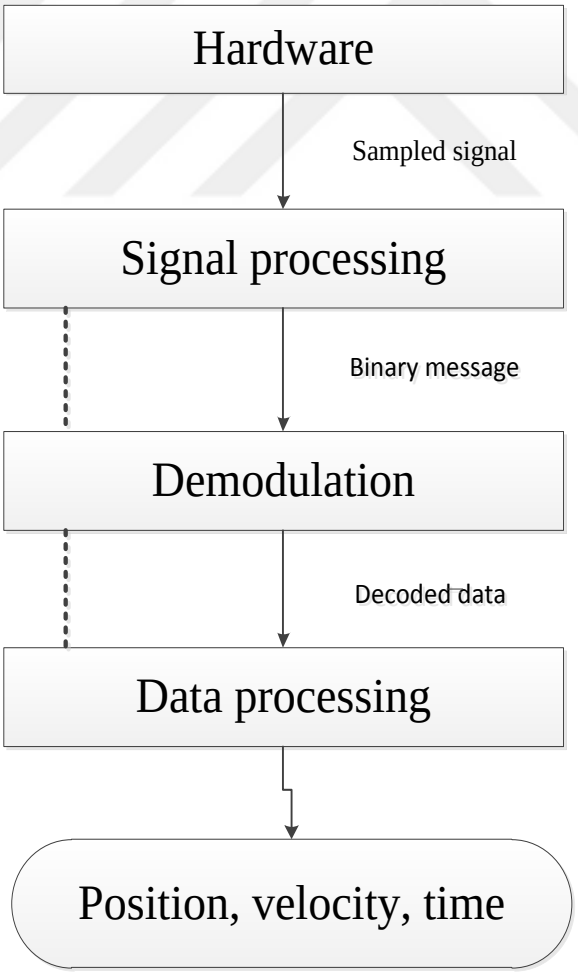

Figure 2.5 Logical steps of the receiver signal process

The receiver calculates its time measurements based on the reference time specified in each package received from the satellite, and knowing that the transmission time of a navigation message is about 12.5 minutes. Thanks to the fragmentation, we obtain a higher rate of measurements, which also means an increase of the refreshing position rate and that leads to a more accurate tracking. The navigation message is modulated at 50 bps and is formed by 25 pages or frames (30 seconds). At the identical time, a frame is divided into 6 seconds and 5 sub frames, every sub frame contents of 0.6 seconds with 10 words [28].

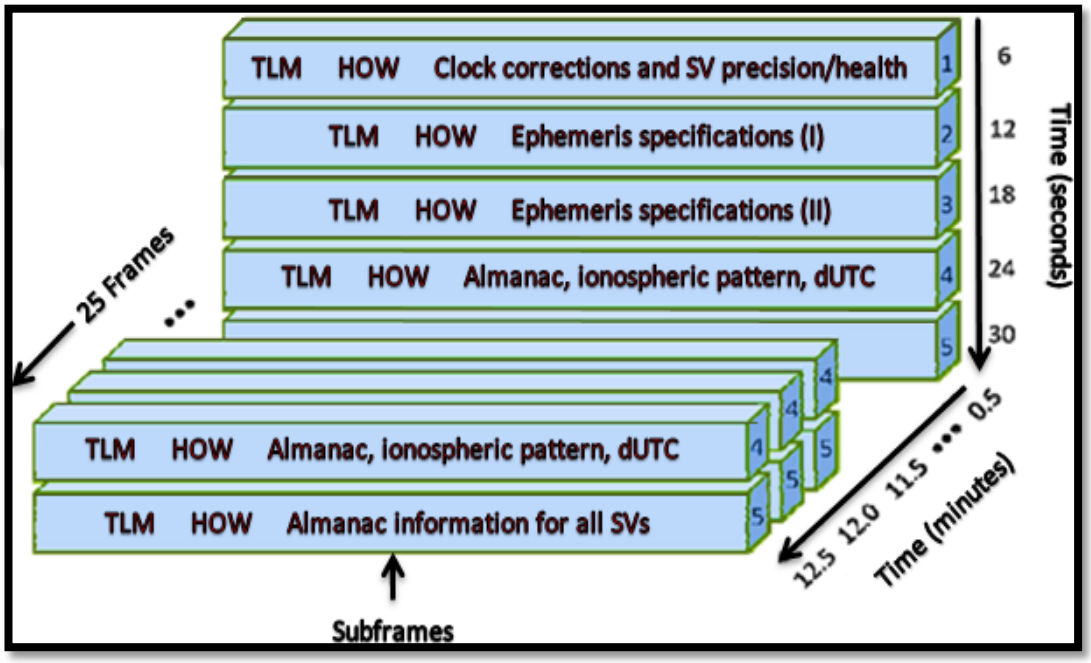

Figure 2.6 Fragmentation of the navigation message

As one can see in the above Figure 2.6, there is a kind of header represented in every sub frame. Specifically, the TLM and the HOW are needed to synchronize and to indicate the time when the first word of the sub frame was transmitted, respectively.

2.3.1. Criterion of the GPS Time

In announcing the time scale of GPS which is cited to coordinated universal time (UTC) time point zero, the big unit utilized is one week, described as 604,800 s. The counter illustrating the 1.5 s time periods is the Z-count, in a particular the structure in Figure 2.7. Its 19 LSBs illustrate the TOW area: 1.5 s epochs within a

week number, limiting from 1 to $604{,}800/1.5 = 403{,}199$; the 10 MSBs are on the converse consecutive number of the present GPS week of the Z-count. The present 1.5 s interval is distinguished simultaneously by the two areas from the starting time.

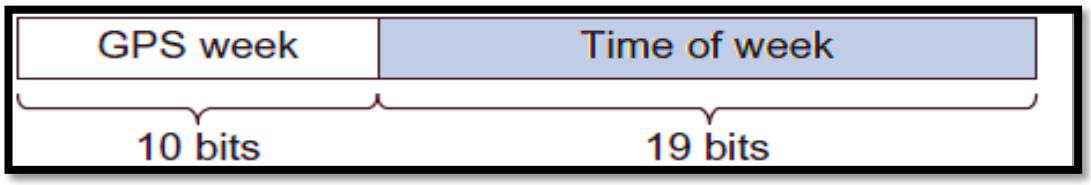

Figure 2.7 Z- count exemplification

The TOW is readjust to zero at the end of each GPS week, and the raises number of the GPS week carries on the counter. Just if we assume the 17 MSBs of the TOW, we gain in expressions 6-second periods of the counter time. Hence, a counter of sub farmes describes on the range of the GPS time by the HOW [29]. In reality, a period of each sub frame is expressed as:

$$\underbrace{10}_{\text{words}} \cdot \underbrace{30}_{\text{bits}} \cdot \underbrace{20}_{\text{code periods in 1 bit}} \cdot \underbrace{1\text{ ms}}_{\text{code duration}} = 6\text{ s}. \tag{2.2}$$

Figure 2.8 illustrates by the satellites the transmitting of the navigation message and by the employers how they are obtained. With the same time of reference, most of the GPS satellites are coincide, so they all at precisely time t_{sub} transmit out the navigation messages. At which the TX of each message sub frame begins the calculation of the time by the HOW.

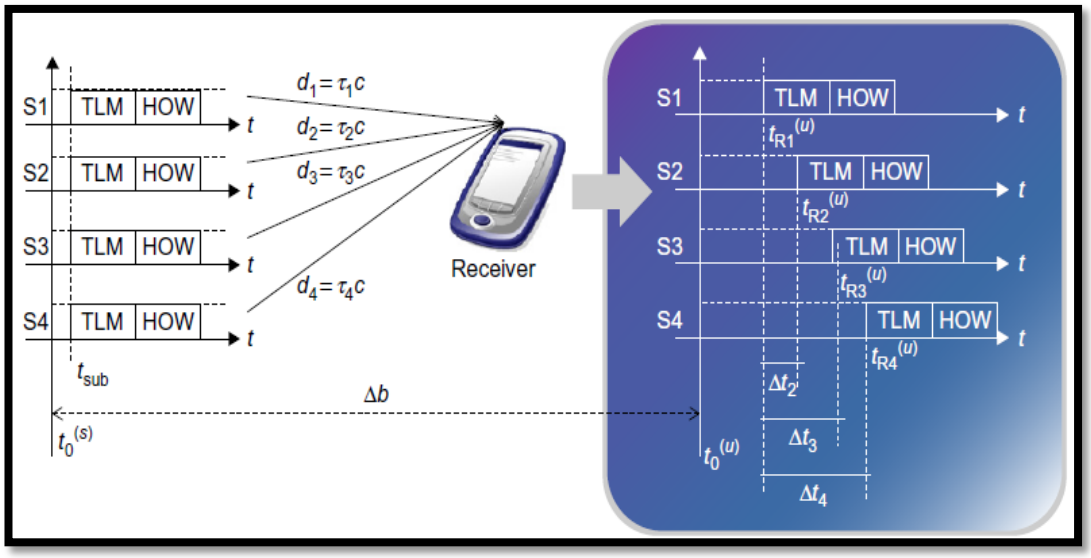

Figure 2.8 Messages information

At the same time the messages of satellite originated, and reach at varying times of RX, because of the varied distances of satellite/RX. On the base of the varied receipt periods $t_{R_i}^u, i = 1, \cdots, 4$ the range of user time approximating the value of the *i*th pseudo range begins with the receiver. It can be examined that if the user's location (x_u, y_u, z_u) and satellite ephemerides (x_1, y_1, z_1) are cognized, by doing a single pseudo range, ρ_1. Once t_u is calculated, an immobile receiver can solve for t_u, it can be deducted from the receiver clock time, t_{rcv}, to get GPS system time, t_E. (In the development of the user location solution, *Tu* was indicated as the time of GPS system, which illustrated the immediate in the time of the system when the signal arrived the receiver of user by satellite. However, at any special time we require to describe the time of GPS system and will utilize the parametric quantity *tE*). At any special time, describing the clock time of the receiver:

$$\boldsymbol{t_{rcv} = t_E + t_u} \tag{2.3}$$

so that:

$$\boldsymbol{t_E = t_{rcv} - t_u} \tag{2.4}$$

from UTC, t_{UTC} is calculated as follows:

$$\boldsymbol{t_{UTC} = t_E - \Delta t_{UTC}} \tag{2.5}$$

where Δt_{UTC} Δt_{LS} illustrates the integer leap second number and a partial estimate of the disparity between the time of UTC and GPS system modulo as δt_A. [In the message of navigation data, the control part gives polynomial factors (*A*0, *A*1, and *A*2) that are utilized to calculate the partial difference between the time of UTC and GPS system (USNO) [4]. Hence, t_{UTC} can be calculated as follows by the receiver:

$$\begin{aligned} \boldsymbol{t_{UTC}} &= \boldsymbol{t_E - \Delta t_{UTC}} \\ &= \boldsymbol{t_{rcv} - t_u - \Delta t_{UTC}} \\ &= \boldsymbol{t_{rcv} - t_u - \Delta t_{LS} - \delta t_A} \end{aligned} \tag{2.6}$$

2.3.2. Comparative Pseudo Range Measurements

The reception times of the receiver registers, beginning at $t_0^{(u)}$ of the satellite TLMs on its own time range. Each measurement of the receiver clock opposite the GPS time and by the same unknown offset time $\Delta b = t_0^{(u)} - t_0^{(s)}$, $t_{Ri}^{(u)}$ is influenced. The estimated pseudo ranges in this manner clarified in Table 2.1.

Table 2.1 Pseudo range mensuration depending on relative times

CH	Transmit Time	Received Time	Difference	Pseudo range
1	300 s	t_{R1}=300.063 s	63 ms	18,900 km
2	300 s	t_{R2}=300.068 s	68 ms	20,400 km
3	300 s	t_{R3}=300.076 s	76 ms	22,800 km
4	300 s	t_{R4}=300.090 s	95 ms	28, 500 km

The measurement of the related delta-pseudo ranges can also depend on the method, by assuming the reference of the pseudo ranges $(i = 1)$. Table 2.2 computing the difference of a time. When the first TLM is obtained, the measurements of the Δt_i are restart and it can be achieved by means of counters.

Table 2.2 Measurement of pseudo range depending on the time differences

CH	Received Time	Transit Time	Pseudo range
1	0	70 ms	21,000 km
2	$0 + \Delta t_2 = 5\ ms$	75 ms	22,500 km
3	$0 + \Delta t_3 = 7\ ms$	77 ms	23,100 km
4	$0 + \Delta t_4 = 12\ ms$	82 ms	24,600 km

As the mean of the satellite time diffusion, the initial value of pseudo range is arbitrarily placed by the receiver, or in reality on the range of the user time is calculated. Arranging a selected received time or selecting a mean of a propagation time is equal to placing a special value of Δb.

By resolving the next equations in the four unknowns x_u, y_u, z_u (The user location), and the difference of Δb, the calculation of time and location are acquired:

$$\begin{aligned}
&\sqrt{(x_1 - x_u)^2 + (y_1 - y_u)^2 + (z_1 - z_u)^2} - c.\Delta b = \rho_1 \\
&\sqrt{(x_2 - x_u)^2 + (y_2 - y_u)^2 + (z_2 - z_u)^2} - c.\Delta b = \rho_1 + c.\Delta t_2 \\
&\sqrt{(x_3 - x_u)^2 + (y_3 - y_u)^2 + (z_3 - z_u)^2} - c.\Delta b = \rho_1 + c.\Delta t_3 \\
&\sqrt{(x_4 - x_u)^2 + (y_4 - y_u)^2 + (z_4 - z_u)^2} - c.\Delta b = \rho_1 + c.\Delta t_4
\end{aligned} \tag{2.7}$$

Where ρ_1 represents the first pseudo range and x_i, y_i, and z_i represent the coordinates of the satellite $(i = 1, \cdots, 4)$ obtained from the ephemeris [30]. In the immediate time varied from begin of a sub frame, the calculation of location and time can also be reiterated. As illustrated in Figure 2.9, sub farme is obtained each time from a definite satellite, the receiver begins a local counter, from the *i*th sub frame starting at the instant time and estimates the passed times δt_i, where the location is calculated, $t_m^{(u)}$, from which it gets the variance $\Delta t_i = \delta t_{max} - \delta t_i,\ i = 2,3,4$.

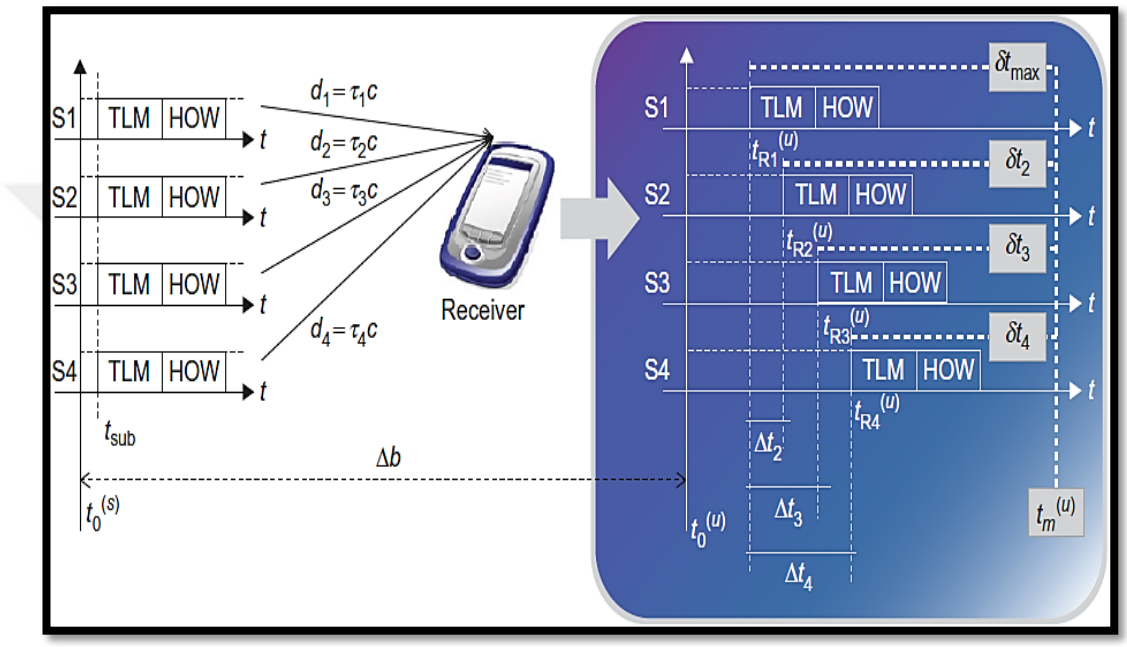

Figure 2.9 Transmission and reception with regard to time

2.3.3. Numerical Formation of the Signals

It is conceivable to provide the numerical term of the several signals, pediment from all the previous discussion. GPS are given by S1 and S2:

$$\boldsymbol{S_1 = A_p(P \oplus D)cos(2\pi L_1 t + \emptyset) + A_c(C/A \oplus D)sin(2\pi L_1 t + \emptyset)} \quad (2.8)$$

$$\boldsymbol{S_2 = B_p(P \oplus D)cos(2\pi L_2 t + \emptyset)} \quad (2.9)$$

where 1.57542 MHz represents L1, L2 represents 1.2267 MHz, D represents the information bits of the navigation message, P is the code chips, C/A is the L1 code chip, A_p and A_c are on L1 the particular amplitudes of the P and C/A codes, and B_p represents L2 on the amplitude of P-code. The particular amplitudes for C/A at 2128.5 dBm 17 are defined, on L1 the 2131.5 dBm for P code, and on L2 2131.5

dBm for P. To produce the signals of GPS, all utilized frequencies are acquired at 10.23 MHz from an ultra-stable oscillator single frequency toned. The signal has to pass several layers of the atmosphere, while travelling to the receiver from the satellite [31]. This passing causes of the two influences: on the signal the softly down and the declination of its way. The first influence is essential and must be discarded, either by dual frequency analysis 25 or by suitable modelling.

2.4. Principles of Pseudo Range Error

The reliability in the user location approximation relies on a sophisticated reaction of different parameters. The GPS reliability relies on the "quality" of the mensuration as well as ephemeris of the satellite. User equivalent range error (UERE) is the uncertainty of the pseudo range. On the last evaluated location, the effect of the UERE is also dependant on some "geometric" elements defining along the user in the sky how the satellites are replaced [24]. In reality, the varied locations of the satellite influence the reliability of the numeral processes. Numerically, the equations in some states are ill stated; that is, errors on the pseudo range of a small measurement give on the last location evaluates big errors.

The sources of error that influence the pseudo ranges can be categorized as follows:

- Control of system: measurement errors, errors on the clocks and ephemeris.
- Delay of ionospheric: the radio wave's velocity relies on the intensity of clear electrons over the proliferation way.
- Delay of troposheric and atmospheric fading: the delay of propagation and fading rely on the temperature, air ministration, and pressure.
- Multipath: various "copies" following several propagation of the transferred signal come to the receiver ways made by near to the receiver sprinkling items and the existence of reflective surfaces.
- Noise of receiver and sensitivity of clock.
- Influences of uncompensated relativistic.
- Selective availability (SA): to locate the reliability of the GPS for civil users, deliberate perturbation to the transferred rating codes.

In the initial proposal, the errors caused by the Doppler influence can be disregarded. Since for the shift of the pertinent carrier frequency, the receiver has anyhow to calculate and match it. An irregular contribution of error is provided by all the earlier

sources that is statistically detached, on each pseudo range the whole error turns out to be:

$$\boldsymbol{\sigma_{UERE} = \sqrt{\sum_j \sigma_j^2}\ (\mathrm{m})} \tag{2.10}$$

where σ_j^2 is the difference of each source. Tables 2.3 and 2.4 show a concept in a theoretical receiver of the UERE magnitude order, namely pseudo range measurements of the error schedule for the PPS, SPS, and GPS, respectively [8, 14].

Table 2.3 Error schedule of GPS PPS Pseudo range [8]

Segment	Error Source	1σ Error (m)
Space	Satellite clock stability Satellite perturbation Other (thermal radiation, etc.)	3.0 1.0 0.5
Control	Ephemeris prediction error Other (thrusters, etc.)	4.2 0.9
User	Ionospheric delay Tropospheric delay Receiver noise and resolution Other (interchannel bias, etc.)	2.3 2.0 1.5 1.2 0.5
UERE	Total (rms)	6.6

Table 2.4 Error structure of GPS SPS Pseudo range [14]

Segment	Error Source	1σ Error (m) With SA	1σ Error (m) Without SA
Space	Satellite clock stability Satellite perturbation Selective availability (no longer active) Other (thermal radiation, etc)	3.0 1.0 32.3 0.5	3.0 1.0 - 0.5
Control	Ephemeris prediction error Other (thrusters, etc.)	4.2 0.9	4.2 0.9
User	Ionospheric delay Tropospheric delay Receiver noise and resolution Multipath	0.5 1.5 1.5 2.5 0.5	5.0 1.5 1.5 2.5 0.5
UERE	Total (rms)	33.3	8.0

2.5. Reference of Coordinate Systems

One needs to know which varied references are presently being utilized by the interest of the navigation system. Certainly, when comparisons between varied locating systems are requested, this is also the uppermost significance. When a locating system is an integration of different techniques; this is especially the states that are pointed to referential varied systems. It is important to describe the earthy design, as well as the introduction of geographic referencing systems. As the locating of satellite-based systems utilizes special signals, there is in theory no requiring for such a personification. The necessity for an exact accordance between the personifications of the Earth and actuality is a remarkable subject. Figure 2.10 illustrates the form of ellipsoid design. In order to be as near as possible to the geoid, this numerical design has been selected and it is described by some other factors such as the its surface f, small axis b, or the first eccentricity e, and by its long axis. In reality, the vertical important characteristic to the regional tangent does not cross the ellipsoid centre, except at the poles and the tropical plane as shown in Figure 2.11. This explains just a numerical personification of the geoid.

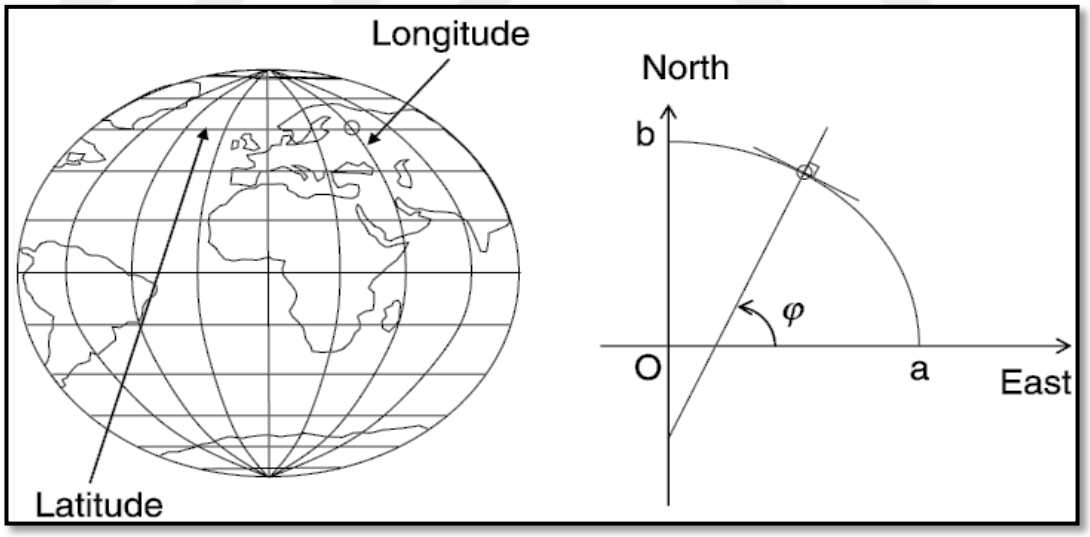

Figure 2.10 Ellipsoid representation

In which the estates of both the satellite and the receiver can be characterized, it is important to select a coordinate of reference. To subedit the maths issue of the satellite navigation. In this punctuation, the expressions of speed and position vectors are ideal for picture states of the satellite and the receiver that calculated in a coordinate of Cartesian system.

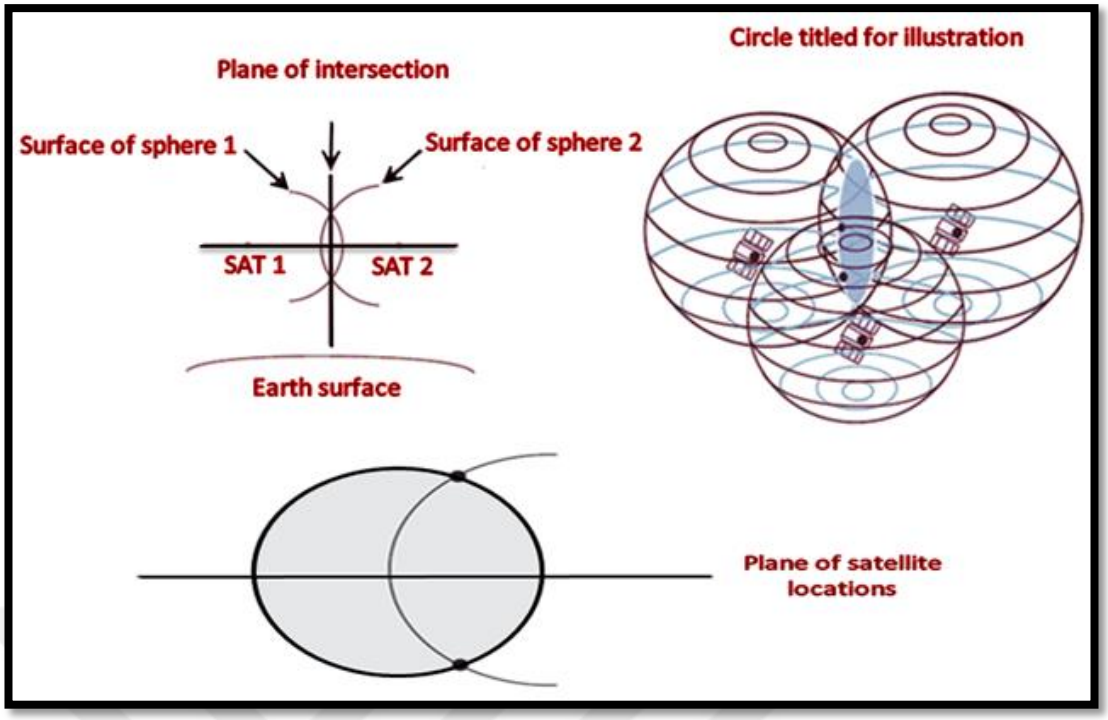

Figure 2.11 Fragmentation of the navigation message

2.6. Coordinate Earth- Fixed/Centred System

It is more suitable to utilize a coordinate system ECEF for the aim of calculating the location of GPS receiver that turns with the Earth. In such a coordinate system, it is simple to calculate the height parameters, longitude, latitude that the receiver illustrates. As with the coordinate of inertial (ECI) system, the ECEF coordinate system utilized for GPS and its *xy*-plane coincident with the Earth's equatorial plane. Anyways, in the system of ECEF, in the direction of 0° longitude refers to the +*x*-axis, and in the direction of 90°E refers to +*y*-axis longitude. Therefore, the *x*-, *y*-, and *z*-axis revolve with no longer characterize and the earth in the interior space of the stable orientations. In this system, in the way of the geographic north pole, the z-axis is selected to the sheet of equatorial to be ordinary, herewith accomplishing the coordinate system of the right-hand. The orbit software of GPS calculation contains the transmutations between the coordinate systems of ECEF and ECI. By the application of turning matrices, such transmutations are achieved to the speed vectors and satellite location in the coordinate system of the ECI [32].

2.6.1 Calculations of Longitude, Latitude, and Height

As illustrated in Figure 2.12 with the point O along the earth centre, the coordinate system of ECEF to the WGS 84 ellipsoid reference is added. With the relevance to the ellipsoid reference, we can know the parameters of longitude, latitude, and height. In this way, these factors are named geodetic [12]. Granted a vector in the system of ECEF of user receiver's location u =(*xu*, *yu*, *zu*), the geodetic longitude (λ) as the angle between the *x*-axis and the user can be calculated in the *xy*-sheet

$$\lambda = \begin{cases} \boldsymbol{arctan}\left(\frac{y_u}{x_u}\right), & \boldsymbol{x_u \geq 0} \\ \boldsymbol{180^0 + arctan}\left(\frac{y_u}{x_u}\right) & \boldsymbol{x_u < 0 \ \ and \ y_u \geq 0} \\ \boldsymbol{-180^0 + arctan}\left(\frac{y_u}{x_u}\right) & \boldsymbol{x_u < 0 \ \ and \ y_u < 0} \end{cases} \tag{2.11}$$

The angles of negatively harmonize to degrees of west longitude explained in equation 2.11. In expressions of the standard ellipsoid, the geodetic factors of latitude (ϕ) and height (*h*) are described at the user's receiver. In Figure 2.12, by the unit vector the standard ellipsoid is characterized. Precisely the standard ellipsoid does not indicate to the Earth centre, unless the user is on the equator or the poles. The height compared to the ellipsoid of the world geodetic system (WGS 84) calculated by a GPS receiver. In the horizontal sheet, the dissimilarity between the restricted data such as European Datum 1950 and North American Datum 1983, and WGS 84 can also be important [33].

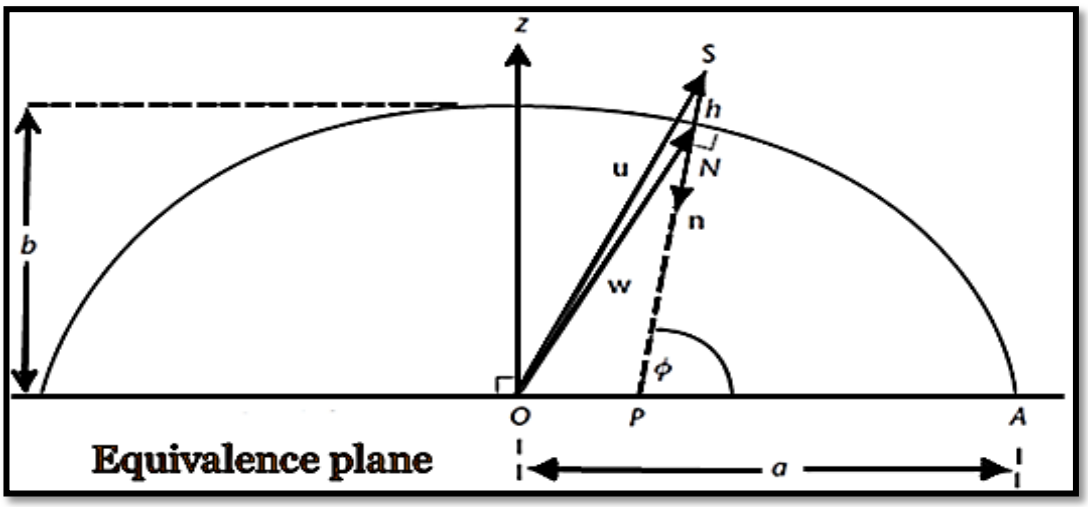

Figure 2.12 Ellipsoidal sample of earth

The height of geodetic is artlessly the lowest distance between the ellipsoid of the reference and user. Geodetic latitude ϕ into the equatorial (*xy*) sheet is the angle between the omission of n and the ellipsoid standard vector n. Conventionally, if *zu* > 0 then ϕ is selected to be positive, and if *zu* < 0 then ϕ is selected to be negative. Regarding to Figure 2.12, the angle of non-precision approach (NPA), on the reference ellipsoid to the user N is the nearest indicate, where the equatorial sheet crossed by the line P on the way, and A on the equator is the nearest indicate to P [15]. Various solutions have been arranged both reduplicate and closed for the calculations from Cartesian coordinates (*x, y, z*) of curvilinear geodetic coordinates (ϕ, λ, *h*). A common and extremely approximate reduplicate manner is defined in Table 2.5 for the calculations illustrated a, *b*, *e*2, and *e* ′+2.

Table 2.5 Calculation of ECEF parameters

Height and Latitude in names of ECFF Parameters
$p = \sqrt{x^2 + y^2}$
$\tan u = \left(\frac{z}{p}\right)\left(\frac{a}{b}\right)$
Iteration Loop
$cos^2u = \frac{1}{1 + tan^2u}$
$sin^2u = 1 - cos^2u$
$\tan \varphi = \frac{z + e'^2 b\, sin^2u}{p + e^2 a\, cos^2u}$
$\tan u = \left(\frac{a}{b}\right) tan\varphi$
Until tan u converges, then
$N = \frac{a}{\sqrt{1 - e^2 sin^2\varphi}}$
$b = \frac{p}{cos\varphi} - N \quad \varphi \neq \pm 90^{\circ}$
$b = \frac{z}{\sin \varphi} - N + e^2 N \quad \varphi \neq 0$

2.7. PRN Codes Utilizing Position Calculation

Direct sequence spread spectrum (DSSS) gives a shape for the essential and limiting transmission of the navigation data signals, such as the health of the satellite and ephemerides. PRN codes are the limiting signals where BPSK modulates the carrier frequencies of the satellite. These codes deterministic in reality and have spectral characteristics like sequences of random binary. In Figure 2.13 an easy

example of a sequence of concise PRN code is illustrated [34]. A foreseeable model has these codes, which can be inflected by appropriately receiver. The Y and P codes are implied as enciphered code. During cryptology, the Y-code is just attainable to the users of PPS.

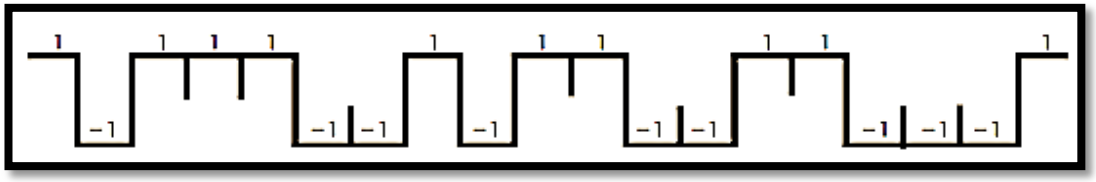

Figure 2.13 Ranging of PRN code

The main discernible between the receiver and transmitter of the GPS system is the time of diffusion of the electromagnetic wave. A measurement of the pseudo range between them provided by the time multiplied by the velocity of light. To explain the principles of working on the GPS, a basic example of positioning which is a boat near the coast will be explained. Let's assume that a lighthouse with recognized coordinates, emitting acoustic signals periodically [9]. Suppose also a boat with a perfectly synchronized clock to the lighthouse's clock receiving the signal just 30 seconds after the lighthouse is emitting the signal. Arriving from the beacon to the receiver, the 30 seconds to the propagation time will adjust. Assuming that the propagation time of the sound in the air is about 335 m/s, it is simple to compute the distance between both objects.

$$\boldsymbol{d = 335m/s\,.\,30s = 10,050m = 10.05km} \tag{2.12}$$

Due to the nature of the sound, the boat will be placed over a point of the circle with radius d that described by the transmitter source as shown in Figure 2.14. If another lighthouse is added, the boat will receive two different signals, one from every transmitter, so the whole circle will be reduced to only the intersection points of both circles. In addition, with a third lighthouse, the ambiguity of the position explained is solved [35].

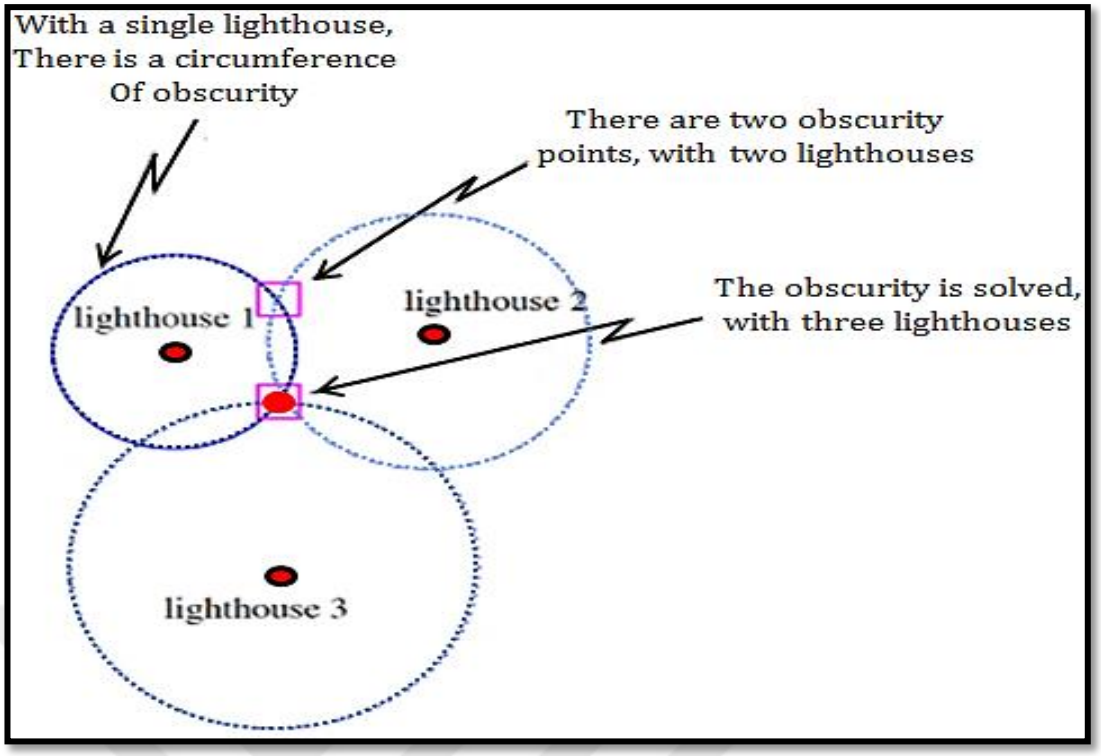

Figure 2.14 2D Positioning

The preceding example, states the basic principle of GPS working. Considering the space of GPS as 3 dimensions, another "lighthouse" is needed with a view to resolving the obscurity. Summarising the example, these are the highlights from one system to the other [1]:

- One supposes that their coordinates are realized in the state of the beacon. In the GPS satellite state, from the transferred ephemerides these are computed.

- In the GPS locating, by the propagation time of a signal, the spaces between satellites and receiver are computed from the satellite to the receiver.

Figure 2.15 illustrated the junction between the circles generates an area in which the receiver can be found, the greater is desynchronize between clocks, the greater is the area of uncertainty [36].

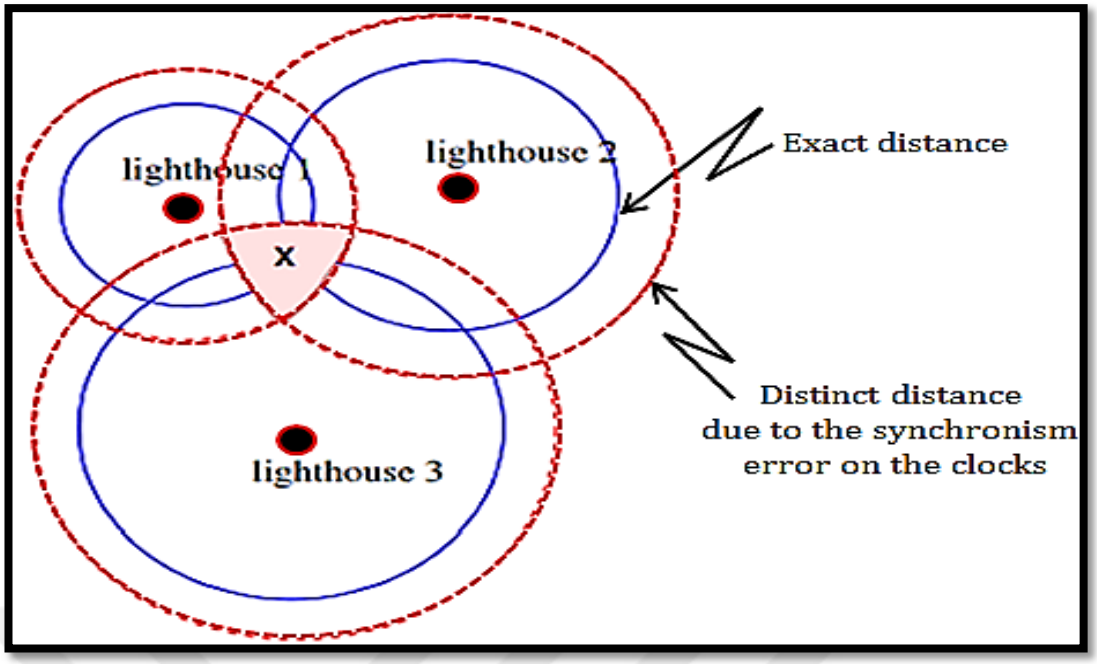

Figure 2.15 Clock error effect on positioning

Moreover, the size of the area not only relies on the synchronism error but the source position with regard to the receiver transmitter. Figure 2.16 exemplifies this state, which called dilution of precision (DOP).

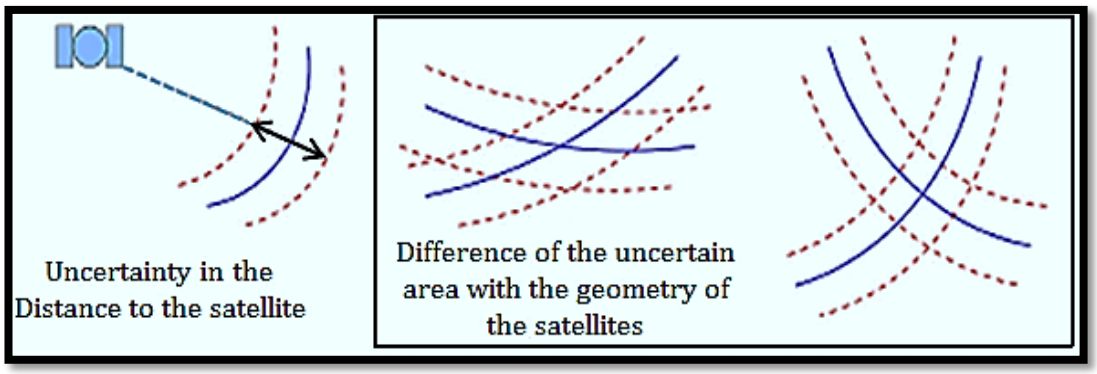

Figure 2.16 Dilution of precision effect

In order to minimize synchronism errors, GPS satellites have extremely perfect atomic clocks with the stabilities of about 10^{-13}. Commercial receivers use quartz clocks much more unstable, but less expensive [8]. The way to combat the ambiguity for the end user is to predict the error of synchronism when the coordinates are calculated.

2.7.1. Computation of User Location

In respect of three dimensions to calculate the offset t_u and user location (x_u, y_u, z_u), four satellites outcoming pseudo range mensurations are produced in the system of equations

$$\boldsymbol{\rho_j = \|s_j - u\| + ct_u} \tag{2.13}$$

where j indicates the satellites and extents from 1 to 4. Equation (2.13) can be increased in the unknowns x_u, y_u, z_u and t_u and into the next group of equations:

$$\boldsymbol{\rho_1 = \sqrt{(x_1 - x_u)^2 + (y_1 - y_u)^2 + (z_1 - z_u)^2} + ct_u} \tag{2.14}$$

$$\boldsymbol{\rho_2 = \sqrt{(x_2 - x_u)^2 + (y_2 - y_u)^2 + (z_2 - z_u)^2} + ct_u} \tag{2.15}$$

$$\boldsymbol{\rho_3 = \sqrt{(x_3 - x_u)^2 + (y_3 - y_u)^2 + (z_3 - z_u)^2} + ct_u} \tag{2.16}$$

$$\boldsymbol{\rho_4 = \sqrt{(x_4 - x_u)^2 + (y_4 - y_u)^2 + (z_4 - z_u)^2} + ct_u} \tag{2.17}$$

where x_j, y_j, and z_j indicate the jth satellite's location in three dimensions. These equations of nonlinear for the unknowns can be resolved by involving either (1) neared-shape solutions [15], (2) filtering, or (3) linearization of the antagonistic proficiencies. We can express the offset of the correct location (x_u, y_u, z_u) from the sacrificial location $(\hat{x}_u, \hat{y}_u, \hat{z}_u)$ by a displacement $(\Delta x_u, \Delta y_u, \Delta z_u)$, if we know around where the receiver is. About the closest location by extending (2.14) to (2.17) in a Taylor series, we can get as linear functions the offset location $(\Delta x_u, \Delta y_u, \Delta z_u)$ of the pseudo range mensurations and known coordinates. As follows, this step is defined. Let an individual pseudo range be clarified using:

$$\boldsymbol{\rho_j = \sqrt{(x_j - x_u)^2 + (y_j - y_u)^2 + (z_j - z_u)^2} + ct_u} \tag{2.18}$$

$$\boldsymbol{= f(x_u, y_u, z_u, t_u)}$$

Utilizing the near location $(\hat{x}_u, \hat{y}_u, \hat{z}_u)$ and bias time evaluates $\hat{t}_u$, a near pseudorange can be computed:

$$\boldsymbol{\hat{\rho}_j = \sqrt{(x_j - \hat{x}_u)^2 + (y_j - \hat{y}_u)^2 + (z_j - \hat{z}_u)^2} + c\hat{t}_u} \tag{2.19}$$

$$\boldsymbol{= f(\hat{x}_u, \hat{y}_u, \hat{z}_u, \hat{t}_u)}$$

As declared previously, the location of unidentified user and the clock offset of the receiver are assumed to comprise an incremental and near components:

$$\begin{aligned} \boldsymbol{x_u} &= \boldsymbol{\hat{x}_u} + \Delta \boldsymbol{x_u} \\ \boldsymbol{y_u} &= \boldsymbol{\hat{y}_u} + \Delta \boldsymbol{y_u} \\ \boldsymbol{z_u} &= \boldsymbol{\hat{z}_u} + \Delta \boldsymbol{z_u} \\ \boldsymbol{t_u} &= \boldsymbol{\hat{t}_u} + \Delta \boldsymbol{t_u} \end{aligned} \tag{2.20}$$

Therefore, we can write

$$\boldsymbol{f(x_u, y_u, z_u, t_u) = f(\hat{x}_u + \Delta x_u, \hat{y}_u + \Delta y_u, \hat{z}_u + \Delta z_u, \hat{t}_u + \Delta t_u)} \tag{2.21}$$

About the closest point and combined presaged, the clock offsets $(\hat{x}_u, \hat{y}_u, \hat{z}_u, \hat{t}_u)$ of receiver can be extended by a Taylor series:

$$\begin{aligned} f(\boldsymbol{\hat{x}_u + \Delta x_u, \hat{y}_u + \Delta y_u, \hat{z}_u + \Delta z_u, \hat{t}_u + \Delta t_u}) &= \boldsymbol{f(\hat{x}_u, \hat{y}_u, \hat{z}_u, \hat{t}_u)} \\ &+ \frac{\boldsymbol{\partial f(\hat{x}_u, \hat{y}_u, \hat{z}_u, \hat{t}_u)}}{\boldsymbol{\partial \hat{x}_u}} \boldsymbol{\Delta x_u} + \frac{\boldsymbol{\partial f(\hat{x}_u, \hat{y}_u, \hat{z}_u, \hat{t}_u)}}{\boldsymbol{\partial \hat{y}_u}} \boldsymbol{\Delta y_u} \\ &+ \frac{\boldsymbol{\partial f(\hat{x}_u, \hat{y}_u, \hat{z}_u, \hat{t}_u)}}{\boldsymbol{\partial \hat{z}_u}} \boldsymbol{\Delta z_u} + \frac{\boldsymbol{\partial f(\hat{x}_u, \hat{y}_u, \hat{z}_u, \hat{t}_u)}}{\boldsymbol{\partial \hat{t}_u}} \boldsymbol{\Delta t_u} + \cdots \end{aligned} \tag{2.22}$$

$$\begin{aligned} \frac{\boldsymbol{\partial f(\hat{x}_u, \hat{y}_u, \hat{z}_u, \hat{t}_u)}}{\boldsymbol{\partial \hat{x}_u}} &= -\frac{\boldsymbol{x_j - \hat{x}_u}}{\boldsymbol{\hat{r}_j}} \\ \frac{\boldsymbol{\partial f(\hat{x}_u, \hat{y}_u, \hat{z}_u, \hat{t}_u)}}{\boldsymbol{\partial \hat{y}_u}} &= -\frac{\boldsymbol{y_j - \hat{y}_u}}{\boldsymbol{\hat{r}_j}} \\ \frac{\boldsymbol{\partial f(\hat{x}_u, \hat{y}_u, \hat{z}_u, \hat{t}_u)}}{\boldsymbol{\partial \hat{x}_u}} &= -\frac{\boldsymbol{x_j - \hat{x}_u}}{\boldsymbol{\hat{r}_j}} \\ \frac{\boldsymbol{\partial f(\hat{x}_u, \hat{y}_u, \hat{z}_u, \hat{t}_u)}}{\boldsymbol{\partial \hat{z}_u}} &= -\frac{\boldsymbol{z_j - \hat{z}_u}}{\boldsymbol{\hat{r}_j}} \\ \frac{\boldsymbol{\partial f(\hat{x}_u, \hat{y}_u, \hat{z}_u, \hat{t}_u)}}{\boldsymbol{\partial \hat{t}_u}} &= \boldsymbol{c} \end{aligned} \tag{2.23}$$

where

$$\boldsymbol{\hat{r}_j = \sqrt{(x_j - \hat{x}_u)^2 + (y_j - \hat{y}_u)^2 + (z_j - \hat{z}_u)^2}} \tag{2.24}$$

substituting (2.21) and (2.23) into (2.24) yields

$$\boldsymbol{\rho_j = \hat{\rho}_j - \frac{x_j - \hat{x}_u}{\hat{r}_j} \Delta x_u - \frac{y_j - \hat{y}_u}{\hat{r}_j} \Delta y_u - \frac{z_j - \hat{z}_u}{\hat{r}_j} \Delta z_u + c t_u} \tag{2.25}$$

We have now finished the linearization of (2.25) with regard to the unknowns $\Delta x_u, \Delta y_u, \Delta z_u$, and Δt_u. By rearranging this term with the unknown amounts on the right and the known amounts on the left that provides:

$$\widehat{\boldsymbol{\rho}}_{\boldsymbol{j}} - \boldsymbol{\rho}_{\boldsymbol{j}} = \frac{\boldsymbol{x_j - \hat{x}_u}}{\hat{\boldsymbol{r}}_{\boldsymbol{j}}} \Delta \boldsymbol{x_u} + \frac{\boldsymbol{y_j - \hat{y}_u}}{\hat{\boldsymbol{r}}_{\boldsymbol{j}}} \Delta \boldsymbol{y_u} - \frac{\boldsymbol{z_j - \hat{z}_u}}{\hat{\boldsymbol{r}}_{\boldsymbol{j}}} \Delta \boldsymbol{z_u} - \boldsymbol{c t_u} \tag{2.26}$$

For expedience, and by presenting new variables, we will facilitate the earlier equation where:

$$\begin{aligned} \Delta \boldsymbol{\rho} &= \widehat{\boldsymbol{\rho}}_{\boldsymbol{j}} - \boldsymbol{\rho}_{\boldsymbol{j}} \\ \boldsymbol{a_{xj}} &= \frac{\boldsymbol{x_j - \hat{x}_u}}{\hat{\boldsymbol{r}}_{\boldsymbol{j}}} \\ \boldsymbol{a_{yj}} &= \frac{\boldsymbol{y_j - \hat{y}_u}}{\hat{\boldsymbol{r}}_{\boldsymbol{j}}} \\ \boldsymbol{a_{zj}} &= \frac{\boldsymbol{z_j - \hat{z}_u}}{\hat{\boldsymbol{r}}_{\boldsymbol{j}}} \end{aligned} \tag{2.27}$$

In (2.27) the a_{xj}, a_{yi}, and a_{zj} expressions indicate the way cosines pointing from the close user location to the *j*th satellite of the unit vector. For the *j*th satellite, the illustration of the unit vector is as:

$$\boldsymbol{a_j} = \left(\boldsymbol{a_{xj}}, \boldsymbol{a_{yi}}, \boldsymbol{a_{zj}}\right)$$

Equation (2.27) can be rewritten more merely as:

$$\Delta \boldsymbol{\rho_j} = \boldsymbol{a_{xj}} \Delta \boldsymbol{x_u} + \boldsymbol{a_{yj}} \Delta \boldsymbol{y_u} + \boldsymbol{a_{zj}} \Delta \boldsymbol{z_u} - \boldsymbol{c} \Delta \boldsymbol{t_u}$$

We now have four unknowns: $\Delta xu, \Delta yu, \Delta zu, and\ \Delta tu,$ which can be resolved to four satellites by the mensuration of strutting rating [37]. By resolving the group of linear equations, the unidentified terms can be calculated as follows:

$$\begin{aligned} \Delta \boldsymbol{\rho_1} &= \boldsymbol{a_{x1}} \Delta x_u + \boldsymbol{a_{y1}} \Delta y_u + \boldsymbol{a_{z1}} \Delta z_u - c \Delta t_u \\ \Delta \boldsymbol{\rho_2} &= \boldsymbol{a_{x2}} \Delta x_u + \boldsymbol{a_{y2}} \Delta y_u + \boldsymbol{a_{z2}} \Delta z_u - c \Delta t_u \\ \Delta \boldsymbol{\rho_3} &= \boldsymbol{a_{x3}} \Delta x_u + \boldsymbol{a_{y3}} \Delta y_u + \boldsymbol{a_{z3}} \Delta z_u - c \Delta t_u \\ \Delta \boldsymbol{\rho_4} &= \boldsymbol{a_{x4}} \Delta x_u + \boldsymbol{a_{y4}} \Delta y_u + \boldsymbol{a_{z4}} \Delta z_u - c \Delta t_u \end{aligned} \tag{2.28}$$

These equations by making the explanations can be set in a matrix pattern:

$$\Delta\boldsymbol{\rho} = \begin{bmatrix} \Delta\boldsymbol{\rho_1} \\ \Delta\boldsymbol{\rho_2} \\ \Delta\boldsymbol{\rho_3} \\ \Delta\boldsymbol{\rho_4} \end{bmatrix} \quad \boldsymbol{H} = \begin{bmatrix} \boldsymbol{a_{x1}} & \boldsymbol{a_{y1}} & \boldsymbol{a_{z1}} & \mathbf{1} \\ \boldsymbol{a_{x2}} & \boldsymbol{a_{y2}} & \boldsymbol{a_{z2}} & \mathbf{1} \\ \boldsymbol{a_{x3}} & \boldsymbol{a_{y3}} & \boldsymbol{a_{z3}} & \mathbf{1} \\ \boldsymbol{a_{x4}} & \boldsymbol{a_{y4}} & \boldsymbol{a_{z4}} & \mathbf{1} \end{bmatrix} \quad \Delta\boldsymbol{x} = \begin{bmatrix} \Delta x_u \\ \Delta y_u \\ \Delta z_u \\ -c\Delta t_u \end{bmatrix}$$

one obtains,

$$\Delta\boldsymbol{\rho} = \boldsymbol{H}\Delta\boldsymbol{x} \tag{2.29}$$

which has the solution

$$\Delta\boldsymbol{x} = \boldsymbol{H^{-1}}\Delta\boldsymbol{\rho} \tag{2.30}$$

As soon as the unknowns are calculated, the user's coordinates *xu*, *yu*, *zu* and the clock offset t_u of the receiver are then computed by (2.28). This plan of linearization will accomplish fully so long as the supplanting $(\Delta x_u, \Delta y_u, \Delta z_u)$ is within the near vicinity of the linearization point. By the reliability of the user necessities, the passable supplanting is transcribed. This step is repeated with $\hat{\rho}$ being subrogated by a new evaluate, if the supplanting depends on the computed point of coordinates *xu*, *yu*, and *zu* does transcend the suitable value of pseudo range. In truth, the real user-to-satellite measurements are deteriorated by distinct errors, such as multipath, from the described ephemeris the deflection of the satellite way, and noise mensuration. These errors, as illustrated here in the sets of vector +**x** interpret to errors:

$$\boldsymbol{\epsilon_x} = \boldsymbol{H^{-1}}\boldsymbol{\epsilon_{meas}} \tag{2.31}$$

where $\boldsymbol{\epsilon_x}$ represent the vector consisting the mensuration of the pseudo range errors and $\boldsymbol{\epsilon_x}$ is the vector in the clock offset of the receiver and user location that characterized errors. The contribution of error $\boldsymbol{\epsilon_x}$ by making mensuration to more than four satellites can be reduced, which will result like to (2.31) in an over determined solution set of equations. Each of these profluent measurements will consist contributions of the independent error.

CHAPTER 3

TERRESTRIAL BASED LOCALIZATION SYSTEM

3.1. Basic Concept of Indoor Localization System

In the current era, there is a pressing need for the location-aware systems/services such as GPS (as the most popular one) beside the popular computing theory's applications. However, GPS is not the appropriate choice for indoor circumstances due to the imprecise precision and the need for a LOS communication with satellites [38]. Therefore, the infrared, ultrasonic, electro-magnetic field are possible alternatives with some constraints in each one. One of the significant automatic identifications is the RFID; which has been implemented for indoor localization with a high performance. It has many excellent characteristics like the compactness, non-LOS readability, high security and data-rate, contactless communications with a low cost. As a result, it became the key research in the computing fields. Despite its advantages, it suffers from many difficulties in the localization service as it needs a large number of infrastructures for determining the location precisely, in addition to the lack RSSI functions in most RFID devices; which is helpful in the accuracy improvement. Also, the radio propagation in the indoor cases suffers from several issues like the rare LOS path, severe multipath, absorption, reflection and diffraction [7].

According to the mentioned issues beforehand, an improved RFID indoor localization algorithm has been presented in this research with highlighting other methods like the LANDMARC and virtual reference elimination (VIRE). The innovation points of the proposed algorithm can be summarized as below: first, a mechanism will be employed to deploy RFID tags and readers; second, combining the K-nearest neighbours (KNN) algorithm and free space path loss model to generate the RSSI values of virtual reference tags; third, establishing a novel error correction model for adjusting the preliminary target position [20, 39].

3.1.1. Basic of RFID Indoor Localization Algorithms

RF-based localisation differs from other techniques in principles such as triangulation, scene analysis, and proximity for automatic location-sensing in addition to the devices. A lot of RFID techniques were the main focus of many researchers like the SpotOn, longest prefix match (LPM), LANDMARC, VIRE, Simplex, Kalman filtering, Scout, 3-D constraints and so on. LPM and SpotOn are rang-based and depends on the triangulation [7]. SpotOn has an uncomplicated and a classical signal propagation model depending on the RSSI for measuring the distances from the target to multiple readers within multiple directions. While, LPM depends on the time difference of arrival (TDOA) technique instead of RSSI. Both of the two localisation systems require at least three RFID readers.

The range-free is the second category of localisation like the LANDMARC and VIRE that depend on the active RFID reference tags for estimating the locations with benefits from the KNN algorithm; which is one of the simplest techniques of machine learning as well. Its basic principle can be summarized as follows: if a sample lies in a feature space and most of its adjacent (K similar samples) belong to one category, then it will be also belonged to this category. Such a principle will be beneficial in estimating the target location [40].

Depending on the KNN algorithm, the LANDMARC was one of the most effectual techniques; in which it gathers the unknown coordinate of target tags to compare their RSSI values with the coordinates of their known KNN reference tags. Each KNN is estimated by means of its Euclidean distance from the target that is computed from their RSSI values in the direction of each reader. The target coordinates are considered from the weighted average of the KNN coordinates of reference tags. According to the KNN method, the closer reference tag possesses a greater weight compared to other tags. Although LANDMARC is a reasonable solution for RFID indoor localization, it can be enhanced in at least two sides: the low performance within a closed region of highly radio interference/signal multi-path effects and the more reference tags needed for strengthening the positioning precision that adds extra cost of devices and generates severe RF interference phenomenon. Therefore, many researchers have attempted to enhance the

LANDMARC by optimizing the placements of RFID reference tags in a triangular mesh, as an example, in spite of the readers' deployment that has a great role in the localisation process with the impact reduction of the multipath effects. In 2006, an error correction technique has been proposed by Jin, which depends on the triangulation for improving the location accuracy by estimating the location error of the target through the calculations of weighted mean location error of KNN tags. However, there is a need for eliminating a KNN tag from the reference tags' set instead of estimating its location using the KNN algorithm; which in turn increases the location error.

The VIRE technique has a high reputation against the LANDMARC. Where, virtual reference tags are utilized instead of many real tags in the sensing space for supporting wider reference area. In 2007, the tracking precision of VIRE has been enhanced by Zhao from 17% to 73% in comparison with the LANDMARC. In spite of that, the RSSI values of virtual reference tags were computed using a linear interpolation method that is clearly fast and simple but imprecise in complicated cases [41]. According to the Friis model (Schelkunoff and Friis, 1952), the relation between the distance and RSSI value from a reader to a tag must be a polynomial relation. Therefore, it is highly proper to utilize some novel nonlinear methods for generating the RSSI values of the virtual reference tags. The final localization category is a range-based and depends on the sensors' density. Each sensor may be defined as a proximity sensor. Whenever the target signal is obtained through a sensor, its location then applied the same as its receiver. Despite the simplicity of this principle, its reliability depends highly on the sensitivity and density of sensors within the localised area.

3.2. RFID System

The readers and tags are the key blocks of RFID system which operates on multiple frequencies such as 2.4MHz in our scenario. The tag can be either an active or a passive kind. The 1st kind has its own battery life and generates a signal by itself, while the 2nd one can only generate a signal if there's a reader nearby, so it depends on the generated signal from the reader to power it. In this thesis, active tags have been utilized since their ranges are much greater than that of passive tags; which in

turn give more precise, faster reading and a less overhead within more readers' form. Where, they were connected to laptops for the final test. The reader is a simple base-station that reads and records the neighbouring tags, its working details will be demonstrated in the design section. The key element in our thesis is RSSI; which has a value ranges from 0 to 255 and depends on the tags' signal strength. Where, a high value can be obtained whenever a reader is nearby, which represents a high signal strength and vice versa [32].Thus RSSI is our project's cornerstone as it can be useful for calculating the distance between a reader and a tag within a multi-readers system. The tag's location can be triangulated in a 2D or 3D space.

3.2.1. The Background of Indoor localization Technologies

In the recent years, with the rapid advances in mobile communication technologies, indoor positioning technology gradually had people's attention as wireless technology [2]. Wireless location technology is measured by the transmission time of radio waves, phase, and amplitude parameters which calculate the position of the measured object technology. Currently the most widely used applications are a set of universal application of mature outdoor location-based technology. However, in the indoor positioning, system by buildings affect the signal to decay the point where is very weak, where extracting the time information and navigation data directly from the satellite broadcasting is very difficult to achieve with it. Therefore, the use of standard GPS in the indoor becomes very difficult. In addition, the accuracy is difficult to meet the actual requirements in an indoor environment relative to a large standard error of GPS. Another applied location used in outdoor such as a cellular wireless location system is a similar shortage. Therefore, they are not as the ideal indoor location-based technology [42]. In the view of this situation, many specifications designed for indoor location-based technology for obtaining the right indoor positioning system. Currently, more popular indoor positioning technologies are the following:

3.2.1.1. Infrared Radiation Technology (IR)

It is similar to radio waves; an electromagnetic wave propagates at the light's speed. The time measurements within the indoor system is somehow difficult, unless

an accurate time distributed clock is utilized, which is still so costly. In spite of the various methods that were implemented, the detection method is the most popular one that checks simply whether a receiver in the detection space or not in the detection space of the device. Active badge is the earliest and most famous indoor positioning system as shown in Figure 3.1. The operation principle of the system is depending on whether the user can carry the badge received modulated infrared signal emitted by the badge to find out whether the user's location is in the detection area of the reader. If the signal is detected, that implies the user's location in the detection area. Table 3.1 presents the global features of an infrared positioning system. The positioning type differs a little from the previous ones. "Symbolic" means that the positioning is not defined in the spatial coordinates (either absolute or relative way), but in terms of room numbers or names [35]. As a result, it would be possible to know the location of a person; in which corridor, office or room, instead of its absolute positioning.

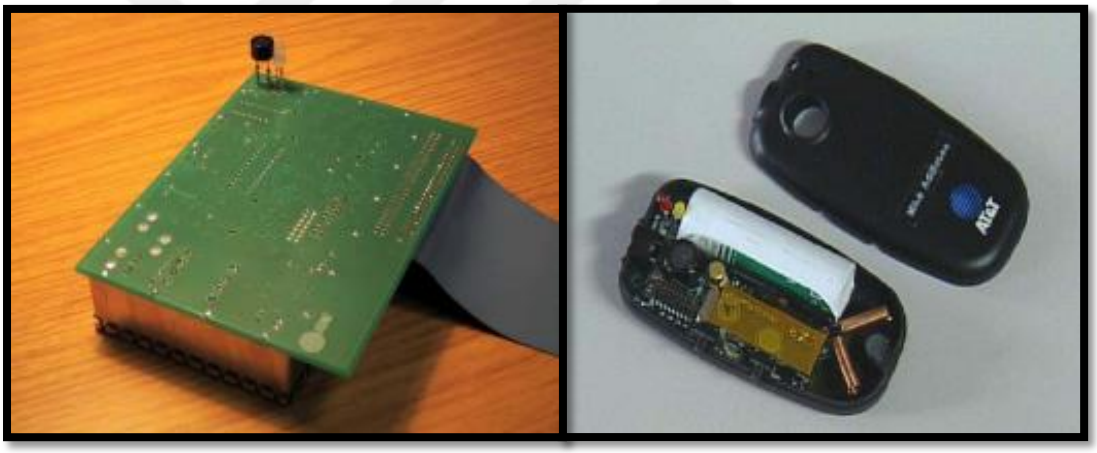

Figure 3.1 Active badges of indoor positioning system

The precision and range figures are related to this principle. The positioning precision is "room class" and is unable to meet indoor positioning accuracy requirements. The single beacon's coverage is one room. Therefore, multiple beacons are required for multiple rooms within indoor localization cases. IR [30] is utilized for wireless connection between tags through the emitting light. The closer receiver tags detect antennas for sending data information to the location server. Shorter range gives higher RF frequency, which in turn means more waves tend to propagate in a straight-line way. RF has a good precision inside a block, but it can't emit through walls; which represents a disadvantage [40].

Table 3.1 Infrared positioning

Technical description	
Technology	Infrared
Localization	Infrastructure (0.1 Hz)
Positioning	Symbolic
Environments	Indoors
Accuracy	Room
Range	One beacon per room

3.2.1.2. Wireless LANs Technology

The wireless local area network (WLAN) technology has currently a great usage in private and public circumstances, such as companies, universities and so on, as it gives wide network coverage [7]. Therefore, it catches the interest of many researchers for developing its architecture, especially within a building environment, for location-aware systems such as the navigation in museums, depending on the WLAN RF signals.

Most of these systems depend on the RSS computations due to its ease of implementation and require no more hardware. In 2000, the RADAR was the 1st approaches that utilize an extensive calibration phase [7], within an indoor positioning system that depends on the WLAN. Where the Microsoft Company uses RADAR [5] by the signal strength of the wireless local area network (LAN) for estimating the target's location. The system positioning error was around 50% within 3 to 4.3m, and the target positioning was difficult to be transmitted to the personal computer as it is fixed and required to be attached to the PC. Another approach is the propagation time of radio signals which has a linear relationship with the distance in a free air, but has a difficulty in the implementation as it needs a timing of a high-resolution. Multiple access points (APs) are required in the construction of the classic WLAN system or BSs, and a group of MSs served by those APs. The AP unit serves a small group of clients in a typical range that reaches to a few hundred meters, and also depends on the interface between the WLAN and wired network infrastructure. Figure 3.2 illustrates the so-called infrastructure network, where the master stations (MSs) can communicate with each other only under the direct control of a single AP [43].

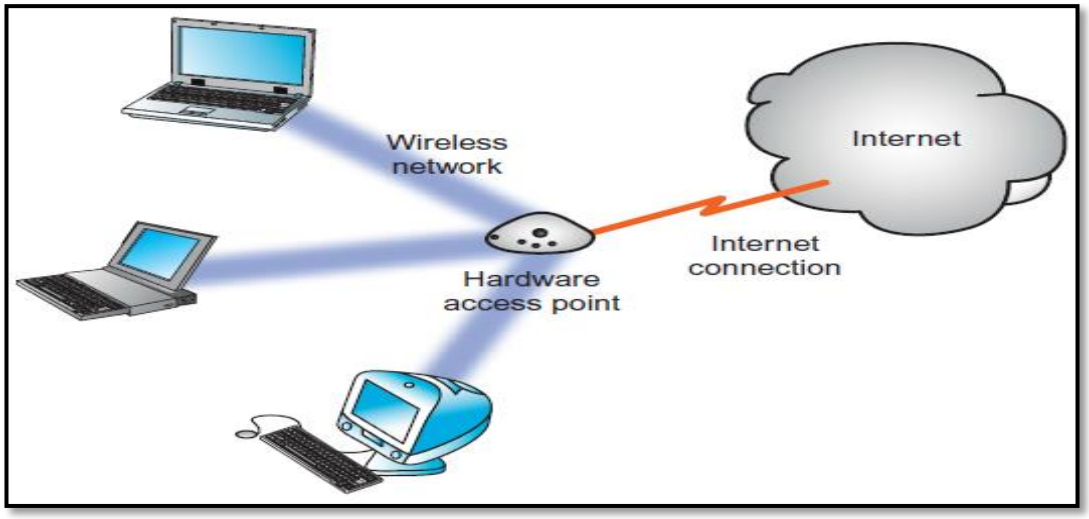

Figure 3.2 Infrastructure network

Figure 3.3 defines the other possible architectures in WLAN applications based on the ad hoc network, where any MS attached to a wireless networking interface card (NIC) can begin a direct communication with other units with no need for a centralized AP to manage all the data traffic.

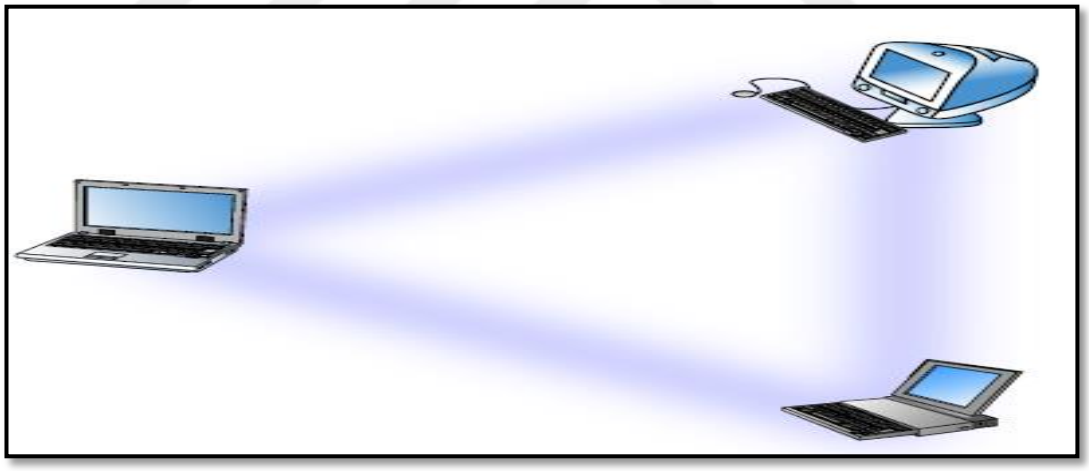

Figure 3.3 Ad hoc networks

The wireless range between the AP and MS is limited and varies based on expected performance and whether it is an indoor or outdoor circumstances. Around 50 to 100 meters is the typical indoor range, but it's become shorter if there is a building that interferes with the radio transmission. While the outdoor range reaches to a few kilometres based on the utilized antennas, environments, and local regulations on emissions. Therefore, many APs can be utilized if the coverage area is too big for a single AP [22].

3.2.1.3. Ultra Wide Band Technology (UWB)

In a high-definition indoor positioning, UWB is promising as it has very precise short distance estimation. It is also an applicable technique for short-range wireless indoor communication that has a high-rate transmission, with low complexity/cost/power consumption [4, 13]. This technology has catched the attention of many manufacturers in the US since February 2002, when the federal communications commission (FCC) opened up a spectrum of 7.5 GHz (from 3.1 to 10.6 GHz) to be utilized by the UWB devices [8]. Due to its high speed and low power consumption, it becomes more reliable in the indoor circumstances. UWB is a pulse based system that utilizes pulses for sending the signal through a wide band of several GHZ, and the destination utilizes a receiver for catching the right pulses to be converted as a data. The positioning system of real-time is high and has a tracking capability and is expected to have a high precision. The UWB classical design utilizes a narrow-baseband time domain pulses of very short duration (in nanoseconds), thereby spreading the radio signal's energy in a uniform manner over a wide-band frequency domain that ranges from extremely low to a few gigahertz. Such a technique is defined as the impulse radio-UWB (IR-UWB). The great benefit behind the short pulse modulation is the capability of estimating the TOA with a well accuracy that reaches to less than a meter which represents an interesting characteristic in the UWB for a positioning system [44].

Therefore, the time represents an embedded UWB characteristic. In addition, the 1st UWB application was implemented in radar, due to the following reasons: its capability to bypass the obstacles and the sharp time discrimination. Thus, UWB technique depends on time computations of the four transmitters (T1-T4) as shown in Figure 3.4, so it is very accurate due to the very short pulse duration (less than 1 ns). Therefore, the time computations are the basic principle to be carried. Although these computations can be very accurate, there will be a problem of global synchronization that results from the 5th UWB module. It can be possible to determine either difference of propagation or propagation time delays after measuring the time from a UWB-equipped mobile terminal and various UWB system modules [11]. Then, a trilateration algorithm is implemented, like that of GNSS systems, for determining the indoor location. Having a good position accuracy based on the precise time measurements.

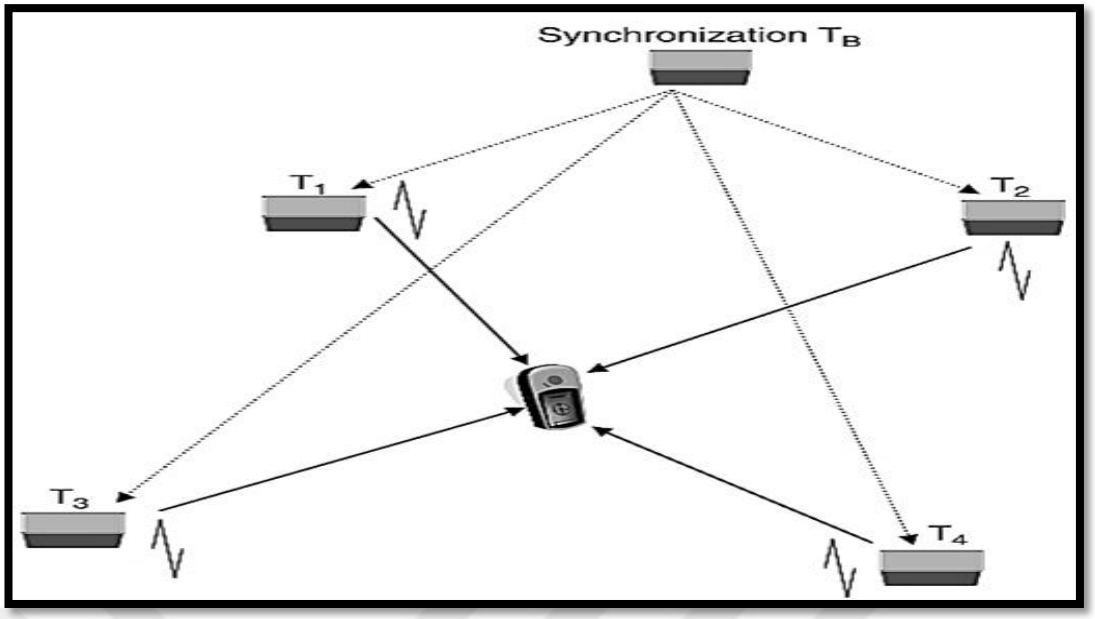

Figure 3.4 UWB approach of positioning

However, a lot of bandwidth is needed for UWB, beside the disturbance that may be created to other communication devices. As a result, its frequency problem has been debated unceasingly. Although it has a very low average power, its pulse duration is so low; which in turn causes a high instantaneous peak of power that will negatively affect its own process and other systems. Yet the UWB is still a research material, as the capabilities of the existing hardware do not match the algorithm's requirements [10].

3.2.1.4. Radio Frequency Identification Technology

An RFID is an electronic label which can be attached to anything for localization. A reader is utilized for supplying a direct power to the label, so it will be capable of transmitting data like the identification number or a location to be detected. These tools are called “RFID tags” that have different sizes/shapes with a very low cost. Consumption of RFID technology is low; it is available in a variety of harsh environment applications and can be widely applied in the manufacturing, logistics, medical treatment, traffic, transport, tracking, security, field equipment and asset management that require a data acquiring and processing [45]. RFID is widely recognized as one of the technique's application of this century's which is the most promising applications. Figure 3.5 illustrates the system of RFID.

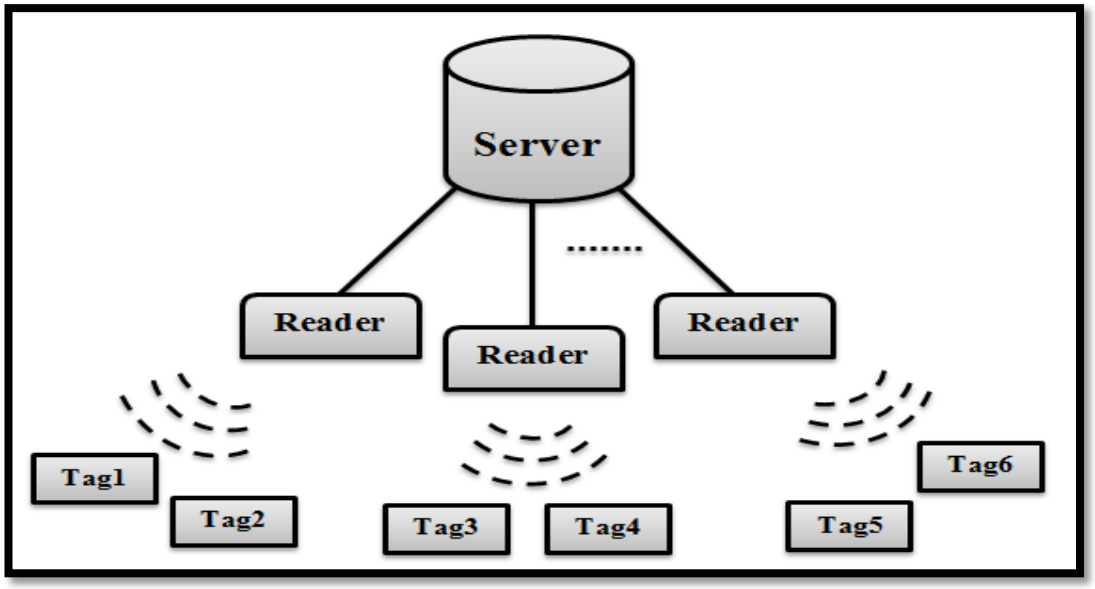

Figure 3.5 RFID system

Table 3.2 gives a properties summary of the RFID-based positioning system that can utilize many tags to be positioned at different locations of wide range due to their low price. The moving terminal has a reader that invigorates the tags when moving close to them. The ultimate range of the current readers is up to 1m (sometimes higher, but that is not common), which in turn gives a 1m accuracy. The positioning technique depends on the tag's returned identifier to the reader, to be read by the location database, as it refers to the location. The attentions of worldwide researchers have been attracted by the RFID since 1948. Nowadays, there are many services that depend on it like the surveillance, automation logistics, automotive systems, and any real time object identifications.

Table 3.2 RFID positioning

Technical Description	
Technology	RFID
Localization	Infrastructure Very limited
Positioning	Symbolic
Environments	Indoors, outdoors
Accuracy	< 1m
Range	< 1m typical

3.3. Typical RFID Technology Applications

The typical applications of RFID technology are listed as:

- **Property's tracking:** It represents the tracking of property within an office, laboratory, or any building. For instance, Bhanage proposed an RFID-based inventory tracking system for supporting a low-cost, long-lived and continuous property's tracking.

- **Automated fee gathering system:** An attached tag to a car's windshield with an RFID reader on the highway fee booth facilitates the automatic charging to the car owner's account for eliminating the driver's stop to pay the fee by hand. Ren & Gao have developed an electronic toll collection system with a new RFID authentication and authorization protocol model, which has the advantages of lower cost, small size, and high reliability.

- **Supply chain tracking:** That means a good tracking using the managing inventory and supply chain. The supply chain field is the main adopter of RFID technique [8]. Many researchers have studied how to utilize RFID technologies, efficiently in supply chain areas. Lin and Bin developed a methodology for exploring and mapping supply chain networks by the methods of RFID-enabled capturing and sharing of the information throughout supply networks.
- **Health-care services:** They are represented by the patient's identification and tracking within a health-care system, by making a link between the patient and the correct medication or doctor. Many industrial companies provide RFID healthcare solutions, such as PDC‟s RFID Wristband System.

- **Tracking within warehouses:** It is represented by the real-time managing and tracking of the incoming or outgoing stores within warehouses or stores. For instance, Zhen developed a control system of RFID-based for logistics resources to formulate and offer the proper solutions within warehouses.

These typical RFID-based applications show that RFID technology can localize or track any object or people in a particular area. Moreover, owing to the gradually reduced cost of RFID tags and readers, it becomes possible to employ a large number of RFID devices in a dense environment. As a result, RFID technology has recently

become more widely used in object identification, mobile robots tracking and navigation, and wearable computing [11]. These successful applications illustrate that RFID has been recognized as a new popular tracking technology by researchers and engineers.

3.3.1. RFID and Asset Tracking

The RFID-model can be constructed using a symbolic positioning and a radio system (due to its simplicity and low cost); where anything can be automatically identified using this system at a distance with no direct line of sight (LoS) with an electromagnetic response /challenge exchange [17]. It was created primarily in the World War II and since then it has become popular due to its cheapness and simplicity. Some trackable tags and base-stations named readers are the basis of this system. The utilized tags/readers in this thesis were freeware design from an Open Beacon company which are the same used in 23rd and 24th Chaos Communication Congress (23C3) RFID visitor tracking program that will be emulated in our thesis. A signal is generated by the tags that represent a singular ID number to be caught by the base stations to process it for locating the tag using the value of the signal power/strength and packet loss. Yet the RFID tags have been utilized for object tracking only before 4 years [18]. An active and passive tag are the two kinds of tag; where the 1^{st} kind has an own power source and produce a signal similar to the classical radio antenna (long range of 1 – 100 meters), while the 2^{nd} one makes a response by returning an electromagnetic field generated by a reader (short range of < 1 meter). The two kinds depend on the singular ID No.; which is especially programmed for a unique tag. The active tag is the one utilized in our system; because of its long-range that is useful for tracking [45].

3.3.2. RSSI Positioning Systems

In order to evaluate the distance between a receiver and transmitter, a received signal strength induction (RSSI) was utilized. The RF signal is the usual utilized one [1]. Computing the distance between a transmitter and an object contributes in locating that object by the triangulation/trilateration technique. In the beginning, an indoor test has been performed for determining the RSSI database of different transmitters [25]; where the results were compared with a data-group of unknown

RSSI to find the perfect match. However, there are two main issues; which are the signal attenuation due to walls and the weak performance of the receivers indoor. In general, there are many obstacles beside the walls within the indoor environment, thus RSSI values are subject to change and become unreliable. As a result, different techniques have been enhanced for a best signal receiving and tracking with developing various sensors for measuring the orientation's angles and strength of a signal.

CHAPTER 4

BOUNDARY VIRTUAL LABEL ALGORITHM

As mentioned in the previous chapter, the VIRE's boundary label positioning accuracy is so low; this chapter mainly focuses on the issue of boundary virtual reference label positioning algorithm (BVIRE). The algorithm by linear regression equation joins the border at boundary of the virtual reference tags. The results under BVIRE algorithm does not add an additional reference label and does not increase the premise of RF interference, so the positioning accuracy of the label which is close to the border compared with the original algorithm has been significantly improved and has better performance.

4.1. The Idea of BVIRE Algorithm

The reason for analysis VIRE algorithm positioning label boundary is to present its low accuracy, fundamentally due to the less result of boundary reference label distribution, so get near the reference tag label to be positioned that is far away from the boundary of the distance. Due to the incorrect reference, the position error is big. Therefore, the positioning accuracy has been improved by adding an additional reference boundary label at the boundaries [47].

4.1.1. The Procedure of Algorithm

Depending on the knowledge of the previous analysis, we can take the boundary by adding a reference label to be located at the boundary of method to ameliorate the exactness of label positioning. However, the introduction of more reference number label at the boundaries, greatly increase the system overhead. Also, it has gone against the original intention of VIRE algorithm. Therefore, we take into account the consideration which uses the boundaries of virtual reference tags replace with the actual reference label. So, we can estimate the signal strength value of boundary

virtual reference label accurately, and we can play the same role with the actual reference label [50]. Thus we proposed the boundary virtual reference label localization algorithm. The flow chart of the algorithm is illustrated in Figure 4.1.

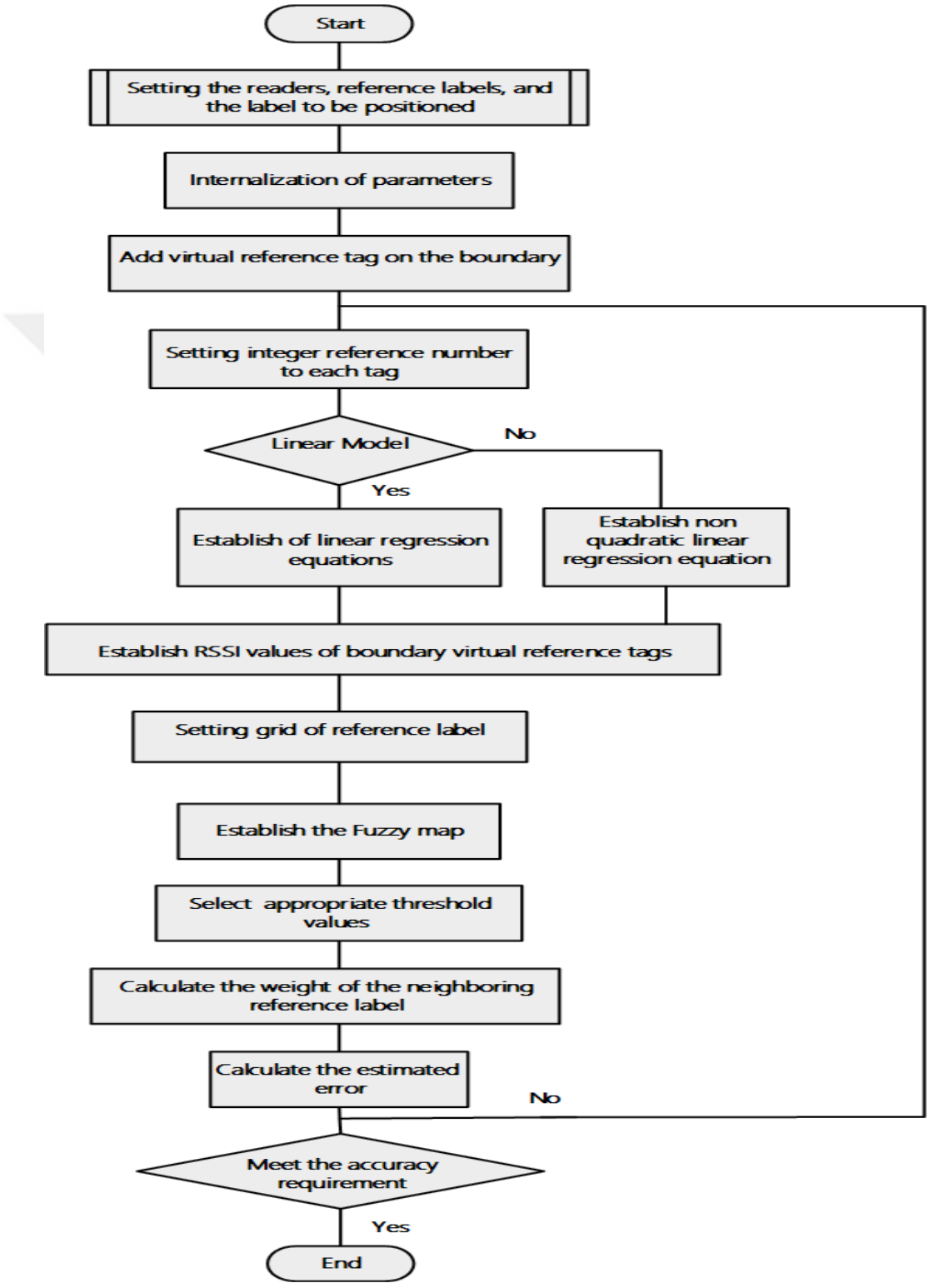

Figure 4.1 Flowchart of BVIRE algorithm

The BVIRE algorithm steps are as follows:

Step 1: According to position build in the flow chart, establishes the reader, reference tag and the tag to be positioned.

Step 2: Introducing path loss model, the distance from the reference label, and RSSI value of the label to be located.

Step 3: Joins the boundary virtual reference tags, by setting the reference integer number to each tag, initially set to 3.

Step 4: Establishes the RSSI value of the regression equation for the border virtual reference label, regression equation, select one linear regression equation or quadratic nonlinear regression equations.

Step 5: Establishes the grid virtual reference label density N value, to join a virtual reference grid label, and to calculate its RSSI values.

Step 6: Establishes the Fuzzy map, select the appropriate threshold values in order to filter out the neighbouring reference label.

Step 7: Calculates the weight of the neighbouring reference label, the weighting of neighbouring reference label obtains the position estimated value of the label to be located.

Step 8: Calculate the estimated error.

Step 9: If it's an estimation error meets the accuracy requirements, then position estimate in step 7 shall be calculated in the final location estimate. If it's an estimation error does not meet the accuracy requirement, then the integer number of the reference label regression num+1 will be deleted, repeat it from steps 3 to 8 until the error of estimation achieves the accuracy requirement.

The above step 4 and step 9 are briefly described. It can be seen based on the simulation analysis, using a quadratic nonlinear regression estimate of RSSI value, we obtained a more accurate linear regression. However the computing complexity is high. Therefore the error precision requirements are high in case of quadratic nonlinear regression, but in other cases the use of a linear regression will be under an element. Due to the number of benchmark reference tag that directly affect the estimates of accuracy. It is clear that using more number of selected benchmark reference tags, the estimated boundary virtual reference RSSI value will be more accurate, and the accuracy of positioning is also higher. However, the more

benchmark reference label leads to more complex computations [51]. So, they just select references to meet the minimum number of errors in the accuracy of labeling requirements. Therefore, the initial situation defined on num (N) is 3, if the precision does not meet requirements; we increase the reference label number until meets the requirements. The experiment showed that when the number of baseline reference label is 4 then it will be capable to meet most of the positioning accuracy requirements.

4.2. Adding the Boundary Virtual Reference Label

As shown in Figure 4.2, we introduced the location of 16 border virtual reference label. We see that from the original value of the reference coordinates labels can readily get the coordinate of the boundaries virtual reference label. In addition, the RSSI value of labels mainly depends on its position that is namely the coordinate values. Therefore, the regression equation can be organized depending on the coordinate values and the RSSI value of the original reference tags.

Figure 4.2 Real time locating system

Also, the reference value is similar in both RSSI of real and boundary virtual reference tags, based on the RSSI of fundamental reference tag in the linear

regression (LR) equation. A real-time updating of the boundaries of virtual reference RSSI and the location label can be performed, whenever the values of RSSI and real reference tag position are changed in a suitable manner with the circumstances. How to construct an LR equation for solving the RSSI of the boundary virtual reference tag is as below:

(1) Constructing a 2D binary LR equation:

$$\boldsymbol{S_{binary(two\ coordinate)} = B_0 + B_1 x + B_2 y} \tag{4.1}$$

where

$$\boldsymbol{B = (X^T X)^{-1} X^T} \tag{4.2}$$

$$X(\boldsymbol{2D}) = \begin{pmatrix} \boldsymbol{1} & \boldsymbol{x_{11}} & \boldsymbol{y_{21}} \\ \boldsymbol{1} & \boldsymbol{x_{12}} & \boldsymbol{y_{22}} \\ \boldsymbol{\vdots} & \boldsymbol{\vdots} & \boldsymbol{\vdots} \\ \boldsymbol{1} & \boldsymbol{x_{1n}} & \boldsymbol{y_{2n}} \end{pmatrix} \tag{4.3}$$

$$\boldsymbol{\hat{\beta}_2 = \frac{\sum_{i=1}^{n} x_i S_i - n\bar{x}\bar{S}}{\sum_{i=1}^{n} x_i{}^2 - n\bar{x}^2} = \frac{\sum_{i=1}^{n}(x_i - \bar{x})\,(s_i - \bar{s})}{\sum_{i=1}^{n}(x_i - \bar{x})^2}}$$

$$\boldsymbol{\hat{\beta}_1 = \bar{s} - \hat{\beta}_2 \bar{x},\ \ \hat{\beta}_0 = \bar{s} - \hat{\beta}_1 \bar{x}} \tag{4.4}$$

$$\boldsymbol{\hat{\beta}} = \begin{pmatrix} \boldsymbol{\hat{\beta}_0} \\ \boldsymbol{\hat{\beta}_1} \\ \boldsymbol{\hat{\beta}_2} \end{pmatrix} \tag{4.5}$$

$$\boldsymbol{S_{|b(two\ coordinate)|} = \hat{\beta}_0 + \hat{\beta}_1 x_{b1} + \hat{\beta}_2 y_{b1}} \tag{4.6}$$

where S_{Binary} is the RSSI value of the real reference label (x, y). B_0, B_1, B_2 define the degradation coefficients of the real reference tag. $X(2D)$ is the label coefficients for two dimensions. $S_{|b(two\ coordinate)|}$ represents an RSSI of boundary virtual reference tag. The tag in Figure 4.2 has demonstrated that using the RSSI and coordinates of the 16 real reference labels, the $\hat{\beta}$ value can be obtained; which defines the degradation factors of the boundary virtual reference tag. Based on equation (4.6), the horizontal and vertical coordinate label (x_{b1},y_{b1}) are utilized to calculate RSSI value $S_{|b|}$ by reader R_1.

(2) Incorporation of one linear degradation equation:

$$\boldsymbol{S_{binary} = B_0 + B_1 x} \tag{4.7}$$

where,

$$\boldsymbol{X(1D)} = \begin{pmatrix} \mathbf{1} & \boldsymbol{x_1} & \boldsymbol{y_1} \\ \mathbf{1} & \boldsymbol{x_2} & \boldsymbol{y_2} \\ \vdots & \vdots & \vdots \\ \mathbf{1} & \boldsymbol{x_n} & \boldsymbol{y_n} \end{pmatrix} \tag{4.8}$$

$$\boldsymbol{S_{|b(binary)|} = \widehat{\beta}_0 + \widehat{\beta}_1 x_{b1}} \tag{4.9}$$

where S_{Binary} defines a "1D" RSSI of the real reference tag (x, y). $B_{0,}$ and B_1, define degradation factors of the real reference tag. $X(1D)$ is a 1D of label coefficients. $S_{|b(binary)|}$ is a "1D" RSSI of boundary virtual reference tag. Let's assume the first row tags are $L_1, L_2, L_{3,}$ and L_4 on the reader R_1 that has RSSI values s_1, s_2, s_3, s_4; then, the RSSI coordinates become $(x_1, s_1), (x_2, s_2), (x_3, s_3), (x_4, s_4)$, and by substituting these factors into the equation (4.1), we obtain $\hat{\beta}_0$ and $\hat{\beta}_1$. We can also have the label x_{b1} on the reader R_1 by the RSSI / $S_{|b|}$. The above steps are repeated for the 3 remaining readers.

(3) Incorporation of quadratic LR equation:

$$\begin{aligned} \boldsymbol{S_{quadratic}} &= \boldsymbol{B_0 + B_1 x + B_2 x^2} \\ &= \boldsymbol{B_0 + B_1 x_1 + B_2 x_2 \rightarrow (x = x_1, x^2 = x_2)} \end{aligned} \tag{4.10}$$

where $S_{quadratic}$ defines a quadratic RSSI of boundary virtual reference tag. x_1, x_2 become the new autonomous factors, thus rewriting the previous equation as below:

$$\boldsymbol{S_{quadratic} = B_0 + B_1 x_1 + B_2 x_2 \rightarrow (x = x_1, x^2 = x_2)} \tag{4.11}$$

According to the previous demonstrations, the same steps of LR eq. 1 are repeated for obtaining an RSSI of the quadratic LR eq.

(4) Incorporation of a logarithmic detour equation:

$$\boldsymbol{S_{logarithmic} = B_0 + B_1 \log x} \tag{4.12}$$

Suppose x'=lg x, then the above equation can be rewritten as:

$$\boldsymbol{S_{logarithmic}} = \boldsymbol{B_0} + \boldsymbol{B_1}\dot{\boldsymbol{x}} \tag{4.13}$$

The LR equations of these forms describe the definite approach sample.

4.2.1. Appending Grid Virtual Reference Labels

Computing the initial coordinates and RSSI of the virtual reference label is performed after calculating the boundaries layout of the virtual reference tag for $n \times n$ net. A boundary net of equally distance unit is included within the boundary virtual references or each four virtual reference tags [16]. Where, each unit within the net is united to the $[(n+1)^2 - 4]$ virtual reference net tag. Additionally to the several real reference tags, a unit net amendment propagation circumference can efficaciously attenuate the approximation error within the location system due to the multipath influence. The principle depends on the simplified stature of perplexity [52]; utilizing a linear data interpolation method to compute the RSSI values and their coordinates. For the horizontal pattern, the RSSI of the virtual reference labels is determined as below:

$$\begin{aligned} \boldsymbol{S_k(T_{p,b})} &= \boldsymbol{S_k(T_{p,b})} + \boldsymbol{P} \times \frac{\boldsymbol{S_k(T_{a+n,b})} - \boldsymbol{S_k(T_{p,b})}}{\boldsymbol{n}} \\ &= \frac{\boldsymbol{P} \times \boldsymbol{S_k(T_{a+n,b})} + (\boldsymbol{n+1-p}) \times \boldsymbol{S_k(T_{p,b})}}{\boldsymbol{n}} \end{aligned} \tag{4.14}$$

In the vertical way, the RSSI value of virtual reference labels can be computed depend on the equation below:

$$\begin{aligned} \boldsymbol{S_k(T_{a,q})} &= \boldsymbol{S_k(T_{p,b})} + \boldsymbol{q} \times \frac{\boldsymbol{S_k(T_{a,b+n})} - \boldsymbol{S_k(T_{a,b})}}{\boldsymbol{n}} \\ &= \frac{\boldsymbol{q} \times \boldsymbol{S_k(T_{a,b+n})} + (\boldsymbol{n+1-q}) \times \boldsymbol{S_k(T_{a,b})}}{\boldsymbol{n}} \end{aligned} \tag{4.15}$$

where $S_k(T_{i,j})$ defines the RSSI in the (i-th row and j-th column) of the virtual tag at the reader R_k, and $a = \lfloor i/n \rfloor, b = \lfloor j/n \rfloor$for $0 \le P = i \bmod n \le n-1$, $0 \le q = j \bmod n \le n-1$.

4.2.2. Choosing the Neighbouring Reference Tags

The overall reference tags (real, virtual, and boundary virtual) were obtained during the aforementioned steps above for RSSI and location coordinates. In addition, all the tags' RSSIs can be read by each reader for locating them. An absolute variance value should be obtained by the reader; in order to locate the tag and its reference; where its value should be smaller as it is closer to the position of the tag to be located.

A fuzzy map of equally sized units was constructed with a cantered reference tag; where the specified threshold (= 2) is no higher than the absolute differential value at position 0. To locate a tag, k was constructed within the k fuzzy chart reader, and the cross neighbouring for all charts is basically optimising the neighbouring reference tag; with fixing a value "1" for each k on the fuzzy chart to neglect any excrescent in position data.

4.3. The Calculation of Weighting Factor

To develop the reliability of positioning, the improvement depends on the basis of weight. The introduction of two weighting factors w_{1i} and w_{2i}. w_{1i} is utilized to describe the signal strength of the selected tag and be positioned adjacent the reference tag (RSSI) of the difference, and the differential value is smaller; the smallest difference that w_{1i} is greater. w_{2i} utilized to describe the optimal density of the selected neighbouring reference tag, the larger density means larger w_{2i}.

$$\boldsymbol{w_{1i} = 1 - \sum_{k=1}^{K} \frac{|S_k(T_i) - S_k(R)|}{K \times S_k(T_i)}} \tag{4.16}$$

$$\boldsymbol{w_{2i} = \frac{n_{ci}}{\sum_{i=1}^{n_a} n_{ci}}} \tag{4.17}$$

where, n_{ci} indicates the number of connections with the neighbouring reference tag i both with the region, n_a represents number of neighbours of reference label to be located during the chosen indoor region. By considering all the elements w_{1i} and w_{2i}, the overall weight will be [53]:

$$\boldsymbol{w_i = w_{1i} \times w_{2i}} \tag{4.18}$$

The positioning of the label for the coordinate values can be computed using the next equation:

$$(\boldsymbol{x}, \boldsymbol{y}) = \sum_{\boldsymbol{i=1}}^{\boldsymbol{n_a}} \boldsymbol{w_i}\,(\boldsymbol{x_i}, \boldsymbol{y_i}) \tag{4.19}$$

the theoretical definition of the approximation error between the coordinates tag to be located and the real coordinates obtained:

$$\mathbf{e} = \sqrt{(\mathbf{x} - \boldsymbol{x_0})^2 + (\mathbf{y} - \boldsymbol{y_0})^2} \tag{4.20}$$

where, (x_0, y_0) represents the real coordinates of the tag to be positioned.

4.4. Circular Error Probability

Circular error probability (CEP) is used to measure the localization estimate accuracy of one strict. CEP is used to measure the estimated position of the value indicators. In the two-dimensional positioning system, CEP defined to contain radius of half random vector realization cantered on average values. If the localization estimator unbiased, CEP is the measure of uncertainty to be positioned relative to the real position of the tag. If the deviation estimator and B is enclosed to the deviation for a 50% probability, estimated location labels to be located at a distance of less than B + CEP [54]. CEP is a complicated function, mostly can be approximated as:

$$\boldsymbol{CEP} = \mathbf{0.75}\sqrt{\boldsymbol{\sigma_x}^2 + \boldsymbol{\sigma_y}^2} \tag{4.21}$$

where, two readers $\sigma_x{}^2$, $\sigma_y{}^2$ are the evaluated variance of the two-dimensional location. For three-dimensional systems, instead of using the ball radius, and CEP circular error probability; we can use the sphere error probability (SEP) rate. As our study was based on a 2D system, the analyses of circular error probability computes at first, the three algorithms' coordinate variances $\sigma_x{}^2$, $\sigma_y{}^2$ and the distance error of standard deviation readers σ_s. CEP value is calculated under three algorithms can be obtained by the formula (4.21).

Table 4.1 shows the value of the three algorithms under the CEP, the maximum CEP of LANDMARC algorithm is 0.6847, the minimum CEP of BVIRE algorithm is 0.1373. When we compared BVIRE algorithm with LANDMARC algorithm, the CEP value decreased by 79.9%, and compared with VIRE algorithm the CEP is

educes 40.0%. Due to the CEP circular error probability table of recruitment, the uncertainty of the label relative to true position, therefore, in the three algorithms, the uncertainty of BVIRE algorithm is to be positioned relative to the true position of the small label.

Table 4.1 Standard deviations and coordinate variances of algorithms

	LANDMARC	**VIRE**	**BVIRE**
$\boldsymbol{\sigma_x^2}$	0.4108	0.0402	0.0143
$\boldsymbol{\sigma_y^2}$	0.4225	0.0416	0.0192
$\boldsymbol{\sigma_s}$	1.4111	0.4987	0.4161

4.5. The Evaluation of Positioning Accuracy

In real environments, evaluating the performance of a variety indoor positioning algorithm, distinguish the various positioning algorithms. The application is very important for the algorithm, therefore we need to determine the location index of the performance evaluation. Currently, the most commonly used evaluation standards have the following several types: mean square error (MSE), root mean square error (RMSE), circular error probability (CEP) and GDOP. The GDOP measures the effect of the reader's position on the positioning precision. Furthermore, the cumulative probability of engineering applications is also often the positioning errors of the cumulative probability distribution function (CDF), probability density function (PDF) and relative positioning error (RPE) as an evaluation standard index. Below each of these evaluations is introduced one by one [55].

4.5.1. The MSE and RMSE

The MSE of localization solution is the highest commonly utilized positioning accuracy evaluation indicators. At the location with the two-dimensional positioning system, MSE is calculated by the following formula:

$$\boldsymbol{MSE = E[(x - x_0)^2 + (y - y_0)^2]} \tag{4.22}$$

Where, $(x_0,\ y_0)$ indicates the actual location of the label to be located, (x, y) represents the estimated position of a tag to be located. Additionally, the RMSE is also utilized for evaluating the positioning accuracy:

$$\boldsymbol{RMSE = \sqrt{E[(x - x_0)^2 + (y - y_0)^2]}} \tag{4.23}$$

In order to determine the accuracy of positioning, typically MSE or RMSE were compared. Generally regarding having the existence of a smooth Gaussian noise, a smooth Gaussian signal is more applicable. In addition, in the non-Gaussian and non-stationary smooth signal, the alternative methods can be used to evaluate the performance of the estimator.

4.5.2. GDOP

GDOP is a technique for measuring the distances, where the geometric relationship between the reader and the position of the label to be located affecting the accuracy of the positioning system. Therefore uses GDOP for measuring the geometrical position's effect on the positioning precision, defines the positioning errors with RMSE ranging error and RMSE ratio. GDOP has characterized the reader and the positioning of the label to be positioned as a result of the geometric position of the label on the relationship between the degrees of magnification ranging error. If the estimator is unbiased, GDOP can be expressed as:

$$\boldsymbol{GDOP = \sqrt{tr[(A^T A)^{-1}]}} \tag{4.24}$$

where, $tr(.)$ is the trace matrix; which represents the matrix elements in the primary diagonal. A feature depends on the coefficient matrix of series linear equation, so some certain characteristic vector quantity establishes, from that Y=AX, here, the reader position Y is defined as M*1 dimensional vector, label position X to be located, we need 2*1 dimensional and unknown vectors [x, y], A is M*2-dimensional matrix, if the $A^T A$ is non-singular matrix and M> 2, the estimated location utilizes the least squares method for obtaining the label to be located as follows:

$$\boldsymbol{X = (A^T A)^{-1} A^T Y} \tag{4.25}$$

When the estimate is unbiased within a 2D system of hyperbolic positioning, the GDOP is:

$$\boldsymbol{GDOP} = \sqrt{\boldsymbol{\sigma_x}^2 + \boldsymbol{\sigma_y}^2}/\boldsymbol{\sigma_s} \tag{4.26}$$

where, σ_s is the ranging error of standard deviation. GDOP and CEP have the following relationship:

$$\boldsymbol{CEP} \approx (\mathbf{0.75}\boldsymbol{\sigma_s})\boldsymbol{GDOP} \tag{4.27}$$

GDOP choose from a big number of tags to be positioned in the desired label indicators. The selected tag should be positioned so that the smallest GDOP can be used as an option to be positioned label position reference when creating the new system.

4.5.3. Cumulative Distribution Function

The above several performance indicators are mainly used in the theoretical analysis; the actual works often use the error (PDF) and (CDF), and other indicators. Many performance analysis of a positioning system was utilized in the CDF. CDF defines the percentage of the number times of a positioning accuracy below the threshold of the total number. For example, position error in the location occupied by the number of 150cm or less in proportion of the number in all localization accounting, referred to as a CDF (150).

4.5.4. Relative Positioning Error

Obviously, positioning accuracy is affected by positioning range. For example, the footwear range of a robotic arm activities during the three-dimensional positioning operation are only a few 10 centimetres. Therefore, the positioning accuracy is required in millimetres. In micro-cellular network positioning system, if the cell radius is about 500 meters, then the positioning accuracy about 100 meters is relatively large. However, if the cell radius is about 15,000 m, then the positioning accuracy about 150 meters is a good positioning accuracy.

To express the relative relationship between the positioning accuracy and positioning range, we are introducing relative positioning error (RPE) concept. If the positioning range (the distance between the reader or effective action between the detection point) of the largest circle (sphere) of the center's radius R_m, then the positioning accuracy δ is:

$$\boldsymbol{RPE = \frac{\delta}{R_m}} \tag{4.28}$$

CHAPTER 5

GPS REPEATER AND FILTERS

5.1. GPS Repeater

The L1 repeater unit has an efficient comprehensive coverage of 35- 40 metres radius from the centre. The signal is radiated in a cone-shaped model that has a 140 degree angle of view built-in antenna. The sub miniature version (SMA) socket connects to the extrinsic antenna feeder cable; in order to power the low noise amplifier (LNA) through the coaxial cable, so the repeater sends 5V DC through it. An extra repeater will be added if a bigger area of encasement is required, by the use of a line amplifier and/or a GPS signal splitter, where all using a primary outdoor antenna. By the availability of outdoor antenna, the GPS repeater can exaggerate the signal and makes that signal available indoor as shown in Figure 5.1.

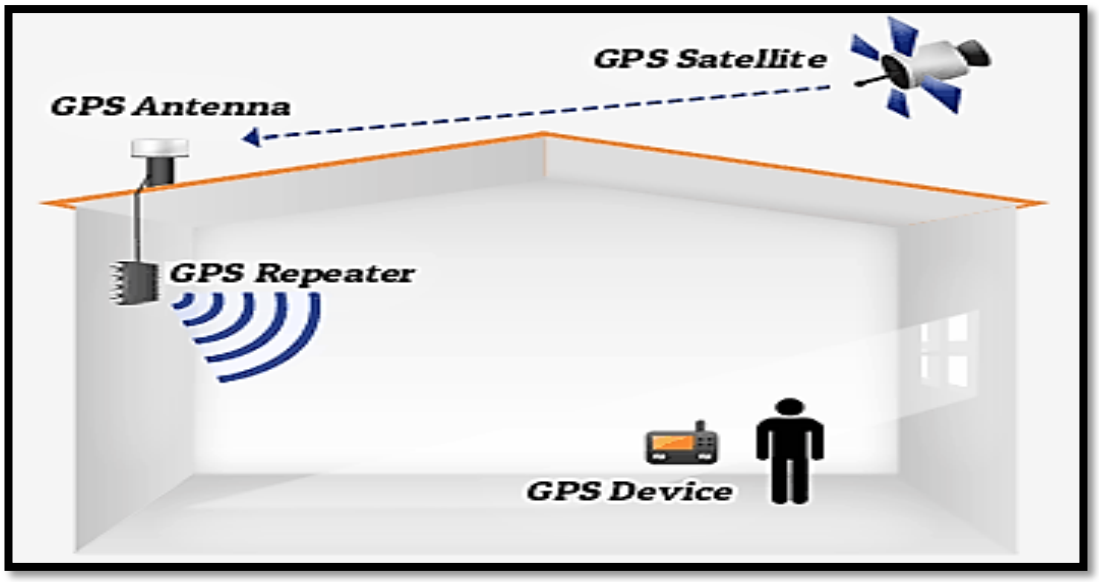

Figure 5.1 Installation of GPS antenna, repeater, and receiver

Inside test facility, a GPS repeater with antenna system provides live satellite signals [56].

- In order to receive GPS signals from satellites, we are not forced to take the devices outdoors
- Rapid Return on Investment (ROI)
- Using one repeater you can coverage area up to 40 metres.

Figure 5.2 Repeater with antenna

The satellite signal will be sent incessantly to the earth, when a GPS satellite is circulating around it. Where, the intensity of the signal will be weekend around -125dBm. Such a weak signal can't permeate into buildings. Sometimes only around the window field, it can be observed. Repeater and antenna shown above in Figure 5.2 are built for the aim of transferring the GPS satellite signal from outdoor to indoor, by re-radiating the signal to make GPS receivers run within testing room, building, especially in the house, and laboratory. Also, to obtain GPS satellite signal outdoor it includes a high frequency, low noise amplifier with an extrinsic high gain active GPS antenna [57]. The amplifier inside it is utilized to enhance the intensity level of GPS satellite signal indoors, the power of accuracy circuit, a signal re-radiation antenna for re-radiation signal indoors. The purpose of the rejuvenation is to supply an indoor locating system, which increases coverage of the outdoors GPS signals in the indoors, and also to equip an indoor positioning system which causes the positioning accuracy same as the outdoor positioning accuracy of GPS. When the receiving conditions are excellent for indoors, the GPS repeaters use to transmit signals where an existing standard receiver of GPS is not capable to calculate a

location. The two hardware dispositions presented below, utilize all the repeaters to iterate the coming signals or repeat the signal from satellite.

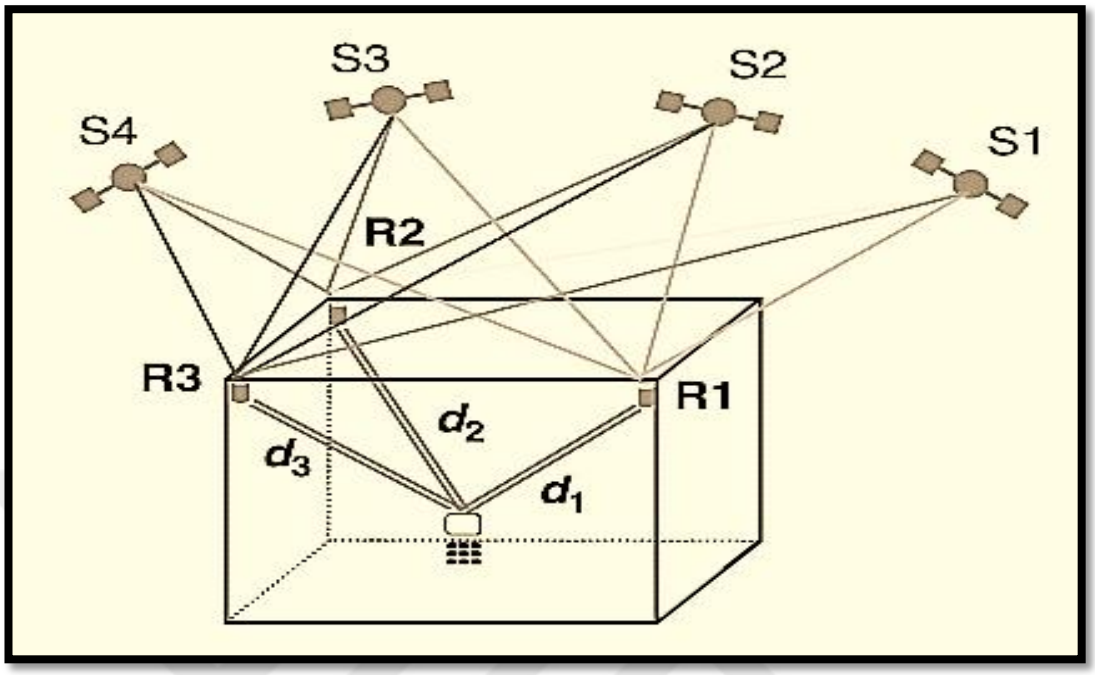

Figure 5.3 The iteration of the incoming signals using three repeaters

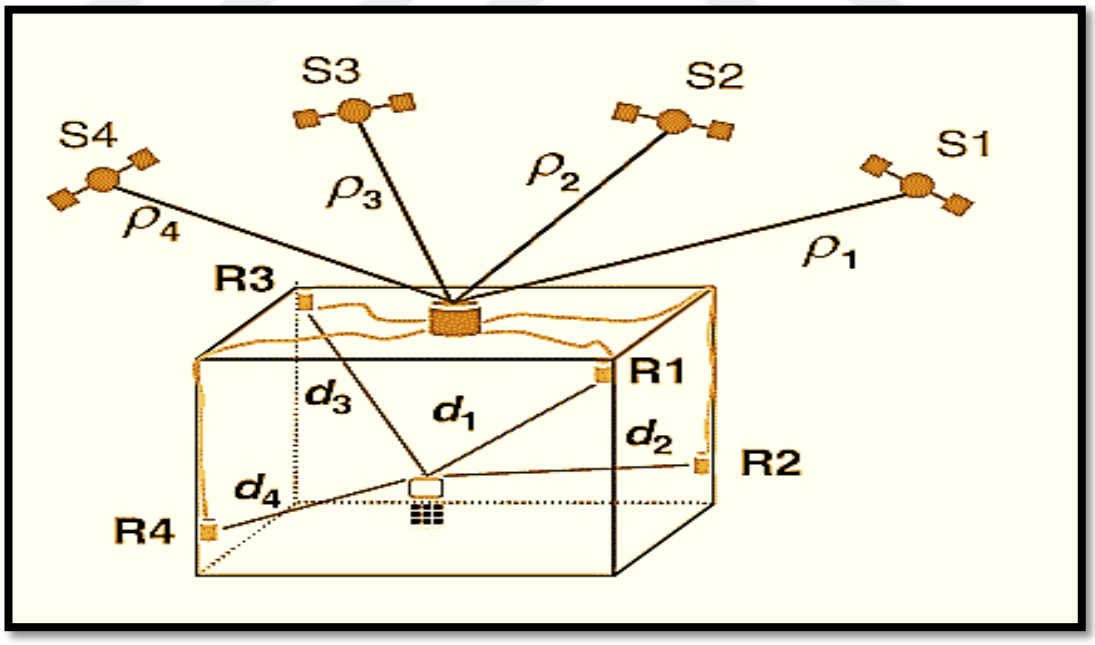

Figure 5.4 The iteration of the incoming signals using four repeaters

The transmitting antenna, receiving antenna, and an amplifying chain are the component of the repeater. Using the repeater, the signals are transmitted indoors from all the satellites. At the indoor receiver location, the deliberations of the

navigation equations that provides the position of the obtaining outdoor antenna drive to a settling vector; which is the essence of all the usual biases with the fourth component. Therefore, it includes the free space expansion delay, the clock bias, and the electronic social system of the repeater, where the delay represents a time equipollent to distance d from repeater to the indoor GPS receiver [11, 58]. For each computation, it is conceivable to obtain two types of data: the repeater's location, the distance d_m between the receiver of the indoor GPS and the repeater "m", and ht_l. The following equations (5.1) and (5.2) are suitable for four repeaters as referring in Figure 5.4 instead of just the three presented in Figure 5.3:

$$\begin{bmatrix} \boldsymbol{ht_1} \\ \boldsymbol{ht_2} \\ \boldsymbol{ht_3} \\ \boldsymbol{ht_4} \end{bmatrix} = \begin{bmatrix} \boldsymbol{ht_l} & + & \boldsymbol{d_1} \\ \boldsymbol{ht_l} & + & \boldsymbol{d_2} \\ \boldsymbol{ht_l} & + & \boldsymbol{d_3} \\ \boldsymbol{ht_l} & + & \boldsymbol{d_4} \end{bmatrix} \tag{5.1}$$

In order to calculate the real location of the indoor GPS receiver, we must find the values of d_1, $d2$, $d3$, and $d4$. It is possible to create a new set from the concluding assortment of equivalences by computing the coordinate differences to remove ht_l.

$$\begin{bmatrix} \boldsymbol{d_2} & - & \boldsymbol{d_1} \\ \boldsymbol{d_3} & - & \boldsymbol{d_1} \\ \boldsymbol{d_4} & - & \boldsymbol{d_1} \end{bmatrix} = \begin{bmatrix} \boldsymbol{ht_2} & - & \boldsymbol{ht_1} \\ \boldsymbol{ht_3} & - & \boldsymbol{ht_1} \\ \boldsymbol{ht_4} & - & \boldsymbol{ht_1} \end{bmatrix} \tag{5.2}$$

The method depends on choosing d_1 then the touch of the two biggest spheres. By their radius $(d_{k2} - d_{m1})$, $(d_3 - d_1)$, and $(d_4 - d_1)$, the three spheres are outlined. Therefore, the extension of the four spheres of radii (d_1, d_2, d_3, and d_4) must be computed to specify the real junction point that represents the location of the receiver of indoor GPS. We need to realize the matching of the effective repeater and the start time. After that and from the mobile receiver of GPS, all arriving clear information will be saved within the program. In every estate, the desired information is:

- The GPS time
- The clock bias
- The rate of clock bias that can be calculated using Doppler shift. The set of equations is given by:

$$\begin{bmatrix} cg_{mes}(g_{R1}) = cg_{obs}(g_{R1}) + dly(R1) + d_1 \\ cg_{mes}(g_{R2}) = cg_{obs}(g_{R2}) + dly(R2) + d_2 \\ cg_{mes}(g_{R3}) = cg_{obs}(g_{R3}) + dly(R3) + d_3 \\ cg_{mes}(g_{R4}) = cg_{obs}(g_{R4}) + dly(R4) + d_4 \end{bmatrix} \quad (5.3)$$

where $cg_{mes}(g_{R_m})$ is the clock bias calculated at time g_{R_m}, $cg_{osc}(g_{R_m})$ is the rate of the clock bias at a time same as the previous time, $dly(Rm)$ represent the repeater's delay, and d_m represent the range between the repeater and the movable receiver. In reality, if the short stability of the receiver's oscillator is unknown, we can use it with a suitable reliability using Doppler shift as shown in the equation below:

$$cg_{OBS}(g_{Rf}) = cg_{OBS}(g_{Rm}) + \sum_{k=i+1}^{f} \Delta cg_{OBS}(g_{Rk}) \quad (5.4)$$

where $\Delta cg_{OBS}(g_{Rk})$ is the range of the clock bias at g_{Rk}. The calculation that carried out by the indoor GPS receiver is definitely similar, so we can calculate a 3D location system using the linearization method [59, 60]. The receiver calculates difference between transmission time and reception time depend on the correlation of a local replication with the received signal. The rule of the recent mechanism when cycling from one repeater to another is to keep on tracking the development of the distances of the pseudo range as explained in Figure 5.5. One of the expectations is the distance of different value from the antenna of transferring indoor of the repeater to the antenna of the indoor receiver. After a total period and for identifying the existing position of the receiver, we should get three differences.

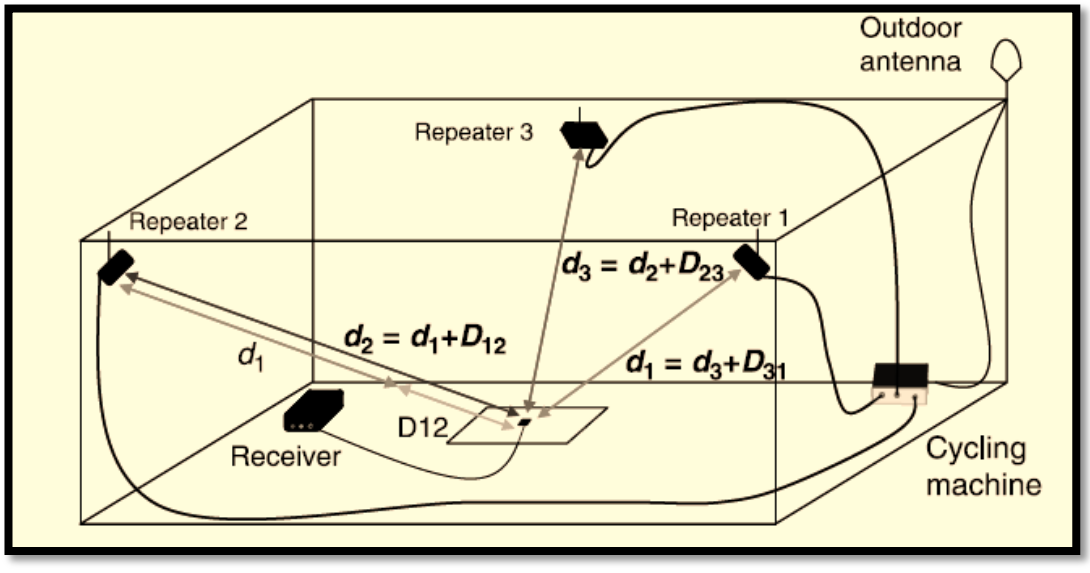

Figure 5.5 The cycling of pseudo from one repeater to another

5.2. Theoretic Sides

The pseudo ranges progression over a little cycle given in Figure 5.6. The following propositions have been prepared in order to comprehend this figure.

- The tardiness caused by the repeaters, such as the cable and electronic tardiness.
- The difference from one time point to the next symbolizes in the providing curve.
- The slope of the receiver's oscillator can be observed.

Distinctly, it comes out that the variance from one repeater to the adjacency can be understood by the receiver in the distance of the pseudo range as acceleration that is discovered from one repeater to the adjacent after the transition. Also, the time required depends on some parameters; which are important in the parliamentary procedure, in order to be capable of following the omissions from one repeater to the adjacent [61, 62].

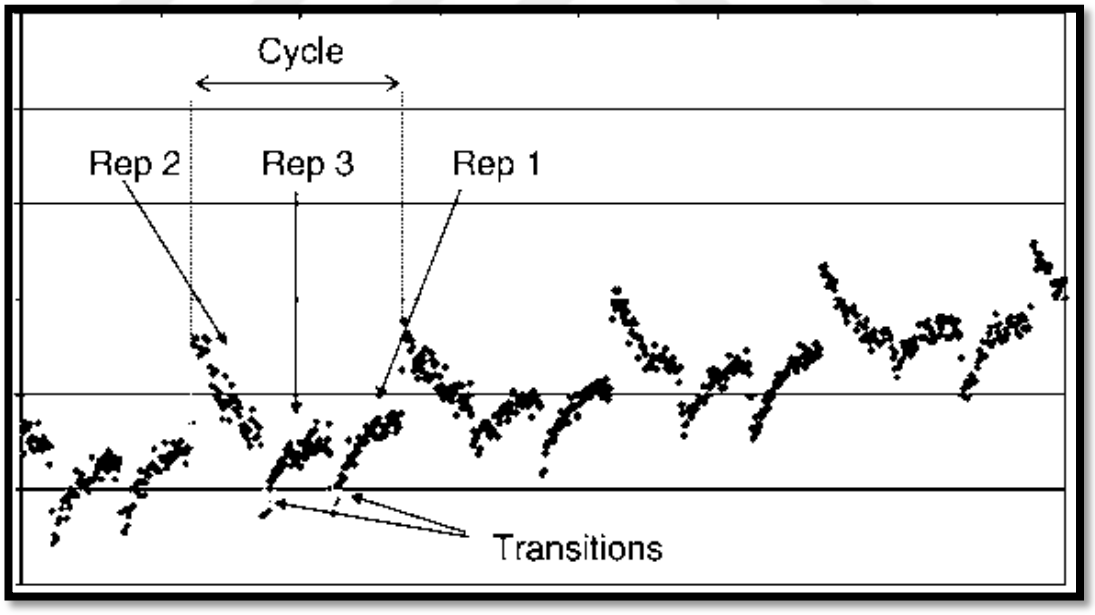

Figure 5.6 The progression of pseudo ranges

In the form of the obtained signal, the signal is changing from one repeater to the next. To obtain the three-dimensional positioning in GPS system; it is required to have at least four satellites. To understand this, the new indoor pseudo ranges term

(PRE_k) between an indoor receiver of GPS and satellite has been written. Also, we should remember that through a repeater RE_k, the signal can be received:

$$\boldsymbol{pre_k(t) = D_{R\to H}(t) + d_k + c.t(t) + \Delta prn(t) + del} \quad (5.5)$$

where $D_{R\to H}$ is the distance of the line-of-sight existing on the ceiling between the antenna of the outdoors and satellite, d_k represent the range between the indoor receiver of GPS and repeater RE_k, t represent the clock bias of receiver, $\Delta prn(t)$ represent the delay of the propagation error, and "del" is the time of propagation connecting the external repeater and antenna RE_k. We assume for the repeaters that all cables are comparable. So, the delay will be the same through RE_1 to RE_4 for all paths.

The signal transforms from repeater RE_k to repeater RE_m, at time t. At the same time, the computed pseudo range through the repeater RE_m becomes:

$$\boldsymbol{pre_k(t+dt) = D_{R\to H}(t+dt) + d_k + c.t(t+dt) + \Delta prn(t+dt) + del} \quad (5.6)$$

Thus, the difference from time $t + dt$ to time t of the pseudo range is calculated by the next equation:

$$\begin{aligned} \Delta \boldsymbol{pre(t+dt) = pre_k(t+dt) - p_{rek}(t)} \\ = \Delta \boldsymbol{D_{R\to H}(t+dt) + \Delta d + c.\Delta[t(t+dt)] + \Delta[\Delta prn(t+dt)]} \end{aligned} \quad (5.7)$$

where

$$\begin{aligned} \Delta \boldsymbol{D_{R\to H}(t+dt) = D_{R\to H}(t+dt) - D_{R\to H}(t)} \\ \Delta \boldsymbol{d = d_m - d_k} \\ \Delta[\boldsymbol{t(t+dt)}] = \boldsymbol{t(t+dt) - t(t)} \\ \Delta[\Delta \boldsymbol{prn(t+dt)}] = \Delta \boldsymbol{prn(t+dt) - \Delta prn(t)} \end{aligned} \quad (5.8)$$

The distances from the two repeaters R_k and R_m are represented by Δd. Here, because its values is small compared with $\Delta D_{R\to H}(t+dt)$ and $\Delta[t(t+dt)]$, we cannot reach it [63]. The next difference time moved to reveal Δd, as Δd is shown just at the transition time between consecutive repeaters. In reality, the signal will still inherit at time t, thus the difference in pseudo range between times t and $t - dt$ does not contain Δd and it as follows:

$$\Delta \boldsymbol{\ell(t) = \ell_k(t) - \ell_i(t-dt) = \Delta D_{S\to A}(t) + c.\Delta[t(t)] + \Delta[\Delta prn(t)]} \quad (5.9)$$

The following equation is acquired when we compute the other difference of the pseudo range to elicit Δd.

$$\Delta \boldsymbol{\ell}(\boldsymbol{t}+\boldsymbol{dt}) - \Delta \boldsymbol{\ell}(\boldsymbol{t}) = [\Delta \boldsymbol{D}_{\boldsymbol{R}\rightarrow\boldsymbol{H}}(\boldsymbol{t}+\boldsymbol{dt}) - \Delta \boldsymbol{D}_{\boldsymbol{R}\rightarrow\boldsymbol{H}}(\boldsymbol{t}) + \boldsymbol{c}.\{\Delta[\boldsymbol{t}(\boldsymbol{t}+\boldsymbol{dt})] - \Delta[\boldsymbol{t}(\boldsymbol{t})]\} + \{\Delta[\Delta \boldsymbol{prn}(\boldsymbol{t}+\boldsymbol{dt})] - \Delta[\Delta \boldsymbol{prn}(\boldsymbol{t})]\} + \Delta \boldsymbol{d} \quad (5.10)$$

If the transference of the signal is very quick between repeater RE_k and RE_m (that means, dt is so small), double differences of t, $D_{\boldsymbol{D}_{\boldsymbol{R}\rightarrow\boldsymbol{H}}}$, and Δprn will be negligible and the double difference in the pseudo range will be minimized to $\Delta_{mk} = \Delta d = d_m - d_k$. In conclusion, we have the following arrangement for the system:

$$\begin{aligned} \Delta_{\boldsymbol{12}} &= \boldsymbol{d_1} - \boldsymbol{d_2} \\ \Delta_{\boldsymbol{23}} &= \boldsymbol{d_2} - \boldsymbol{d_3} \\ \Delta_{\boldsymbol{34}} &= \boldsymbol{d_3} - \boldsymbol{d_4} \\ \Delta_{\boldsymbol{41}} &= \boldsymbol{d_4} - \boldsymbol{d_1} \end{aligned} \quad (5.11)$$

The distances d_k is defined by the receiver's coordinates (x_f, y_f, z_f) and repeaters's coordinates RE_k $(x_{REk}, y_{REk}, z_{REk}, k = 1, \ldots, 4)$, it is as shown below:

$$\Delta_{\boldsymbol{12}} = \boldsymbol{d_1} - \boldsymbol{d_2}$$

$$= \sqrt{(\boldsymbol{x_{RE1}} - \boldsymbol{x_f})^2 + (\boldsymbol{y_{RE1}} - \boldsymbol{y_f})^2 + (\boldsymbol{z_{RE1}} - \boldsymbol{z_f})^2} - \sqrt{(\boldsymbol{x_{RE2}} - \boldsymbol{x_f})^2 + (\boldsymbol{y_{RE2}} - \boldsymbol{y_f})^2 + (\boldsymbol{z_{RE2}} - \boldsymbol{z_f})^2}$$

$$\Delta_{\boldsymbol{23}} = \boldsymbol{d_2} - \boldsymbol{d_3}$$

$$= \sqrt{(\boldsymbol{x_{RE2}} - \boldsymbol{x_f})^2 + (\boldsymbol{y_{RE2}} - \boldsymbol{y_f})^2 + (\boldsymbol{z_{RE2}} - \boldsymbol{z_f})^2} - \sqrt{(\boldsymbol{x_{RE3}} - \boldsymbol{x_f})^2 + (\boldsymbol{y_{RE3}} - \boldsymbol{y_f})^2 + (\boldsymbol{z_{RE3}} - \boldsymbol{z_f})^2}$$

$$\Delta_{\boldsymbol{34}} = \boldsymbol{d_3} - \boldsymbol{d_4}$$

$$= \sqrt{(\boldsymbol{x_{RE3}} - \boldsymbol{x_f})^2 + (\boldsymbol{y_{RE3}} - \boldsymbol{y_f})^2 + (\boldsymbol{z_{RE3}} - \boldsymbol{z_f})^2} - \sqrt{(\boldsymbol{x_{RE4}} - \boldsymbol{x_f})^2 + (\boldsymbol{y_{RE4}} - \boldsymbol{y_f})^2 + (\boldsymbol{z_{RE4}} - \boldsymbol{z_f})^2}$$

$$\Delta_{41} = \boldsymbol{d_4 - d_1}$$

$$= \sqrt{\left(\boldsymbol{x_{RE4} - x_f}\right)^2 + \left(\boldsymbol{y_{RE4} - y_f}\right)^2 + \left(\boldsymbol{z_{RE4} - z_f}\right)^2}$$

$$- \sqrt{\left(\boldsymbol{x_{RE1} - x_f}\right)^2 + \left(\boldsymbol{y_{RE1} - y_f}\right)^2 + \left(\boldsymbol{z_{RE1} - z_f}\right)^2} \qquad (5.12)$$

Table 5.1 Repeater specifications

Technical Description	
Type of technology	RF at 1.575 GHz
Location	Mobile receiver
Performance of Environments	Indoors
Accuracy	$\sim 1 - 2\ m$
Range	RF repeater range

The position of the indoor GPS receiver in this system is represented by these unknown variables (x_f, y_f, z_f) as explained in equation (5.12). Either using a hyperbolic or linearization method, the solution is carried away in order to solve the algorithm [64]. Evaluating the differences Δ_{mk} based on positioning represents the main problem of indoor repeater. While transferring from one repeater to the adjacent, these differences are corresponding to the code phase. Table 5.1 epitomized the universal features of a repeater positioning system. The repeater system presents more advantages in the arbitrage with pseudolites specified in the electronic design of the repeater itself. Since it is simpler, and has no near influence, as there is perpetually just one repeater that transfers at an assumed time. Therefore, it removes the discrepancy issue from different transmitters. Time differential method that is carried out is considered as a real significant advantage of this approach. In normal GNSS receivers, there is required following the pseudo range and the generated omissions by repeater cycling that are not looking for. This is the reason behind the precision approach with the repeater rather than the correlation part that accomplished based on the conductance of the part of the feedback loop [65, 66].

Distinctly, there is some disadvantage of the repeaters; which is the different procedure of the surroundings indoor and outdoor; since the receiver would require to exchange from one process to the other. However, it is not as a big trouble, since we can consider a comparative concept of using wide LAN for indoors and GNSS for outdoors.

5.3. Tracking and Positioning of Bayesian Filtering

In order to increase the locating system's accuracy, we have used a proper statistical instruments that combine data which are Bayesian filter. For calculating the density function of an unknown probability, the approximation of recursive Bayesian is a common probabilistic approach along utilizing of time incoming measurements and a design of numerical process. Probabilistically from observations the Bayesian filters calculate a dynamical province of a system. In the estimation of position, the terminal position is the state, and sensors of giving observations that are functions of the state [30, 67].

In our state, the target location is the state vector x, whereas the measures coming from suitable repeater are z. Each element of x and z are pointed to a specific approximation time t_k, demonstrated with *k* in the notation of the discrete-time. Two sequential time appraisals are spaced by $\Delta t_k = t_{k+1} - t_k$ seconds. The two classical Bayesian estimators are the maximum a posteriori (MAP) and the minimum mean square error (MMSE). The previous estimates the mean of the a posteriori probability density function:

$$\hat{\boldsymbol{x}}_{\boldsymbol{MMSE}} = \int \boldsymbol{x}\boldsymbol{p}_{\boldsymbol{x}|\boldsymbol{z}}(\boldsymbol{x}|\boldsymbol{z})\boldsymbol{dx} \tag{5.12}$$

whereas the later estimates the a posteriori probability density function's method

$$\hat{\boldsymbol{x}}_{\boldsymbol{MAP}} = \boldsymbol{arg\ max}\{\boldsymbol{p}_{\boldsymbol{x}|\boldsymbol{z}}(\boldsymbol{x}|\boldsymbol{z})\} \tag{5.13}$$

If the a posteriori probability density function $\boldsymbol{p}_{\boldsymbol{x}|\boldsymbol{z}}(\boldsymbol{x}|\boldsymbol{z})$ is hard to set, the integration of (5.12) or the maximization of (5.13) can be highly complicated or if the random variable **X** has a high dimension. In this state, instead of the total vector the MMSE or MAP estimation can be used to single elements of **X** ; for example, if $X = [X_1, \cdots, X_N]$, then the MMSE estimate of X_k is yield by the mean of a posteriori distribution of the marginal $pX_{x|Z}(.|z)$ of the variable X_k. The approach of consecutive Bayesian by utilizing sequential measurements of the system outputs provides a recursive estimate of the state of the system [68].

5.3.1. The Derivate of Kalman Filter

An optimum Bayesian recursive filter is the Kalman filter that calculates the linear dynamical system case from a series of noisy measurements when the next suppose applied [69, 70]:

- v_{k-1} and w_k are drawn from Gaussian densities of known parameters
- $f_{k-1}(x_{k-1}, u_{k-1}, v_{k-1})$ is a well-known linear function of (x_{k-1}, u_{k-1}) and v_{k-1}
- $h_k(x_k, w_k)$ is a well-known linear function of x_k and w_k

Just under the above- aforementioned extremely compelled circumstances, the Kalman filter (KF) accomplishes optimum MMSE solution. When the dependence of mensuration on states is nonlinear, and when noises ordinarily cannot be assumed zero-biased or distributed, in some applications they may not hold. In such cases, we have to repair to suboptimal Bayesian filters because the estimator of MMSE is complicated. The extended Kalman filter (EKF) [71] has been excessively utilized among the suboptimal filters for various years. To linearise observance and/or the state transition equations of the EKF through the extension of a Taylor-series extension, the basic plans is assumed about the mean of the pertinent Gaussian and apply to this linearized design of the linear KF.

For several theoretical systems, EKF has been depicted that has nonlinear state update and/or measurement equations and/or state update [21]. In fact, about the present mean of the state EKF linearizes the observation design [72]. As a result, with difficulty and depends on how the dynamic system performance of the EKF and the measurements are designed. The state-space design can be written, if just the supposable about the noises hold:

$$\boldsymbol{x_k = f(x_{k-1}, u_{k-1}) + v_k} \tag{5.14}$$

$$\boldsymbol{z_k = h(x_k) + w_k} \tag{5.15}$$

where $v_k \sim N(0, R_k)$, $w_k \sim N(0, R_k)$, and f and h are nonlinear.

5.3.1.1. Tracking of the Bias NLOS with Extended Kalman Filter

It is well known that on approximates of TOA, the non-line of sight (NLOS) locating presents a bias, decreasing locating algorithm's accuracy. In peculiar, because of the status of NLOS, from stronger fading the first incoming endures the following arrivals and hence incorrect data of TOA are acquired. In the case of multipath, the arrivals of the later signal cause a greater impulse of supplanting restraint, a simple frequency flat channel is utilized by the algorithms which supposes then the time of bias to be calculated. The locating of outcoming system handling with those approximates can just give an approximation of biased location. In order to minimize this type of error, a more complete state-space design is probable to specify that contains for each node where the bias distance to be evaluated as an extra element [52, 73]. Therefore, the aim of the related EKF is to develop the accuracy of locating by tracking not just the velocity and location and of the unknown movable node, but also the bias because of the propagation of NLOS.

This approximation with bias tracking is named EKF and is depicted below shortly. The state vector is described as $x_k^{(BT)} = [x_k^T \quad b_k^T]^T$, where the vector x_k is that described in (5.14) and the vector set b_k are the bias of measurement distance at each node. The matrix of the state transmission:

$$\boldsymbol{F_k^{(BT)}} = \begin{bmatrix} \boldsymbol{F_k} & \boldsymbol{0} \\ \boldsymbol{0} & \boldsymbol{I_M} \end{bmatrix} \tag{5.16}$$

where M is the anchor node number. The vector of model noise is $v_k = [0_2, \quad v_s, \quad v_b]^T$, where v_s and v_b are the noise vectors of bias and velocity with covariance matrices $Q_{s,k}$ and $Q_{b,k}$, respectively. The distance measurements are additive with the given bias, for the EKF the observation equation can be scripted as:

$$\boldsymbol{z_k} = \boldsymbol{h}(\boldsymbol{x_k}) + \boldsymbol{b_k} + \boldsymbol{w_k} \tag{5.17}$$

so that the matrix $H_k^{(BT)}$ of TOA-based measurement turns out to be:

$$\boldsymbol{H_k^{(BT)}} = [\boldsymbol{H_{dist,k}} \quad \boldsymbol{I_M}] \tag{5.18}$$

5.3.1.2 Adaptive EKF

This section concentrates on an adaptive extended Kalman filter (AEKF) technique suggested [13, 74] at low dynamics for tracking movable objects that utilizing from immovable anchor nodes of the RSS measurements.

When a KF is utilized, a sensibility of a commonly analysis is achieved that best fits the design in order to determine the mathematical parameters to the real object paths. These parameters rely on factors where such analyses are powerfully state-dependent that alteration in varied scenarios such as the difference of noise, the dynamics of objects, and sampling frequency. According to the provisions where the system is readjust and applied, AEKFs try to automatically modify relevant parameters of the model if the environment changes. The aim behinds this adaptive access is to the utilizing of the EKF behind this adaptive access to calculate the path loss model of some parameters that utilized for the measurements of RSS. In a typical manner after a posterior linear regression on a scale of semi logarithmic and a scene analysis movement, such parameters are observed where at a distance d_0, the P_0 is intercept, and the exponent of path-loss α represents the slope. The variance of the difference between the model and real measurements is expressed as the shadowing variance σ_{dB}^2. If the parameters of the propagation model are calculated by the EKF itself, then the analysis of such off-line scene can in base be avoided [75]. To apply this, it is conceivable at a given close-in distance to implicate the mean received power P_0 and exponent of path-loss into the state vector:

$$\boldsymbol{x_k^{(Ad)}} = [\boldsymbol{x_k^T}, \boldsymbol{\alpha}, \boldsymbol{P_0}]^{\boldsymbol{T}} \tag{5.19}$$

where x_k can be any state vector, for example, the state models of the P, position velocity (PV), or position velocity acceleration (PVA) [15]. The function of the state transition of the parameters α and P_0 are static and the correspondence matrix is:

$$\boldsymbol{F_k^{(Ad)}} = \begin{bmatrix} \boldsymbol{F_k} & \boldsymbol{0_{4\times2}} \\ \boldsymbol{0_{2\times4}} & \boldsymbol{I_2} \end{bmatrix} \tag{5.20}$$

Whereas the covariance of the process noise matrix becomes:

$$\boldsymbol{Q_k^{(Ad)}} = \begin{bmatrix} \boldsymbol{F_k} & \boldsymbol{0_{4\times2}} \\ \boldsymbol{0_{2\times4}} & \boldsymbol{I_2} \end{bmatrix} \tag{5.21}$$

Where $\sigma_{\tilde{\alpha}}^2$ and $\sigma_{\tilde{P}_0}^2$ are the noise variance related to the state variable α and P_0 respectively [76]. The observation is a vector containing the measurements of RSS between *M* anchor and nodes. From the long normal model the symmetrical Jacobian $H_k^{(Ad)}$ is derived as:

$$\boldsymbol{H_k^{(Ad)}} = \begin{bmatrix} & -\mathbf{10}\ \mathbf{log_{10}}\left(\boldsymbol{x_{k|k-1}}, \boldsymbol{x_{A1}}\right)/\boldsymbol{d_0} & \mathbf{1} \\ \boldsymbol{H_{RSS,k}} & \vdots & \vdots \\ & -\mathbf{10}\ \mathbf{log_{10}}\left(\boldsymbol{x_{k|k-1}}, \boldsymbol{x_{AM}}\right)/\boldsymbol{d_0} & \mathbf{1} \end{bmatrix} \tag{5.22}$$

The ability to calculate online the covariance noise is the basic benefit of this algorithm at each iteration of KF, to execute statistical analysis thus avoiding the necessity on historical information.

The covariance matrix of the noise measurement to be utilized on the next iteration $\hat{R}_{RSS,k+1|k+1}$ is calculated as a convex set of the present estimate $\hat{R}_{RSS,k|k}$ and the square of the innovations $\tilde{y}_k$ and the posteriori state approximation covariance matrix $P_{k|k}$ figured into the measurements. For fast convergence, in an exponential moving rate truncated to a window size *w*, the acquisition range λ_k is modified which permitting detection of further changes in the noise:

$$\begin{aligned} \widehat{\boldsymbol{R}}_{\boldsymbol{RSS,k+1|k+1}} &= (\mathbf{1} - \boldsymbol{\lambda_k})\widehat{\boldsymbol{R}}_{\boldsymbol{RSS,k|k}} + \boldsymbol{\lambda_k}\widehat{\boldsymbol{R}}_{\boldsymbol{RSS,k+1|k}} \\ \widehat{\boldsymbol{R}}_{\boldsymbol{RSS,k+1|k}} &= \boldsymbol{diag}\ (\tilde{\boldsymbol{y}}_{\boldsymbol{k}})^{\mathbf{2}} + \boldsymbol{H_k P_{k|k} H_k^T} \\ \boldsymbol{\lambda_k} &= \left(\mathbf{1} - (\mathbf{1}/\boldsymbol{w})\right)/(\mathbf{1} - (\mathbf{1} - (\mathbf{1}/\boldsymbol{w}))^{\mathbf{2}}) \end{aligned} \tag{5.22}$$

Likewise, for the covariance of the noise process:

$$\widehat{\boldsymbol{Q}}_{\boldsymbol{k+1|k+1}}^{\boldsymbol{(Ad)}} = (\mathbf{1} - \boldsymbol{\lambda_k})\widehat{\boldsymbol{Q}}_{\boldsymbol{k|k}}^{\boldsymbol{(Ad)}} + \boldsymbol{\lambda_k}\widehat{\boldsymbol{Q}}_{\boldsymbol{k+1|k}}^{\boldsymbol{(Ad)}} \tag{5.23}$$

$$\widehat{\boldsymbol{Q}}_{\boldsymbol{k+1|k}}^{\boldsymbol{(Ad)}} = \boldsymbol{diag}(\hat{\boldsymbol{x}}_{\boldsymbol{k|k}} - \hat{\boldsymbol{x}}_{\boldsymbol{k|k-1}})^{\mathbf{2}} - \left(\boldsymbol{P_{k|k}} - \boldsymbol{P_{k|k-1}} + \widehat{\boldsymbol{Q}}_{\boldsymbol{k|k}}^{\boldsymbol{(Ad)}}\right)$$

5.3.2. Particle Filter

According to a sampling manner, the particle filter realizes the updates of the bayes filter that frequently pointed to as sequential importance sampling. The key benefit of particle filters to characterize densities of unreasonable probability is their capability. Furthermore, the particles of particle filter on areas of the state space are very effective with high probability. However, these methods increase in an exponential manner because the worst case complexes of them in the state space

dimensions, when utilizing particle filters to issues of high-dimensional approximation, one has to be watchful.

In the update steps and prediction that implied the integrals for rating, the main idea is to estimate an integral expectation of the form:

$$\boldsymbol{I(g) = E_{p(x)}\{g(x)\} = \int g(x)p(x)dx} \tag{5.24}$$

By the following average:

$$\boldsymbol{I_{N_s}(g) = \frac{1}{N_s}\sum_{i=1}^{N_s} g\left(x^{(i)}\right)} \tag{5.25}$$

where $\{x^{(i)}\}_{i=1}^{N_s}$ are independent samples drawn from the distribution $p(x)$. However, $p(x)$ in an effective way from which it is hard to draw samples in a complex posterior distribution from, particularly in nonstandard states, and high dimensional. A markov chain monte carlo (MCMC) methods is a probable solution structure [31, 77], but to recursive approximation issues its reiterative model is not well appropriate. By the group of the particle filters (PFs) the more sophisticated methods that permit recursions are characterized.

In particle filtering, the belief functions $Bel(x_k)$ and over a group of weighted samples are parameterized:

$$\boldsymbol{\left\{< x_k^{(i)}, \omega_k^{(i)} > | i = 1, \cdots, N_s\right\}} \tag{5.26}$$

Where N_s is the number of particles, and $\omega_k^{(i)} > 0 \; \forall i, k$ are the weights normalized as $\sum_{i=1}^{N_s} \omega_k^{(i)} = 1$. The property of the estimation in (5.26) relies on the number of particles N_s. In order to minimize the perplexity, in the areas where the target is positioned, the sampling can be more impenetrable. If we could generate N_s independent and identically distributed random samples $\left\{X_{0:k}^{(i)}, i = 1, \cdots, N_s\right\}$ according to the posterior $p(X_{0:k}|Z_{1:k})$, we would estimate this distribution as:

$$\boldsymbol{\hat{p}(X_{0:k}|Z_{1:k}) = \frac{1}{N_s}\sum_{i=1}^{N_s} \delta\left(X_{0:k} - X_{0:k}^{(i)}\right)} \tag{5.27}$$

Where $\delta(.)$ is the Dirac delta function, and acquire the estimation:

$$\boldsymbol{\hat{I}(g_k) = \int g_k(X_{0:k})\hat{p}(X_{0:k}|Z_{1:k})dX_{0:k} = \frac{1}{N_s}\sum_{i=1}^{N_s} g_k\left(X_{0:k}^{(i)}\right)} \tag{5.28}$$

Which is established to converge $I(g_k)$ and to be unbiased as N_s increases under the weak supposition [78]. Regrettably, to expeditiously design samples it is

commonly inconceivable from the posterior $p(X_{0:k}|Z_{1:k})$ because it is far from being Gaussian and multivariate. By means of the importance sampling idea, this issue can be worse. Essentially, a density function of posterior probability includes the estimation by a group of N_s weighted random samples:

$$\boldsymbol{p(x_k|z_{1:k}) \approx \sum_{i=1}^{N_s} \omega_k^{(i)} \delta\left(x_k - x_k^{(i)}\right)} \tag{5.29}$$

A proposal distribution has been described since the $p(x_k|z_{1:k})$ is not known, which is instead $p(x_k|z_{1:k})$ suitable to sample. Thus, the posterior is estimated taken from an arbitrary importance density function $\pi(X_{0:k}|Z_{1:k})$ by a group of weighted random samples. The selected proposal distribution can be factorised:

$$\boldsymbol{\pi(x_k|Z_{1:k}) = \pi(x_k|x_{k-1}, z_{1:k}).\pi(x_{k-1}|z_{1:k-1})} \tag{5.30}$$

Then, in the evaluation of $I(g_k)$ we can write:

$$\boldsymbol{I(g_k) = \frac{\int g_k((X_{0:k})\omega(X_{0:k})\pi(X_{0:k}|Z_{1:k})dX_{0:k})}{\int \omega(X_{0:k})\pi(X_{0:k})}} \tag{5.31}$$

Where the term $\omega(X_{0:k})$ is pointed to as importance weight and is described as:

$$\boldsymbol{\omega(X_{0:k}) = \frac{p(X_{0:k}|Z_{1:k})}{\pi(X_{0:k}|Z_{1:k})}} \tag{5.32}$$

Then, after producing N_s independent and identically distributed particles $\left\{X_{0:k}^{(i)}; i = 1, \cdots, N_s\right\}$ according to $\pi(X_{0:k}|Z_{1:k})$, we can compute the estimate of $I(g_k)$ as:

$$\boldsymbol{\hat{I}(g_k) = \frac{\frac{1}{N_s}\sum_{i=1}^{N_s} g_k\left(X_{0:k}^{(i)}\right)\omega\left(X_{0:k}^{(i)}\right)}{\frac{1}{N_s}\sum_{i=1}^{N_s} \omega\left(X_{0:k}^{(i)}\right)} = \sum_{i=1}^{N_s} g_k\left(X_{0:k}^{(i)}\right)\tilde{\omega}_k^{(i)}} \tag{5.33}$$

where $\tilde{\omega}_k^{(i)}$ are the normalised importance weights described by:

$$\boldsymbol{\tilde{\omega}_k^{(i)} = \frac{\omega\left(X_{0:k}^{(i)}\right)}{\sum_{i=1}^{N_s} \omega\left(X_{0:k}^{(i)}\right)}} \tag{5.34}$$

However, this result which is a very suitable characteristic is not recursive for online proceeding of information. Every time new information z_{k+1} becomes available, along the sequence of total state. All the importance weights require to be recalculated, with the computational complexness increasing with time. One manner to utilize the importance sampling solution while preserving reclusiveness is by

means of the sequential importance sampling (SIS) idea. Resorting to the factorization of the proposed function (5.30) and iterating, we can get samples from:

$$\boldsymbol{x_k^{(i)} \sim \pi(X_{0:k}|Z_{1:k}) = \pi(x_0) \prod_{m=1}^{k} \pi(x_m|X_{0:m-1}, Z_{1:m})} \tag{5.35}$$

With weights of the related importance $\widetilde{\omega}_k^{(i)}$ that can be recursively calculated as:

$$\boldsymbol{\widetilde{\omega}_k^{(i)} \propto \widetilde{\omega}_{k-1}^{(i)} \frac{p\left(z_k|x_k^{(i)}\right) p\left(x_k^{(i)}|x_{k-1}^{(i)}\right)}{\pi\left(x_k^{(i)}|x_{0:k-1}^{(i)}, Z_{1:k}\right)}} \tag{5.36}$$

Indeed, after the normalization, the estimation of $I(g_k)$ becomes:

$$\boldsymbol{\hat{I}(g_k) = \sum_{i=1}^{N_s} g_k\left(x_k^{(i)}\right) \widetilde{\omega}_k^{(i)}} \tag{5.37}$$

Substantially the structure of (6.70)–(6.71) is simpler than the one verbalised in (5.33)–(5.34) because at time k the earlier does not need to adjust past trajectories $x_{0:k-1}^{(i)}$ and saves an important amount of computational load and memory [79]. A crucial matter is the selection of $\pi(.)$ design. Additionally from which it is simple to create samples to being a statistical distribution, the function of significance must have a support that contains the actual posterior. The group occlusion of function $\pi(.)$ statements must contain the one of $p(X_{0:k}|Z_{1:k})$. Then, the posterior approximation is:

$$\boldsymbol{\hat{p}(x_k|Z_{1:k}) = \sum_{i=1}^{N_s} \omega_k^{(i)} \delta\left(x_k - x_k^{(i)}\right)} \tag{5.38}$$

To the actual posterior and under weak suppositions, $N_s \to \infty$ is the converges of the most estimation. Notice that the most certainly convergences are equal in probability to one. The support of the selected importance density $(\bar{\pi})$ contains the support of the posterior pdf $(\bar{p})$, if these suppositions hold:

$$\begin{gathered} \boldsymbol{\bar{\pi} = \{x_k \in x | \pi(x_k|Z_k) > 0\}} \\ \boldsymbol{\bar{p} = \{x_k \in x | p(x_k|Z_k) > 0\}} \\ \textbf{And } \boldsymbol{\bar{p} \subseteq \bar{\pi}} \end{gathered} \tag{5.39}$$

However, it is well known for limited N_s that when *k* grows, for all particles except for one the weights $\widetilde{\omega}_k^{(i)}$ incline to be zero. Therefore, the algorithm fails to characterize in the posterior distribution of adequate manner. In other words, the importance weights of the unconditioned discrepancy increase over time [41]. This is

known as the devolution phenomenon and represents a significant obstacle for the SIS method. We can present a chosen step normally known as resampling in order to determine this. A classic selection step with replacement of N_s new particles comprise of resampling according to its importance weight from the produced group of particles. Other more advanced schemes contain graded resampling, polynomial, or balance [80]. Because the resampling step is in an inherent manner and it cannot be executed with other procedures pipelined, so it is worthwhile referring a checkpoint in any parallel affectation.

5.4. New Resampling of MPF Sequential

An execution of new importance sampling sequential with a resampling step is a sequential importance resampling (SIR) which presented to forbid the devolution issue clarified above. For the choice of the importance function of density $\pi\left(X_{0:k}^{(i)}|Z_{1:k}\right)$, it is possible to utilize the transition density $p\left(x_k|x_{k-1}^{(i)}, z_k\right)$, which by a motion equation can be described. The importance function has been clarified by reducing the discrepancy of the importance weights stated upon the observations up to time *k*, and the assumed trajectory $X_{0:k}^{(i)}$ and $Z_{1:k}$. Then, from (5.36) and the likelihood function $\omega_k^{(i)} = \omega_{k-1}^{(i)} p\left(z_k|x_k^{(i)}\right)$ we observe that the weights of importance can be calculated directly. SIR, although requiring the capability to sample from $p\left(x_k|x_{k-1}^{(i)}, z_k\right)$ and to evaluate $p\left(z_k|x_k^{(i)}\right)$, which may not have in the universal state an analytic result. Regarding the distributions of noise p_{v_k} and p_{w_k} this is matched to taking equations (5.14) and (5.15) as reciprocally independent. We make utilize of the efficient sample size N_{eff} for the step of resampling [81]. This is clarified as:

$$\boldsymbol{N_{eff}} = \frac{\boldsymbol{N_s}}{\boldsymbol{1+Var_{\pi(\cdot|Z_{1:k})}\{\omega(X_{0:k})\}}} \tag{5.40}$$

which precisely cannot be measured but can be easy evaluated by $\widehat{N}_{eff} = (\sum_{i=1}^{N_s}(\omega_k^{(i)})^2)^{-1}$. The resampling step will be applied whenever $\widehat{N}_{eff}$ decreases below a given threshold N_{thres}, which is usually chosen to be $N_{thres} = 2N_s/3$. The general flow chart of the SIR operation is explained in Figure 5.7, whereas the process of the algorithm is defined in Figure 5.8.

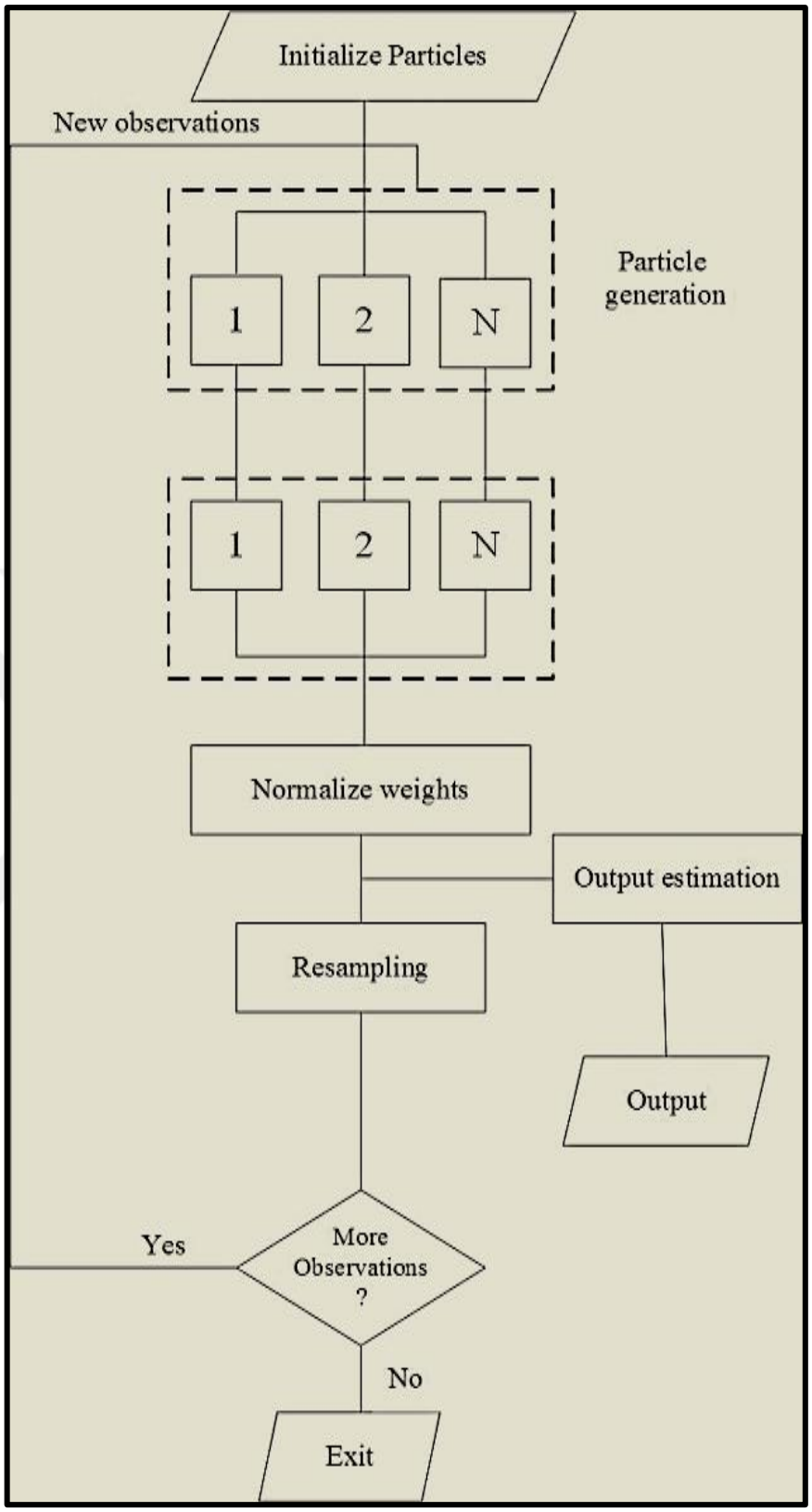

Figure 5.7 SIR algorithm's flowchart.

Require: px_0, pv_k, pw_k, observations $\boldsymbol{Z}_{1:K}$ and $\boldsymbol{U}_{1:K}$.
Ensure: $\hat{x}_k$ approximates x_k as $N_s \to \infty$.
Initialization: set $k = 0, \left\{x_0^{(i)}\right\}_{i=1}^{N_s} = \frac{1}{N_s}$ and generate N_s samples $\left\{x_0^{(i)}\right\}_{i=1}^{N_s}$ from p_{x_0}.
for k=1 to **K do**
for i=1 to N_s **do**
Sample $\tilde{x}_k^{(i)} \sim p\left(x_k | x_{k-1}^{(i)}\right) \leftrightarrow Generate\ v_{k-1} \sim p_{v_{k-1}}$ *and simulate*

$$\tilde{x}_k^{(i)} = Fx_{k-1}^{(i)} + Bu_{k-1} + Gv_{k-1}.$$

Evaluate importance weight $\tilde{\omega}_k^{(i)} = \tilde{\omega}_{k-1}^{(i)} p\left(z_k | \tilde{x}_k^{(i)}\right) = \omega_{k-1}^{(i)} pw_k \left(z_k - h\left(\tilde{x}_k^{(i)}\right)\right)$
end for
Normalize weight $\omega_k^{(i)} = \frac{\tilde{\omega}_k^{(i)}}{\sum_{i=1}^{N_s} \tilde{\omega}_k^{(i)}}$
Compute $\hat{N}_{eff} = \frac{1}{\sum_{i=1}^{N_s} \left(\omega_k^{(i)}\right)^2}$
if $\hat{N}_{eff} \geq N_{threshold}$ **then**
Set $x_k^{(i)} = \tilde{x}_k^{(i)}\ \forall i$
else
Resampling with replacement N_s particles $\left\{\tilde{x}_k^{(i)}\right\}_{i=1}^{N_s}$ according to the importance weights $\omega_k^{(i)}$
Reset weights to $\omega_k^{(i)} = \frac{1}{N_s}\ \forall i$
end if
Compute $\hat{x}_k = \sum_{i=1}^{N_s} \omega_k^{(i)} x_k^{(i)}$
end for

Figure 5.8 New resampling algorithm of MPF

5.5. A Brief Introduction to some Nonlinear Filters

For the state approximation the most public form is defined as recursive Bayesian estimation. This is the optimum method for any procedure of estimating a state pdf, given a measurement of a model and a system as:

$$\boldsymbol{x_k} = \boldsymbol{f}(\boldsymbol{x_{k-1}}, \boldsymbol{u_k}, \boldsymbol{v_k}) \tag{5.41}$$

$$\boldsymbol{y_k} = \boldsymbol{h}(\boldsymbol{x_k}, \boldsymbol{w_k}) \tag{5.42}$$

We shortly discuss these estimators in this part, recursively which computes for each time-step a new evaluate. Depending on the evaluate for the new measurements and former time step.

5.5.1. Unscented Kalman Filter

The filter begins by increasing the state vector to L dimensions, where L represents the dimension's sum in the vector of main state, deal with noise and its measurement. The covariance matrix to a L^2 matrix is likewise increased. Together this forms increased covariance matrix P^a and state evaluates vector x^a :

$$\boldsymbol{x}_{\boldsymbol{k-1}}^{\boldsymbol{a}} = \begin{bmatrix} \boldsymbol{x}_{\boldsymbol{k-1}} \\ \boldsymbol{0}_{\boldsymbol{w}} \\ \boldsymbol{0}_{\boldsymbol{v}} \end{bmatrix} \tag{5.43}$$

$$\begin{aligned} \boldsymbol{P}_{\boldsymbol{k-1}}^{\boldsymbol{a}} &= \boldsymbol{E}\{(\boldsymbol{x}_{\boldsymbol{k-1}}^{\boldsymbol{a}} - \widehat{\boldsymbol{x}}_{\boldsymbol{k-1}}^{\boldsymbol{a}})(\boldsymbol{x}_{\boldsymbol{k-1}}^{\boldsymbol{a}} - \widehat{\boldsymbol{x}}_{\boldsymbol{k-1}}^{\boldsymbol{a}})^{\boldsymbol{T}}\} \\ &= \begin{pmatrix} \boldsymbol{P}_{\boldsymbol{k-1}} & \boldsymbol{0} & \boldsymbol{0} \\ \boldsymbol{0} & \boldsymbol{Q}_{\boldsymbol{k-1}} & \boldsymbol{0} \\ \boldsymbol{0} & \boldsymbol{0} & \boldsymbol{R}_{\boldsymbol{k-1}} \end{pmatrix} \end{aligned} \tag{5.44}$$

In such a method the next step comprises of producing 2L+1 sigma-points that they jointly capture the entire covariance and mean of the increased state. To comprise these points the χ^a matrix is selected, and its columns are computed as follows:

$$\begin{aligned} \boldsymbol{\chi}_{\boldsymbol{0},\boldsymbol{k-1}}^{\boldsymbol{a}} &= \boldsymbol{x}_{\boldsymbol{k-1}}^{\boldsymbol{a}} && \boldsymbol{i} = \boldsymbol{0} \\ \boldsymbol{\chi}_{\boldsymbol{i},\boldsymbol{k-1}}^{\boldsymbol{a}} &= \boldsymbol{x}_{\boldsymbol{k-1}}^{\boldsymbol{a}} + (\boldsymbol{\alpha}\sqrt{\boldsymbol{L}\boldsymbol{P}_{\boldsymbol{k-1}}^{\boldsymbol{a}}})_{\boldsymbol{i}} && \boldsymbol{i} = \boldsymbol{1}, \cdots, \boldsymbol{L} \\ \boldsymbol{\chi}_{\boldsymbol{i},\boldsymbol{k-1}}^{\boldsymbol{a}} &= \boldsymbol{x}_{\boldsymbol{k-1}}^{\boldsymbol{a}} - (\boldsymbol{\alpha}\sqrt{\boldsymbol{L}\boldsymbol{P}_{\boldsymbol{k-1}}^{\boldsymbol{a}}})_{\boldsymbol{i-L}} && \boldsymbol{i} = \boldsymbol{L+1}, \cdots, \boldsymbol{2L} \end{aligned} \tag{5.45}$$

where the i-th column of the covariance matrix of the square root is represented by the character. The α parameter, in the period $0 < \alpha \leq 1$ calculates the spread sigma-point. Typically, this parameter is low, frequently around 0.001, to prevent the effects of non-local. The outcoming χ_{k-1}^{a} matrix can now be attenuated vertically into the χ_{k-1}^{x} rows, which comprises the state; χ_{k-1}^{v} rows, the χ_{k-1}^{w} rows, which comprises sampled process noise. A weight is also determined to each point of sigma point [82]. By comparing the moments of the sigma-points, these weights are required while presuming a Gaussian propagation with a Taylor series propagation of the models. The out coming weights for mean and covariance evaluated like that:

$$w_0^{(m)} = 1 - \frac{1}{\alpha^2} \qquad i = 0$$

$$w_0^{(c)} = 4 - \frac{1}{\alpha^2} - \alpha^2 \qquad i = 0$$

$$w_i^{(m)} = w_i^{(c)} = \frac{1}{2\alpha^2 L} \qquad i = 1, \cdots, 2L \tag{5.46}$$

By propagating the sigma-points through the measurement, the filter predicts the following cases and computing the covariance matrices with weighted mean:

$$\chi_{k|k-1}^{x} = f(\chi_{k-1}^{x}, u_k, \chi_{k-1}^{w}) \tag{5.47}$$

$$\hat{x}_{k|k-1} = \sum_{i=0}^{2L} w_i^{(m)} \chi_{k|k-1}^{x} \tag{5.48}$$

$$P_{k|k-1} = \sum_{i=0}^{2L} w_i^{(c)} \left[\chi_{k|k-1}^{x} - \hat{x}_{k|k-1}\right]\left[\chi_{k|k-1}^{x} - \hat{x}_{k|k-1}\right]^T \tag{5.49}$$

$$Z_{k|k-1} = h\left(\chi_{k|k-1}^{x}, \chi_{k-1}^{v}\right) \tag{5.50}$$

$$\hat{z}_{k|k-1} = \sum_{i=0}^{2L} w_i^{(m)} Z_{i,k|k-1} \tag{5.51}$$

By first computing of the state and covariance measurements of cross correlation matrices, the predictions are then updated which utilized with new measurements to calculate the Kalman acquisition:

$$P_{zz} = \sum_{i=0}^{2L} w_i^{(c)} [\, Z_{i,k|k-1} - z_{k|k-1}][Z_{i,k|k-1} - \hat{z}_{k|k-1}]^T \tag{5.52}$$

$$P_{xz} = \sum_{i=0}^{2L} w_i^{(c)} [\, \chi_{i,k|k-1}^{x} - \hat{x}_{k|k-1}][Z_{i,k|k-1} - \hat{z}_{k|k-1}]^T \tag{5.53}$$

$$K_k = P_{xz} P_{zz}^{-1} \tag{5.54}$$

$$\hat{x}_{k|k} = \hat{x}_{k|k-1} + K_k\left(z_k - \hat{z}_{k|k-1}\right) \tag{5.55}$$

$$P_{k|k} = P_{k|k-1} - K_k P_{yy} K_k^T \tag{5.56}$$

5.5.2. Centric Difference of Kalman Filter

CDKF is similar to UKF except in choosing groups of sigma-point and equating weights which are chosen as below:

$$\chi_{0,k-1}^{a} = x_{k-1}^{a} \qquad i = 0$$

$$\chi_{i,k-1}^{a} = x_{k-1}^{a} + (\alpha\sqrt{h^2 P_{k-1}^{a}})_i \qquad i = 1, \cdots, L \tag{5.57}$$

$$\chi_{i,k-1}^{a} = x_{k-1}^{a} + (\alpha\sqrt{h^2 P_{k-1}^{a}})_{i-L} \qquad i = L+1, \cdots, 2L$$

$$w_i^{(m)} = w_i^{(c)} = \frac{1}{2h^2} \qquad i = 1, \cdots, 2L \tag{5.58}$$

5.6. Ameliorating Reliability of Modified Particle Filter Depending on GPS Locating

The GPS signal is simple to be stopped by targets since it is in view, such as high trees and buildings. In this status, the GPS receiver locating error will get bigger or get vain, decreasing the accessibility of GPS locating information. And the symmetric errors caused by the influences of multipath signal, will direct to big locating error. In its application, the big issue from the real location is the deflection of locating. The GPS reliability of locating is mostly within 10m, but occasionally locating error can be more than 50m from real location [10, 83]. For this reason, the presentation is utilized to develop the reliability of the particle filtering algorithm of outdoor and indoor and GPS locating.

5.6.1. Characterization of the Motion Case

The output parameters of the GPS receiver in practical applications containing of latitude, longitude, speed, data of orientation angle. The equation of system case and the equation observation of system are put up according to the relevance between the acceleration, speed, and distance [21]. The algorithm just depends on the receiver of output GPS repeater information, no other supplementary equipment, so the algorithm can be utilized in the processing of the GPS data such as transfer position, cars, and ships. We suppose that the altitude is known and fixed in a civilian environment, so that it does not occur.

5.6.2. Incorporation of the System State Equation

Choosing the state variables of the dynamical model:

$$X = [x_e, v_e, a_e, x_n, v_n, a_n, b_t, m_t^T]^T \tag{5.59}$$

where x_e and x_n demonstrate the position element of the east and north, v_e and v_n are eastward and northward velocity elements of the receiver, a_e and a_n are the

precipitation set of east and north, b_t is the GPS clock offset, m_t^T comprise the multipath biases. T indicates the transfer of a matrix or vector. The GPS indicates for the longitude, latitude, and velocities over east and north respectively.

By the integration of the location, the velocity is acquired. As a Gauss Markov way, the clock drift of GPS is commonly characterized which is unified to produce the clock offset of GPS [84]. The state equation of the uninterrupted system is following:

$$\dot{\boldsymbol{X}}(\boldsymbol{t}) = \boldsymbol{A}\boldsymbol{X}(\boldsymbol{t}) + \boldsymbol{U} + \boldsymbol{W}(\boldsymbol{t}) \tag{5.60}$$

where

$$\boldsymbol{U} = \begin{bmatrix} \mathbf{0} \\ \mathbf{0} \\ \frac{\mathbf{1}}{\tau_e}\bar{\boldsymbol{a}}_{\boldsymbol{e}} \\ \mathbf{0} \\ \mathbf{0} \\ \frac{\mathbf{1}}{\tau_n}\bar{\boldsymbol{a}}_{\boldsymbol{n}} \end{bmatrix}, \quad \boldsymbol{W}(\boldsymbol{t}) = \begin{bmatrix} \mathbf{0} \\ \mathbf{0} \\ \boldsymbol{\omega}_{\boldsymbol{e}} \\ \mathbf{0} \\ \mathbf{0} \\ \boldsymbol{\omega}_{\boldsymbol{n}} \end{bmatrix} \tag{5.61}$$

where ω_e and ω_n yield noise. τ_e and τ_n are the acceleration change of the northward and eastward associated constant time. By acquiring the discrete state equation of the system and discretization the equation of the continuous system:

$$\boldsymbol{X}_{\boldsymbol{k}} = \emptyset_{\boldsymbol{k},\boldsymbol{k-1}}\boldsymbol{X}_{\boldsymbol{k-1}} + \boldsymbol{U}_{\boldsymbol{k}} + \boldsymbol{W}_{\boldsymbol{k}} \tag{5.62}$$

where,

$$\boldsymbol{X}_{\boldsymbol{k}} = [\boldsymbol{x}_{\boldsymbol{\varepsilon}}(\boldsymbol{k}) \quad \boldsymbol{v}_{\boldsymbol{\varepsilon}}(\boldsymbol{k}) \quad \boldsymbol{a}_{\boldsymbol{\varepsilon}}(\boldsymbol{k}) \quad \boldsymbol{x}_{\boldsymbol{n}}(\boldsymbol{k}) \quad \boldsymbol{v}_{\boldsymbol{n}}(\boldsymbol{k}) \quad \boldsymbol{a}_{\boldsymbol{n}}(\boldsymbol{k})]^{\boldsymbol{T}}$$
$$\emptyset_{\boldsymbol{k},\boldsymbol{k-1}} = \boldsymbol{diag}\{\emptyset_{\boldsymbol{e}(\boldsymbol{k},\boldsymbol{k-1})}, \emptyset_{\boldsymbol{n}(\boldsymbol{k},\boldsymbol{k-1})}\} \tag{5.63}$$

Assume, $\alpha_e = \frac{1}{\tau_e}, \alpha_n = \frac{1}{\tau_n}$ then, $\emptyset_{e(k,k-1)}$ and $\emptyset_{n(k,k-1)}$ are respectively:

$$\emptyset_{\boldsymbol{e}(\boldsymbol{k},\boldsymbol{k-1})} = \begin{bmatrix} \mathbf{1} & \boldsymbol{T} & \boldsymbol{\alpha}_{\boldsymbol{e}}^{\mathbf{-2}}(\mathbf{-1} + \boldsymbol{\alpha}_{\boldsymbol{e}}\boldsymbol{T} + \boldsymbol{e}^{-\alpha_e T}) \\ \mathbf{0} & \mathbf{1} & (\mathbf{1} - \boldsymbol{e}^{-\alpha_e T})\boldsymbol{\alpha}_{\boldsymbol{e}}^{\mathbf{-1}} \\ \mathbf{0} & \mathbf{0} & \boldsymbol{e}^{-\alpha_e T} \end{bmatrix}$$
$$\emptyset_{\boldsymbol{n}(\boldsymbol{k},\boldsymbol{k-1})} = \begin{bmatrix} \mathbf{1} & \boldsymbol{T} & \boldsymbol{\alpha}_{\boldsymbol{n}}^{\mathbf{-2}}(\mathbf{-1} + \boldsymbol{\alpha}_{\boldsymbol{n}}\boldsymbol{T} + \boldsymbol{e}^{-\alpha_n T}) \\ \mathbf{0} & \mathbf{1} & (\mathbf{1} - \boldsymbol{e}^{-\alpha_n T})\boldsymbol{\alpha}_{\boldsymbol{n}}^{\mathbf{-1}} \\ \mathbf{0} & \mathbf{0} & \boldsymbol{e}^{-\alpha_n T} \end{bmatrix}$$

$$\boldsymbol{U}_{\boldsymbol{k}} = [\boldsymbol{u}_1 \quad \boldsymbol{u}_2 \quad \boldsymbol{u}_3 \quad \boldsymbol{u}_4 \quad \boldsymbol{u}_5 \quad \boldsymbol{u}_6]^{\boldsymbol{T}} \tag{5.64}$$

In equation (5.65),

$$u_1 = [-T + 0.5\alpha_e T^2 + (1 - e^{-\alpha_e T})\alpha_e^{-1}]\alpha_e^{-1}\bar{a}_e$$
$$u_2 = [T - (1 - e^{-\alpha_e T})\alpha_e^{-1}]\bar{a}_e$$
$$u_3 = (1 - e^{-\alpha_e T})\bar{a}_e$$
$$u_4 = [-T + 0.5\alpha_n T^2 + (1 - e^{-\alpha_n T})\alpha_n^{-1}]\alpha_n^{-1}\bar{a}_n$$
$$u_5 = [T - (1 - e^{-\alpha_n T})\alpha_n^{-1}]\bar{a}_n$$
$$u_6 = (1 - e^{-\alpha_n T})\bar{a}_n$$
$$W_k = [0 \quad 0 \quad \omega_\varepsilon(k) \quad 0 \quad 0 \quad \omega_n(k)] \tag{5.65}$$

Also, the measurements of GPS that associated to the unknown state vector are non-linear. Accordingly, sequential Monte Carlo manners present a suitable structure for the approximation of the state vector as follows [85].

$$z_k = [\varphi_k^{GPS} \quad \lambda_k^{GPS} \quad v_k^{E,GPS} \quad v_k^{N,GPS}]^T \tag{5.66}$$

The GPS readings for the latitude, longitude and velocities were along East, and North respectively. The equation (5.67) indicates the measurement of the design:

$$z_k = \begin{bmatrix} \varphi_k^{GPS} \\ \lambda_k^{GPS} \\ v_k^{E,GPS} \\ v_k^{N,GPS} \end{bmatrix} = h(x_k, v_k) = \begin{bmatrix} \varphi_k + v_k^{\varphi} \\ \lambda_k + v_k^{\lambda} \\ v_k^f sinA_k + v_k^{v^E} \\ v_k^f cosA_k + v_k^{v^N} \end{bmatrix} \tag{5.67}$$

where $v_k = [v_k^{\varphi} \quad v_k^{\lambda} \quad v_k^{v^E} \quad v_k^{v^N}]^T$ is the GPS readings of the noise.

$$\delta_{x_k} = \begin{bmatrix} \delta_\varphi \\ \delta_\lambda \\ \delta_{v^E} \\ \delta_{v^N} \\ \delta A \\ \delta a^{od} \\ \delta\omega_z \end{bmatrix} = \left[I_{7\times7} + \begin{pmatrix} 0 & 0 & 0 & \frac{1}{R_M+h} & 0 & 0 & 0 \\ 0 & 0 & \frac{1}{(R_N+h)cos\varphi} & 0 & 0 & 0 & 0 \\ 0 & 0 & -a^{od}sinA & cosA & 0 & & \end{pmatrix} \Delta t \right] \begin{bmatrix} \delta_\varphi \\ \delta_\lambda \\ \delta_{v^E} \\ \delta_{v^N} \\ \delta A \\ \delta a^{od} \\ \delta\omega_z \end{bmatrix} +$$
$$\begin{bmatrix} 0 \\ 0 \\ 0 \\ 0 \\ 0 \\ \sqrt{2\gamma_{od}\sigma_{od}^2} \\ \sqrt{2\beta_z\sigma_z^2} \end{bmatrix} w_{k-1} \tag{5.68}$$

5.7. An Approximation of Modified Particle Filtering

The unknown parameters interference in a Bayesian structure is depending on the posterior distribution. By evaluating the posterior pdf of the increased state vector $(X_{0:t}, \lambda_{0:t})$, the connected approximation on the GPS measurements of the multipath influences is directed dependent on the measurements up to the present time, expressed as $p(X_{0:t}, \lambda_{0:t}|Y_{1:t})$. A Bayes's formula of recursive application permits to obtain an impracticable outcome to the approximation problem. To produce the pdf posterior of the multipath biases and the navigation cases, the point procedure can be marginalised out:

$$\boldsymbol{p(X_t|Y_{1:t}) = \sum_{i=1}^{n_\Lambda^t} \omega_t^{(i)} p\left(X_t|Y_{1:t}, \lambda_{0:t}^{(i)}\right)} \tag{5.69}$$

where

$$\boldsymbol{\omega_t^{(i)} = P\left[\lambda_{0:t}^{(i)}|Y_{1:t}\right]} \tag{5.70}$$

$$\boldsymbol{\omega_t^{(i)} \propto \prod_{k=1}^{t} p\left(Y_k|\lambda_{0:t}^{(i)}, Y_{1:k-1}\right) P\left[\lambda_k^{(i)}\right]} \tag{5.71}$$

The pdfs $p\left(X_t|Y_{1:t}, \lambda_{0:t}^{(i)}\right)_{t>0}$ and $p\left(Y_k|\lambda_{0:t}^{(i)}, Y_{1:k-1}\right)_{k=1:t}$ gave the nonlinearities of the measurement design. Nevertheless, in an exponential manner rising the sum in (5.69) encases number of discrete series $\lambda_{0:t}$. An exception manner requires to be utilised to save the complexness of computational invariable [86]. Many manners which are depending either on a combining strategy or pruning have been improved in the literature. To develop multipath bias tracking, a precise choice of the particles at each time step permits even if few schemes are utilized. Regarding to a combination of resampling/sampling steps and on the most likely ways $\lambda_{0:t}$ the MPF is centred.

5.7.1. The Procedure of Resampling Method

A straightforward utilize of the statistic test that demonstrate the improper possibility would comprise of instantly discarding particles. However, the properties of PF would not be warranted anymore. As an alternate for the step of resampling, and to design a more effective proposal of distribution, the outcome of the hypothesis test can be utilized for the MPF. The possible flexibility has already been emphasised in selecting the resampling weights [87]. According to the weights of filtering and

instead of resampling, additional weights that reverberate definite "future trend "may be utilized. According to the rule of grandness sampling, the corrected weights are specified by the new group of produced particles, herewith including that the random samples still form an estimation of the object distribution $P[\lambda_t|Y_{1:t}]$. If a jump of the mean is observed, the next rule can be used to calculate the weights of auxiliaries:

$\alpha_t^{(i)} = (\widetilde{w}_t^{(i)})^{\beta}$ for the particles which differ from the outcome of the test;

$\alpha_t^{(i)} = \widetilde{w}_t^{(i)}$, otherwise;

Where the penalisation coefficient $\beta(\beta > 1)$ as the opportunity can be construed that the related particles continue after a few iterations. The modified resampling runs at random choosing a particle $\lambda_t^{(i)}$ from $\{\lambda_t^{(k)}\}_{k=1:N}$ with probability $\alpha_t^{(k)}$. Then the particle allocates the weight of filtering $w_t^{(i)} = w_t^{(k^i)}/\alpha_t^{(k^i)}$ when sample $\lambda_t^{(k^i)}$ is chosen. By favouring the particles which are more likely to live on, this technique at the next time steps assures that to model the particles an effective design are utilized. It can be analysed as an attempt to minimize the variance of the importance weights of MPF. The algorithm permitting us to evaluate the indicator sequence $\lambda_{0:t}$ and the state vector X_t.

5.7.2. Establishment of the Observance Equation

The evaluation of the state vector that constructed by the receiver of GPS is depending on the measurements of satellite [88]. In the following, Z_t represents the measurement vector saving the measurements of GPS at time t from n_t satellites. n_t is probable to change with time due to the geometry of the satellites and the receiver. The output of GPS receiver east position data Z_e, the information of north location Z_n, speed v and angle direction θ are the measurement parameters. The vector defined by:

$$\boldsymbol{Z} = [\boldsymbol{z_e} \quad \boldsymbol{z_n} \quad \boldsymbol{v} \quad \boldsymbol{\theta}]^{\boldsymbol{T}} \tag{5.72}$$

Assuming sampling period T=1s. Then, the relevance between the state parameters and the value of measurement are as follows:

$$\boldsymbol{z_e} = \boldsymbol{x_e} + \boldsymbol{\varepsilon_e}$$

$$z_n = x_n + \varepsilon_n$$
$$v = \sqrt{v_e^2 + v_n^2} + \varepsilon_v$$
$$\theta = arctan\frac{v_e}{v_n} + \varepsilon_\theta \tag{5.73}$$

Thus, the continuous observation equation:

$$Z = \begin{bmatrix} z_e \\ z_n \\ v \\ \theta \end{bmatrix} = \begin{bmatrix} x_e \\ x_n \\ \sqrt{v_e^2 + v_n^2} \\ arctan\frac{v_e}{v_n} \end{bmatrix} + \begin{bmatrix} \varepsilon_e \\ \varepsilon_n \\ \varepsilon_v \\ \varepsilon_\theta \end{bmatrix} \tag{5.74}$$

where ε_e and ε_n represent the reflection noise by GPS receiver of north and east outcome, which can be almost utilized as $(0, \sigma_e^2), (0, \sigma_n^2)$ gaussian white noise. ε_v and ε_θ are the reflection noise of the direction of angle and the speed, which can be almost utilized as $(0, \sigma_v^2), \left(0, \sigma_\theta^2\right)$ non gaussian distribution of white noise. In order to be calculated, the equation of discrete observation is:

$$Z_k = h(X_k) + V_k \tag{5.75}$$

where,

$$Z_k = [z_e(k) \quad z_n(k) \quad v(k) \quad \theta(k)]^T$$
$$h(X_k) = \begin{bmatrix} x_\varepsilon(k) \\ x_n(k) \\ \sqrt{v_\varepsilon^2(k) + v_n^2(k)} \\ arctan\dfrac{v_\varepsilon(k)}{v_n(k)} \end{bmatrix}$$
$$V(k) = \begin{bmatrix} \varepsilon_e(k) \\ \varepsilon_n(k) \\ \varepsilon_v(k) \\ \varepsilon_\theta(k) \end{bmatrix} \tag{5.76}$$

From the above equation, the observation equation is non-linear, by Taylor series the MPF is extended at disregard the second order and at the prognostic value:

$$Z_k = h\left(\widehat{X}_{k,k-1}\right) + H_k\left(X_k - \widehat{X}_{k,k-1}\right) + V_k \tag{5.77}$$

To be simplified,

$$Z_k = H_k X_k + V_k + h\left(\widehat{X}_{k,k-1}\right) + H_k \widehat{X}_{k,k-1} \tag{5.78}$$

Where,

$$\boldsymbol{H_k} = \frac{\boldsymbol{\partial h(X_k)}}{\boldsymbol{\partial X_k}}\Big|_{\boldsymbol{X_k=\hat{X}_{k,k-1}}} = \begin{bmatrix} \boldsymbol{1} & \boldsymbol{0} & \boldsymbol{0} & \boldsymbol{0} & \boldsymbol{0} & \boldsymbol{0} \\ \boldsymbol{0} & \boldsymbol{0} & \boldsymbol{0} & \boldsymbol{1} & \boldsymbol{0} & \boldsymbol{0} \\ \boldsymbol{0} & \boldsymbol{h_1} & \boldsymbol{0} & \boldsymbol{0} & \boldsymbol{h_2} & \boldsymbol{0} \\ \boldsymbol{0} & \boldsymbol{h_3} & \boldsymbol{0} & \boldsymbol{0} & \boldsymbol{h_4} & \boldsymbol{0} \end{bmatrix}$$

$$\boldsymbol{h_1} = \frac{\boldsymbol{v_e}}{\sqrt{\boldsymbol{v_e^2 + v_n^2}}}$$

$$\boldsymbol{h_2} = \frac{\boldsymbol{v_n}}{\sqrt{\boldsymbol{v_e^2 + v_n^2}}}$$

$$\boldsymbol{h_3} = \frac{\boldsymbol{v_n}}{\boldsymbol{v_e^2 + v_n^2}}$$

$$\boldsymbol{h_4} = \frac{\boldsymbol{-v_e}}{\boldsymbol{v_e^2+v_n^2}} \tag{5.79}$$

5.7.3. Data Filtering of Modified Particle Filter for GPS Locating

The elaborated description of modified particle filter algorithm is utilized to develop locating accuracy of GPS from repeater as follows:

(1) Initialization of particle group, k=0:

At the start value X_θ point, N particles are created according to the density of prior probability, particle groups $\{X_\theta^i\}_{i=1}^N$, and putting the initialisation weight value $\omega_0^{(i)} = 1/N$. For $k = 1,2,\cdots,n$. Applying the following steps:

(a) From state equation the priori particles of state prognosis of the system are extracted at time k,

$$\boldsymbol{\{X_{k|k-1}(i): i = 1, 2, \cdots, N\} \sim p(X_k|X_{k-1})} \tag{5.80}$$

(b) The value of weight is updated after the calculated values are accomplished. Depending on the observation equation of the system, the error between the calculated values and the predicted values are used to modify the weight particle, then the weight are computed as follows:

$$\boldsymbol{q_k^i} = \frac{\boldsymbol{1}}{\sqrt{\boldsymbol{2\pi\sigma}}}\boldsymbol{e}^{\frac{\boldsymbol{-(z_k - h(X_k^i))^2}}{\boldsymbol{2\sigma^2}}} \tag{5.81}$$

The weight is normalised:

$$\boldsymbol{\tilde{q}_k^i} = \frac{\boldsymbol{q_k^i}}{\boldsymbol{\sum_{i=1}^N q_k^i}}, \boldsymbol{\sum_{i=1}^N \tilde{\tilde{q}}_k^i = 1} \tag{5.82}$$

(2) Resampling: In order to keep the several of particle samples, the method of Markov Monte Carlo has been utilized to suppress the degradation problem of particle [89]. A new particle group is formed after the sampling, that is $\{\tilde{X}_k^i, i = 0,1,2,\cdots,N\}$. The outcomes in a poorness of the particle system are the resampling step.

(3) Approximation the state of time k parameters $\hat{X}_k$ is predicted by utilizing the group of particles.

(4) Set K=k+1 and go to step (2).

Problematic is that the sequential importance sampling eventually leads to so called weight degeneracy. That is, all but one weight will turn to zero. In a crucial resampling step, in which particles are discarded or duplicated according to their weights, was introduced to counteract this problem. The degree of degeneracy can be assessed by the efficient number of particles (approximately) given by:

$$\boldsymbol{N_{eff}} = \frac{\mathbf{1}}{\sum_{\boldsymbol{i=1}}^{\boldsymbol{N}} (\boldsymbol{w^{(i)}})^{\mathbf{2}}} \tag{5.83}$$

Resampling can be applied whenever N_{eff} falls below a threshold [90]. An approximate marginal filtering density can be obtained by extracting $\{x_k^{(i)}, w_k^{(i)}\}_{i=1}^N$ from $\{x_{0:k}^{(i)}, w_k^{(i)}\}_{i=1}^N$. The algorithm is initialized with appropriate particles and weights $\{x_0^{(i)}, w_0^{(i)}\}_{i=1}^N$. The method proposed in targets is the marginal smoothing distribution. It is sometimes referred to as forward filter backward smoother. The particles from the filtering step are kept but assigned new weights. Initialized with the filtering weights $\{w_K^{(i)}\}_{i=1}^N$ the following update is performed for k=K-1 to k=0:

$$\bar{\boldsymbol{w}}_{\boldsymbol{k}}^{(\boldsymbol{i})} = \sum_{\boldsymbol{j=1}}^{\boldsymbol{N}} \bar{\boldsymbol{w}}_{\boldsymbol{k+1}}^{(\boldsymbol{j})} \frac{\boldsymbol{w}_{\boldsymbol{k}}^{(\boldsymbol{i})} \boldsymbol{p}\left(\boldsymbol{x}_{\boldsymbol{k+1}}^{(\boldsymbol{j})} | \boldsymbol{x}_{\boldsymbol{k}}^{(\boldsymbol{i})}\right)}{\sum_{\boldsymbol{l=1}}^{\boldsymbol{N}} \boldsymbol{w}_{\boldsymbol{k}}^{(\boldsymbol{l})} \boldsymbol{p}\left(\boldsymbol{x}_{\boldsymbol{k+1}}^{(\boldsymbol{j})} | \boldsymbol{x}_{\boldsymbol{k}}^{(\boldsymbol{l})}\right)} \tag{5.84}$$

This category of algorithms permits not just non-Gaussian and/or nonlinear designs to be dealt with, but also sate vectors consisting discrete and continuous variables.

5.8. The Algorithm of Resampling

The drawing of a new particle group is the aim of the resampling algorithm that is supporting the mean of the old one, but formed by new particles with their weights reset to 1/NP. The resampling step is essential to prevent depletion of the particle [85, 91], an undesired phenomenon of particle filters to a single state point where the particle group collapses provoking the filter for the estimation being no longer able to explore new solutions, therefore flexible the robustness of the solution. Several methods are proposed for resampling step. This section overviews the used method, the regularized resampling, and also outlines an alternative method as a suggestion that could improve results in future works.

5.8.1. Regularized Resampling

The implemented resampling solution presented in this thesis is the regularized resampling method [5]. Being P^t the current particle set after correction and normalization, the resampling begins creating a sorted version of that set, labelled as, $\tilde{P}^t$, where the order is established by the particle weights, starting from the most important particle:

$$\widetilde{\boldsymbol{P}}^{\boldsymbol{t}} = \left\{ \left\{ (\boldsymbol{X}_{\boldsymbol{1}}^{\boldsymbol{t}}, \boldsymbol{w}_{\boldsymbol{1}}^{\boldsymbol{t}}), \cdots, \left(\boldsymbol{X}_{\boldsymbol{N_P}}^{\boldsymbol{t}}, \boldsymbol{w}_{\boldsymbol{N_P}}^{\boldsymbol{t}}\right) \right\} | \boldsymbol{w}_{\boldsymbol{j}}^{\boldsymbol{t}} \geq \boldsymbol{w}_{\boldsymbol{j}}^{\boldsymbol{t}} \Leftrightarrow \boldsymbol{i} < \boldsymbol{j}, \forall (\boldsymbol{X}_{\boldsymbol{i}}^{\boldsymbol{t}}, \boldsymbol{w}_{\boldsymbol{i}}^{\boldsymbol{t}}) \in \boldsymbol{P}^{\boldsymbol{t}} \right\} \quad (5.85$$

Once the $\tilde{P}^t$ set is built, a cumulative weight for each particle in $\tilde{P}^t$ is assigned as:

$$\boldsymbol{cw}_{\boldsymbol{i}}^{\boldsymbol{t}} = \sum_{\boldsymbol{j=1}}^{\boldsymbol{i}} \boldsymbol{w}_{\boldsymbol{j}}^{\boldsymbol{t}} \quad (5.86)$$

The computation of these cumulative weights provides a cumulative distribution function of the particle weights over the index i, as it is shown in the Figure 5.9. With such a function, the resampling process draws a random number uniformly distributed, $r \in [0,1]$, and the selected particle to be resampled is:

$$\boldsymbol{X}_{\boldsymbol{R}}^{\boldsymbol{t}} = \boldsymbol{X}_{\boldsymbol{j}}^{\boldsymbol{t}} \in \widetilde{\boldsymbol{P}}^{\boldsymbol{t}} | \boldsymbol{cw}_{\boldsymbol{j-1}}^{\boldsymbol{t}} < \boldsymbol{r} < \boldsymbol{cw}_{\boldsymbol{j}}^{\boldsymbol{t}}, \boldsymbol{r} \sim \boldsymbol{rand}(\boldsymbol{0}, \boldsymbol{1}) \quad (5.87)$$

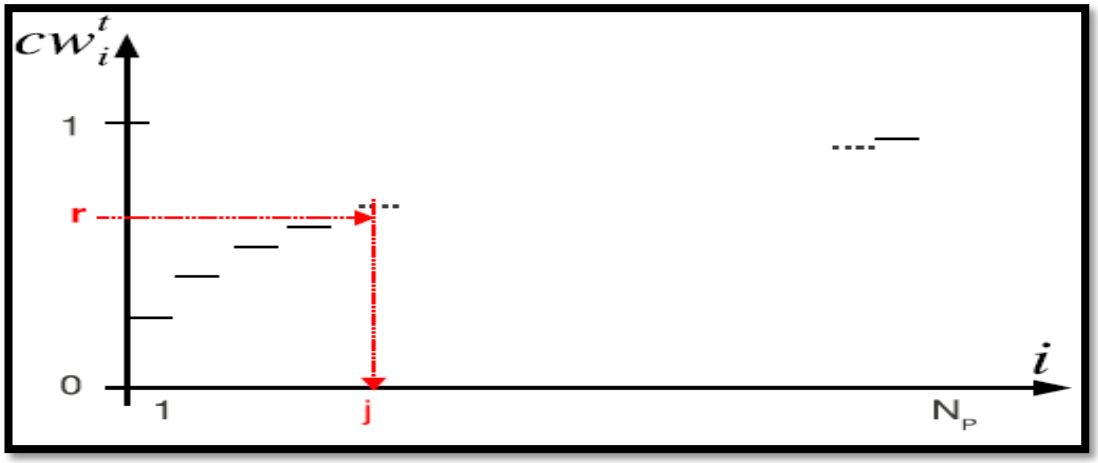

Figure 5.9 Particle index of weights

To avoid the particle depletion phenomenon, a resampling noise, is added when drawing the new particle X_i^t from the selected one X_R^t. This noise should be small with respect to the uncertainty introduced by the probabilistic kinematic model used at the propagation step [92]. Resampling noise is parameterized with a covariance matrix C_γ. Figure 5.10 summarizes the regularized resampling algorithm.

INPUT: P^t, C_γ
Resampled the posterior version (output): P^t
$\bar{P}^t \leftarrow arrangeUsingWeight\ (P^t)$
for $i = 1 \cdots N_P$ **do**
$cw_i^t = \sum_{j=1}^{i} w_j^t$
end for
for $i = 1 \cdots N_P$ **do**
$n = rand(0,1)$
$X_R^t = X_j^t \in \bar{P}^t, j = min\, k, cw_k^t > r$
$X_i^t \sim \aleph(X_R^t, C_\gamma)$
end for
$P^t = \{X_i^t\}, i = 1 \cdots N_P$

Figure 5.10 Regularization of the Resampling algorithm [60]

5.8.2. Low Variance Resampling

Low variance resampling is an alternative method for resampling, where only a random number, $r \in \left[0, \frac{1}{N_P}\right]$, is drawn to choose the first particle to be resampled [90]. From that random value, the rest of the particles are chosen. Adding $1/N_P$ to that initial value in the way indicated in the Figure 5.11 by resampling algorithm of

low variance. This method is quite more efficient in terms of complexity because of it does not need to sort the particle set and it only uses a single random number.

INPUT: P^t, C_γ
Resampled the posterior version (output): P^t
for $i = 1 \cdots N_P$ ***do***
$cw_i^t = \sum_{j=1}^{i} w_j^t$
end for
$n = rand(0, \frac{1}{N_P})$
for $i = 1 \cdots N_P$ ***do***
$X_R^t = X_j^t \in P^t, j = min\, k, cw_k^t > r$
$X_i^t \sim \aleph(X_R^t, C_\gamma)$
$n = n + \frac{1}{N_P}$
end for
$P^t = \{X_i^t\}, i = 1 \cdots N_P$

Figure 5.11 Resampling algorithm of low variance [42]

CHAPTER 6

EXPERIMENTAL RESULTS

6.1. GPS L1 Repeater

The L1 repeater unit has an efficient comprehensive coverage of 35-40 metres radius from the centre. The signal is eradiating in a cone-shaped model that has a 140 degree angle of view built-in antenna. The SMA socket connects to the extrinsic antenna feeder cable; in order to power the LNA through the coaxial cable, so the repeater sends 5V DC through it. An extra repeater will be added if a bigger area of encasement is required, by the use of a line amplifier and/or a GPS signal splitter, where all using a primary outdoor antenna [93]. By the availability of outdoor antenna, the GPS repeater can exaggerate the signal and makes that signal available indoor as shown in Figure 6.1.

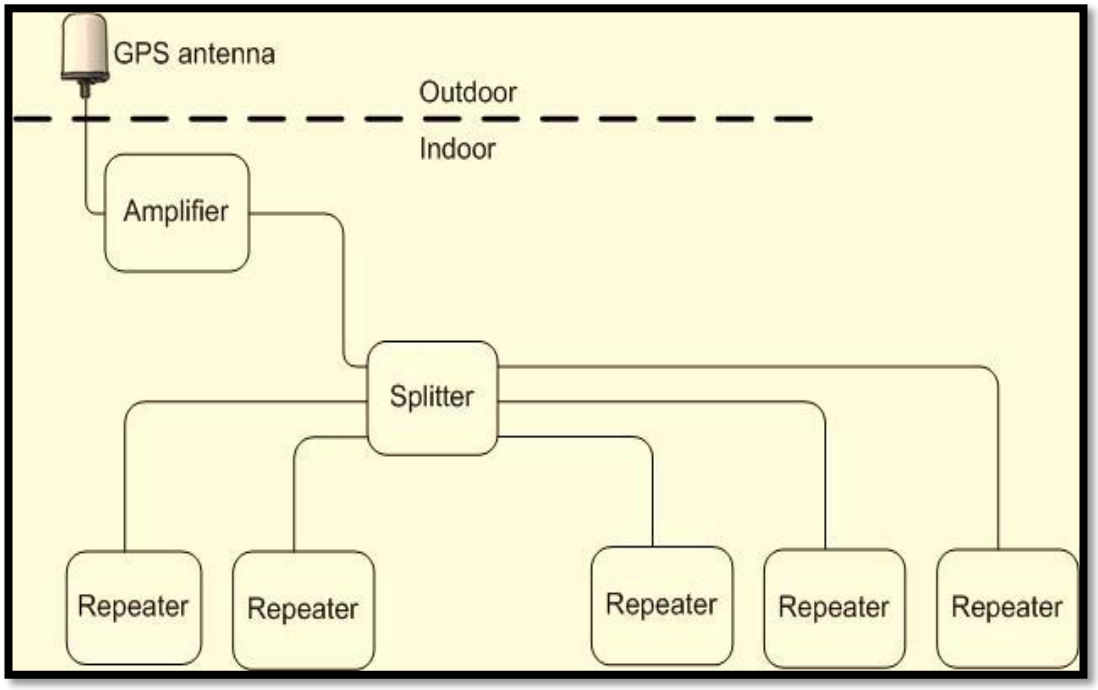

Figure 6.1 Distribution of the signal to repeaters

In our experiment, we have used GPS repeater with a high-gain antenna (HGA) of one meter; which gave us more accurate results as shown below in Figure 6.2.

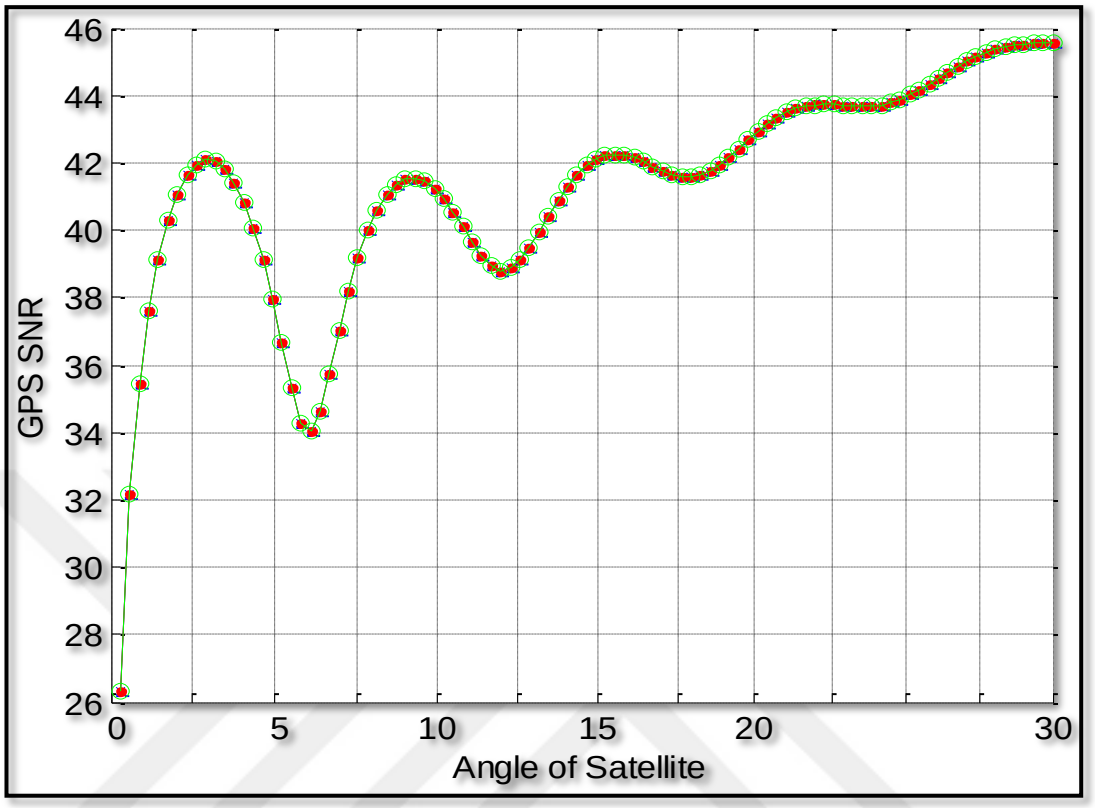

Figure 6.2 Observations of GPS signal to noise ratio

The estimates of SNR technique and the investigation of its performance are shown in Figure 6.2. Where the SNR data are recorded by the GPS receiver and the repeater is used for computing the distance between the receiving antenna and assumed horizontal reflecting surface using the SNR interference pattern. As we can see from the Figure 6.2, the increase in SNR by 30 angles in the red line; which represent our approximation; is near to the original estimation (Green line) that indicates the high accuracy of our system with the estimated high antenna. The SNR designated can be described by:

$$\boldsymbol{SNR = A\cos(\theta + \varphi) = A\cos(\frac{4\pi y}{\lambda}\sin\epsilon + \varphi)} \quad (6.1)$$

where the amplitude is defined by A (based on the antenna gain pattern and the reflecting surface's characteristics), φ defines the phase offset and θ defines the SNR phase. The SNR phase relies on y, that defines the distance between the reflecting

surface and the antenna phase centre (also named as reflector height), λ defines the wavelength of GPS carrier, and ϵ defines the satellite elevation's angle.

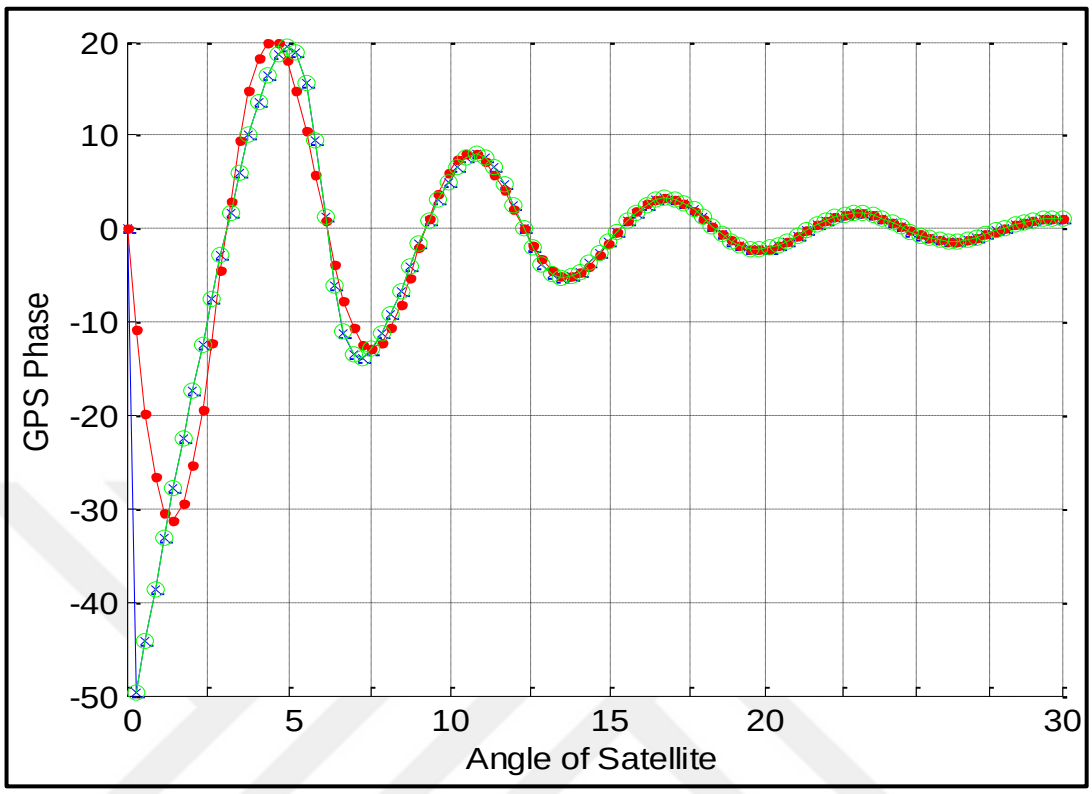

Figure 6.3 observations of indoor GPS phase

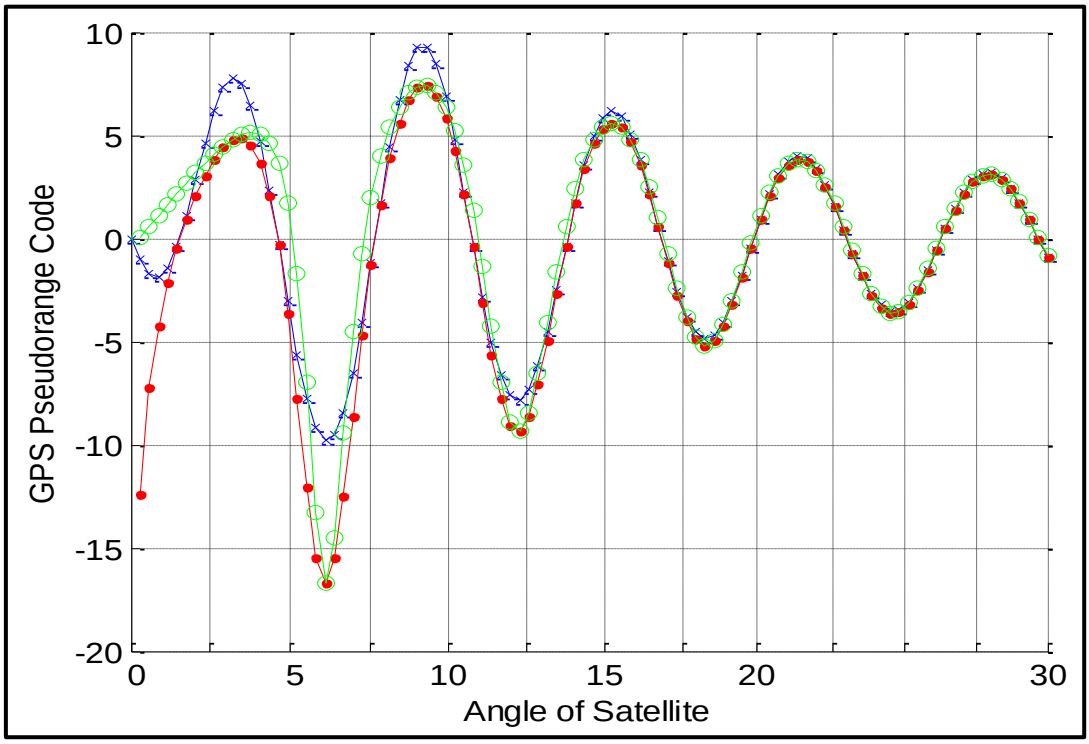

Figure 6.4 Observations of indoor GPS pseudo range code

The antenna has installed perpendicularly on a1-m-high for the results in Figure 6.3 and Figure 6.4. Also, the accurate solution is presented in the two figures by the green form, the approximations by blue form, and the red form represents the small-delay estimation. So the antenna would introduce a fewer artefacts in the position time when it is nearer to the ground. Also, a high antenna would look preferable because multipath errors would be most likely average to zero. Although the indoor GPS pseudo-range error in Figure 6.3 rises without bound in ratio to reverberate height, but indoor GPS phase observations in Figure 6.4 are more significant for long positioning. So, high antennas are more preferable according to the above results.

6.2. Comparison of Performance Results

Figure 6.5 presents the experimental results of different filters. Using the MPF with bias tracking has led to a reduction in both variance (from 15m to less than 3m in the standard deviation) and positioning error (from 25 to 10 m). Therefore, this tracking was a key factor of this reduction gain. The mean square is presented in the TOA estimates with the bias tracking in Figure 6.6.

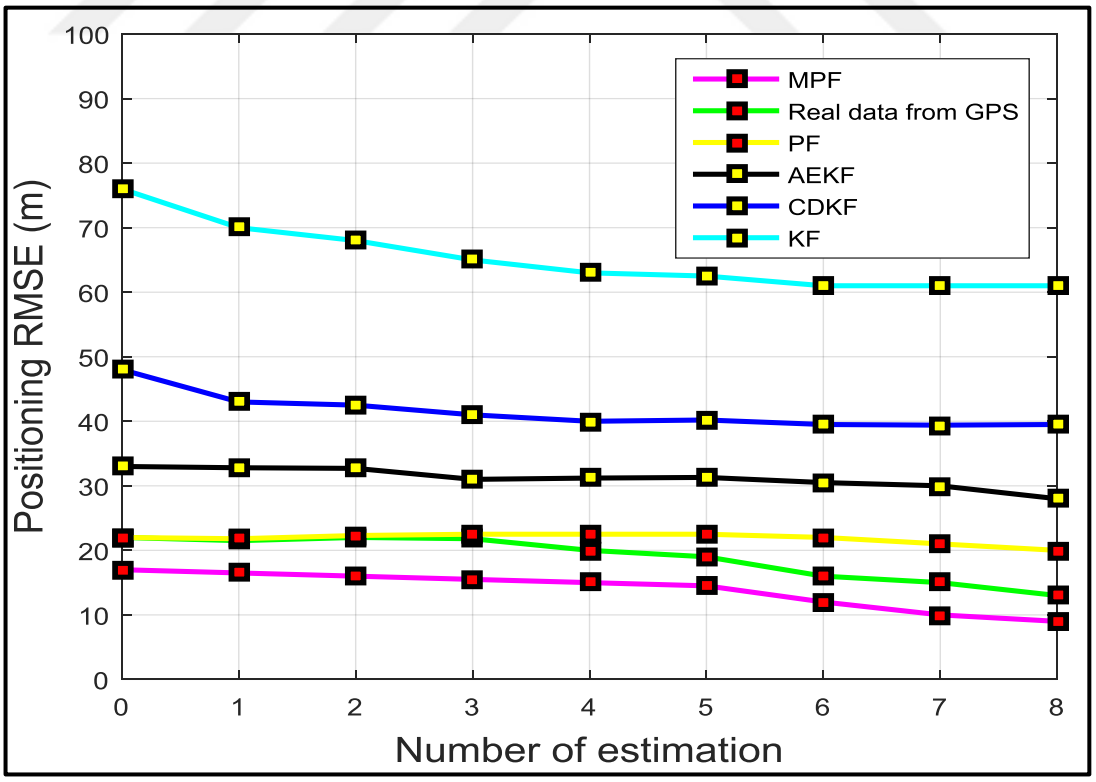

Figure 6.5 RMSE from measurement of four filters

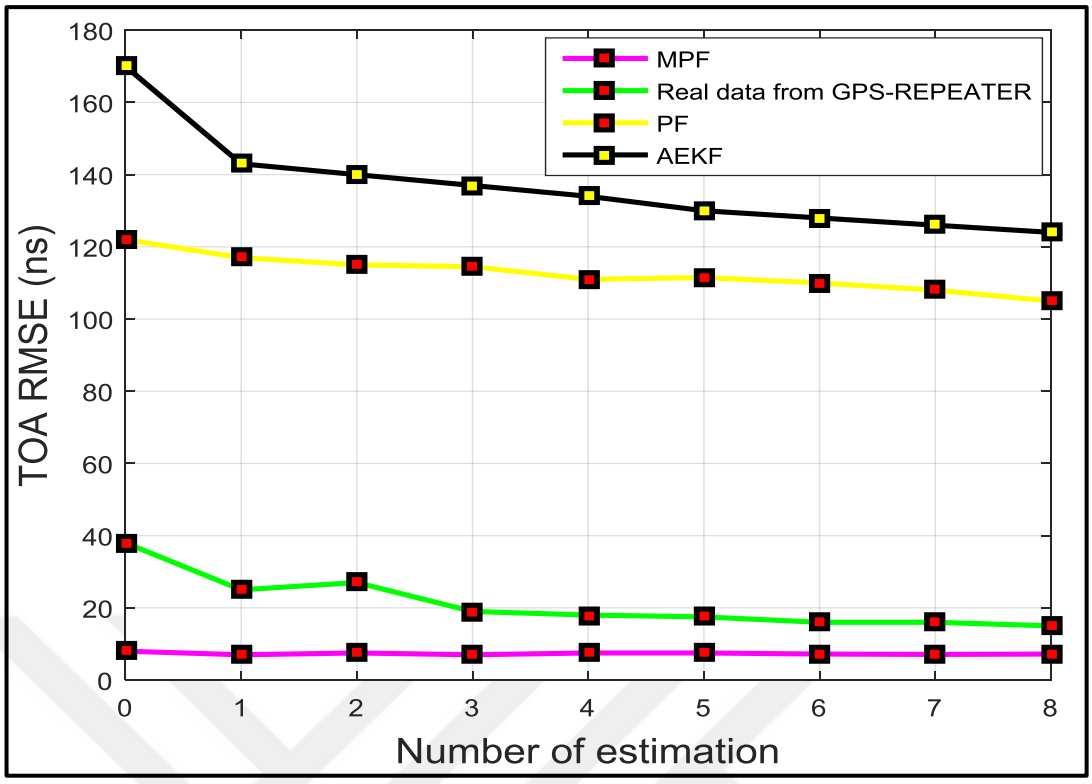

Figure 6.6 TOA RMSE measures of four filters

The execution of the Bayesian filters (MPF) for the structure has been analysed by the computer. The basic features of the reformed environment are outlined in Table 6.1. A receiver utilizing navigation signal of the civilian GPS C/A which has a precorrelation filter of a 1.1 MHz cutoff frequency, and the signal is digitized at 4.308 MHz central frequency of a sampling rate $f_s = 5.714\,MHz$. The results are arranged in a duplicate baseband based on this frequency of the signal's interest. The time of reflection is equal to 1 ms. The reformed scenario is related to a naturalistic geometry of elevation equal to (8^0), M=6 visible satellites with a nominal C/N_0 of 45-dB-Hz. The elevation of the simulated satellites, azimuth, and PRN code numbers are presented in Table 6.2.

Table 6.1 Produced signal parameters

Parameter	Value	Units
$\mathbf{r_c}$	1.023	MHz
$\mathbf{f_s}$	40/7. r_c	MHz
B	1.1	MHz
$\boldsymbol{k/f_s}$	10^{-3}	s
M	6	-
PRN	6-10-15-17-23-26	-
Elev.cutoff	8^0	degrees

Table 6.2 Azimuth and highness values of the apparent satellites

PRN	6	10	15	17	23	26
Azimuth	4	195	77.3	240	155	65
Elevation	5	26.2	33.4	36.1	78.6	29.4

For the latter, two numbers of particles were utilized, one fitness with number of originated MPF sigma points $(N_s) = 2N_x$, and other of $N_s = 500$ particles. The position RMSE was computed in meters after 5s of a process as shown in Figure 6.7 and Figure 6.8. As the summation of the square root, the RMSE is calculated for squared coordinate errors, averaged overruns of 50 Monte Carlo. The algorithm's real capability was developed by adding more correlation samples using resampling algorithm with a new weight as demonstrated in the results. However, raising the particles' weight with resampling algorithm leads to developments in the MPFs algorithm at the income of a greater computational price.

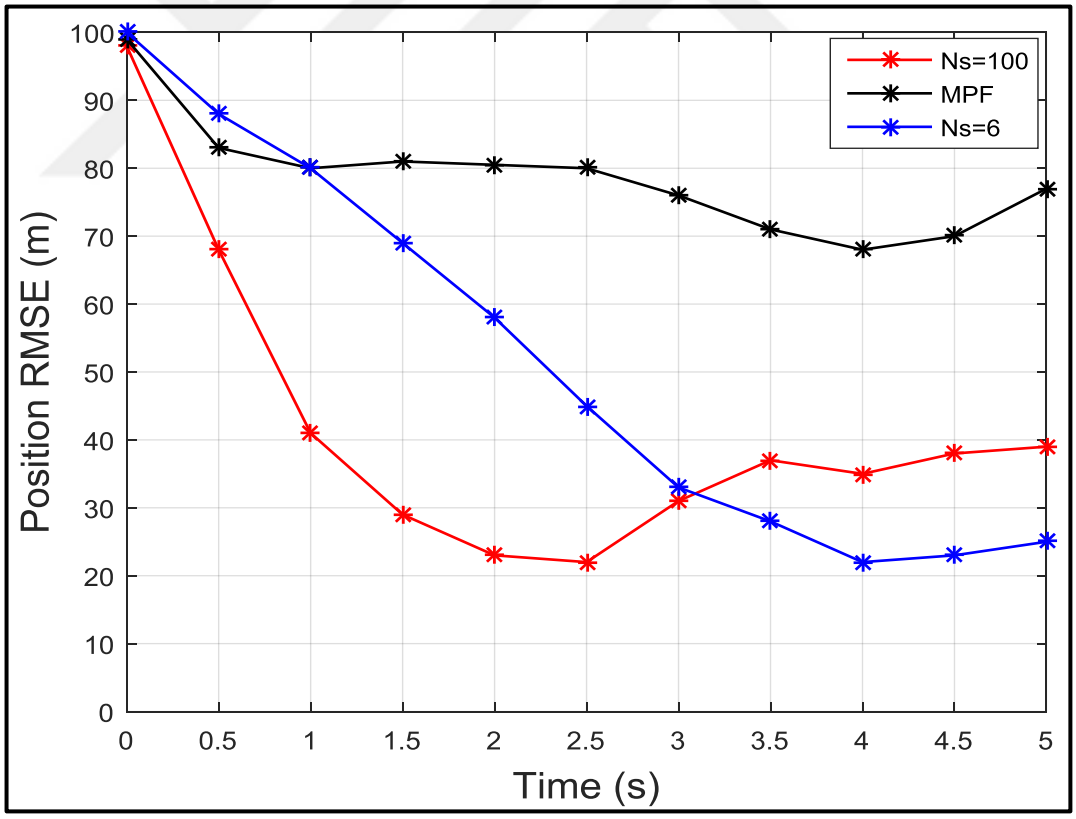

Figure 6.7 Position RMSE with $L_c = 6$ correlation samples

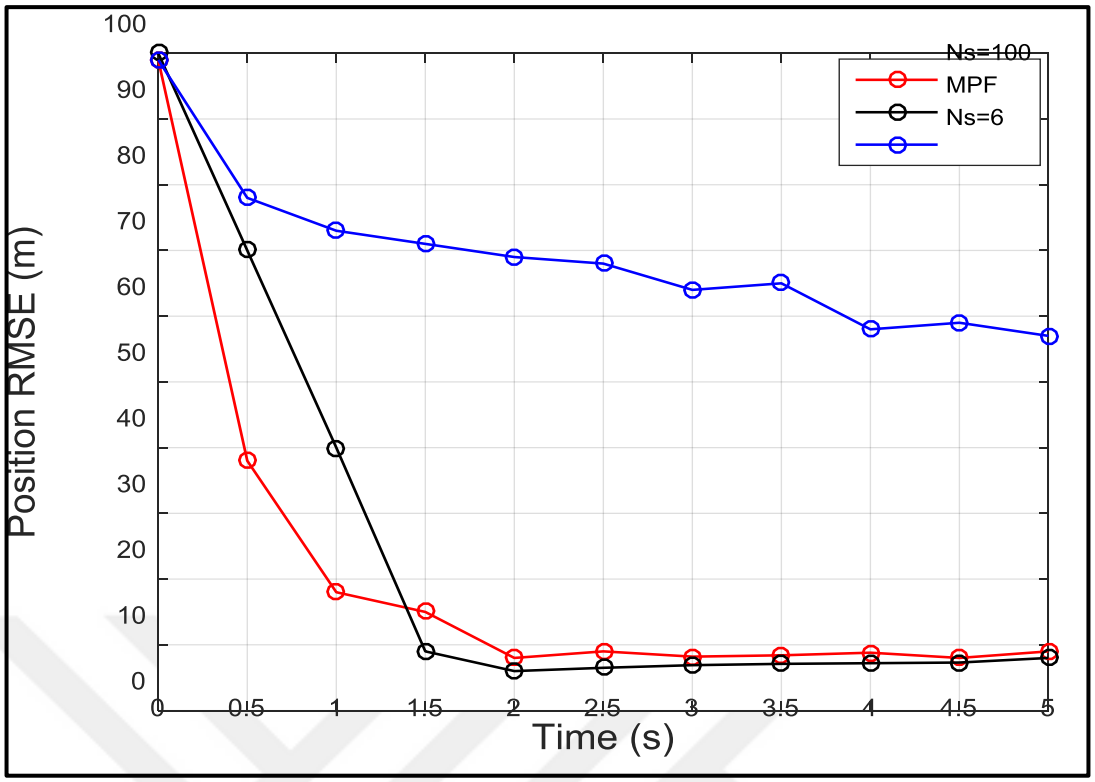

Figure 6.8 Position RMSE with $L_c = 10$ correlation samples

6.3. Influence of the Modified Particle Filter

In our implementation of modified particle filter, the MPF has been accomplished with $N_s = 500$ particles with a term between two consecutive computations $\Delta t_k = 500\ ms$. The key elements of the mobility designs are: $\sigma_p = 0.6$ m, $\sigma_p = 0.28$, $\sigma_p = 0.4$ m, $\sigma_p = 0.09$ m (with fixed speed), $\sigma_p = 0.051$ m (with inconstant speed), $\sigma_p = 0.06$ m. The effect of the mobility design in positioning is examined in Figures 6.9 and 6.10 where the error CDFs of the position acquired with the mobility designs have been associated with the CDF acquired when the mobility design isn't utilized. Thus, the mobility design improves the actual motion of the target and influence of the positioning system.

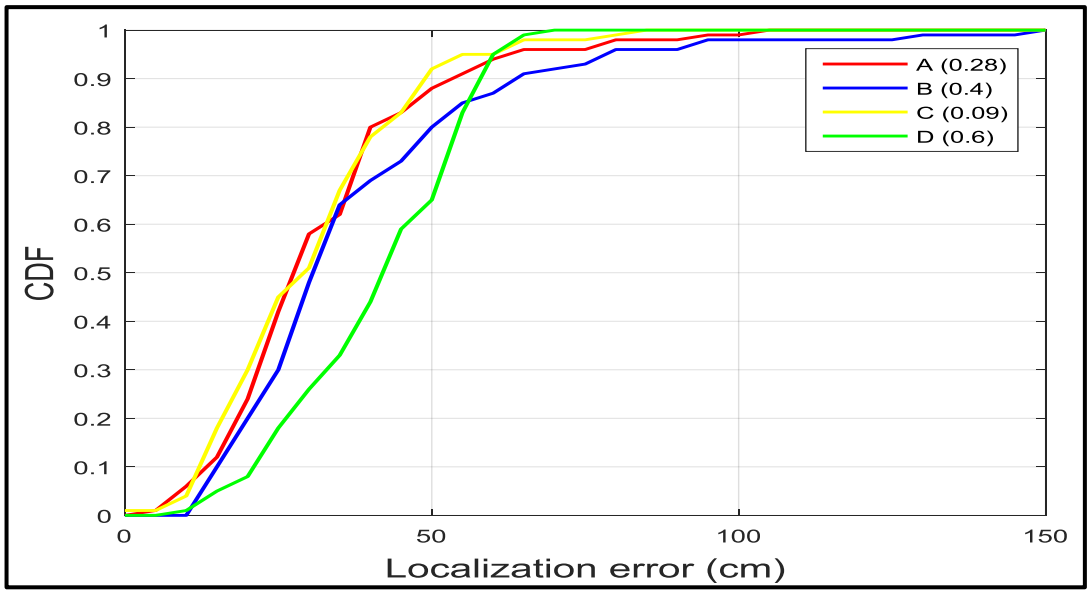

Figure 6.9 Position error of MPF/CDF with fixed speed case

Table 6.3 gives a brief demonstration for the influence of fixed and inconstant speed, respectively. The output probability is described of two dissimilar thresholds, $e_{th} = 1\ m$ and $e_{th} = 0.5\ m$. Due to the mobility models, the performance has been improved when consolidating more data of the used real mobile node speed, particularly in the inconstant speed case. For the MPF designs, a comparison of the CDFs of the position error was shown and the scenario of the inconstant speed is assumed. Table 6.3 presented the RMSE and the related output of the probability.

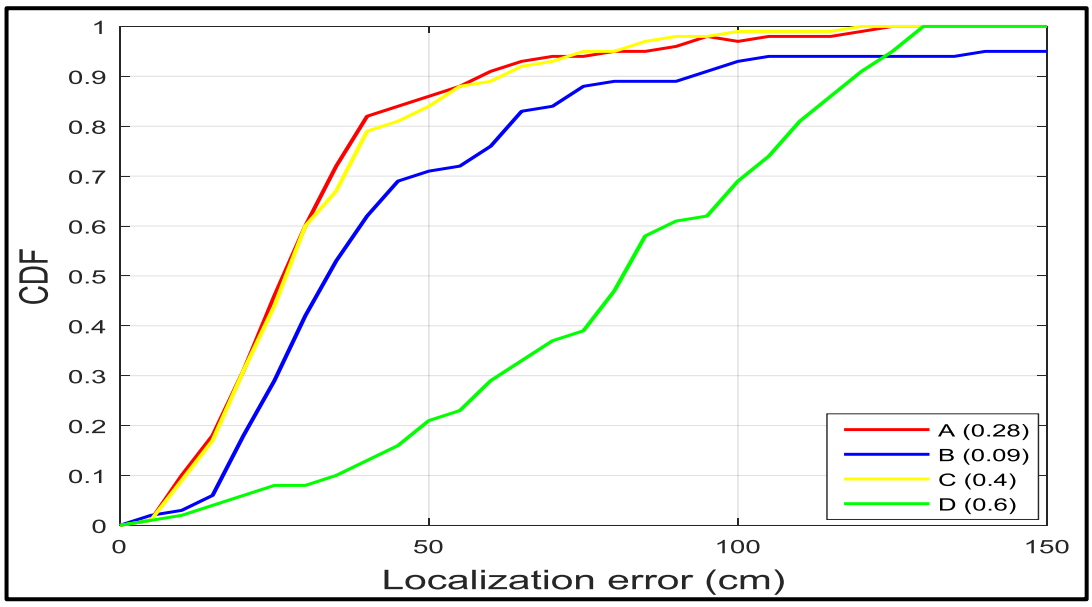

Figure 6.10 Position error of MPF/CDF with unfixed speed case

Table 6.3 MPF RMSE & positioning output probability

Mobility Model	$\mathcal{P}_{out}(e_{th} = 1\,m)$	$\mathcal{P}_{out}(e_{th} = 0.5\,m)$	RMSE (cm)
No mobility	0.02	0.19	44
Mobility1	≈ 0	0.25	40
Mobility2	≈ 0	0.04	29
Mobility3	0.01	0.10	32

6.4. Coping with NLOS Computations

Due to the walls' existence and some furniture, part of the MPF-ranging computations were done in NLOS condition. Therefore, there was a chance for comparing and testing algorithms that were particularly proposed for NLOS signals. Both of MPF-ranging computations (LOS and NLOS) and RSS computations (all LOS) will be utilized next. The representation of the mobile target is as below:

$$\begin{bmatrix} \boldsymbol{x_k} \\ \boldsymbol{y_k} \end{bmatrix} = \begin{bmatrix} \boldsymbol{x_{k-1}} \\ \boldsymbol{y_{k-1}} \end{bmatrix} + \begin{bmatrix} \boldsymbol{v_{1,k}} \\ \boldsymbol{v_{2,k}} \end{bmatrix} \tag{6.2}$$

where the target-coordinates are defined as x_k and y_k at time *k*, the process noise defined as $v_k = [v_{1,k} \quad v_{2,k}]^T$ at time *k*; which is considered as a covariance **Q** of zero-mean non Gaussian operation that is, $v \sim N(0, Q)$. The results were obtained for *N* of known locations as demonstrated beforehand. A lognormal was utilized to model the received power, for its wide usage. The ith result at time *k* is as below:

$$\boldsymbol{z_{i,k}(dBm) = P_0(dBm) - 10\alpha log_{10}\left(\frac{\|r_k - r_i\|}{d_0}\right) + w_{i,k},} \quad \boldsymbol{i = 1, \cdots, N} \tag{6.3}$$

r_i defines a known position of the *i*th receiver, $\alpha = 3.212$ is the exponent of path-loss, and r_k defines the robot's position at time *k*. σ_{dB}^2 represents the diagonal elements of **R**, in which it defines the shadowing variance, where in our case $\sigma_{dB} = 5.55\,dB$. The determined noise set is $w_k = [w_{1,k} \quad w_{2,k} \cdots w_{N,k}]^T$ that is assumed again to be a zero-mean non Gaussian of covariance $R \in R^{N \times N}$. By default, the obtained results are in the noisy-range calculations. The range computation for the ith at time *k* is:

$$z_{i,k} = \|r_k - r_i\| + w_{i,k} \qquad i = 1, \cdots, N \tag{6.4}$$

A user-defined cost function is one of the highest benefits when using MPF; instead of the probabilistic system model; because a little change in the cost function leads to great improvement in the filtering efficiency; which is a beneficial bonus for the application. Where, the filter's cost function has been already altered by the multiplication with a proper weight matrix.

The inverse of the observed rough-range computation, after normalization, of GPS-repeater case was considered as the weight. In our experiment, (from 93 dBm to 30 dBm) was the RSS range. The chosen weight has an inverse relation with the RSS absolute value. Therefore, the method of calculating the weight matrix can be the same with RSS computations instead of range computations. As a result, the obtained weight matrix led to a high performance in the GPS-repeater localization system case. Removing the outliers from the computations has improved the MPF filter. A certain threshold was set above with the expected range of computations that were regarded as outliers. Removing the outliers has improved the performance as the obtained data are corrupted with errors; particularly at the end and start of the target run.

The estimated trajectories shown in Figure 6.11 and Figure 6.12 are for GPS-repeater computations using MPF (with the weight matrix) and using MPF (without weight matrix) respectively. The state model's covariance is the key difference with MPF of fixed speed. The speed variations can be also affected by the faster bias variations.

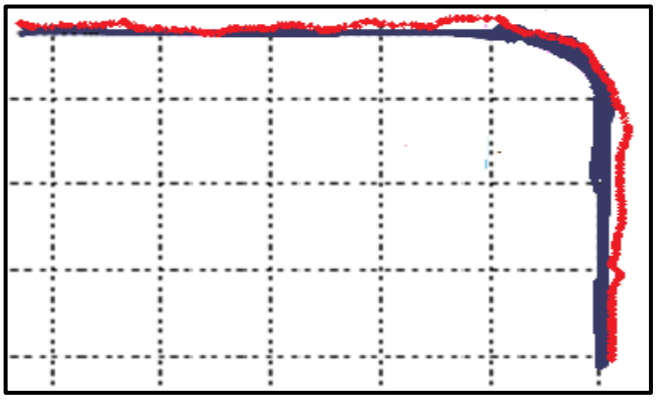

Figure 6.11 Evaluated trajectory using MPF of weight matrix. Cross marks refer to sigma (particles), the solid line defines the robot's real trajectory, and its estimate is defined by curve with markers.

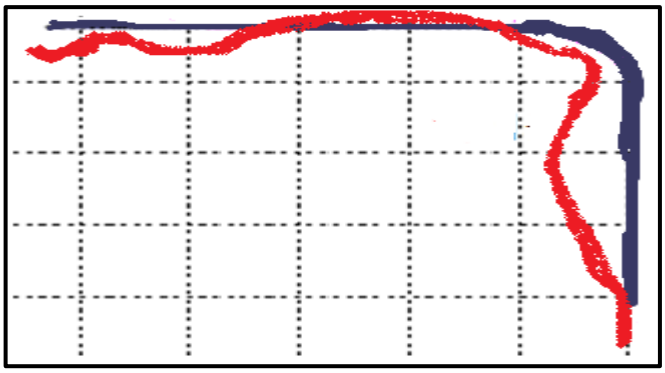

Figure 6.12 Evaluated trajectory using MPF for moving target of variable speed without weight matrix

6.5. Defining a Developed Model

A sample of a totally software GPS-repeater receiver has been characterized through the model of GNSS. The aim was to give an evidence idea of an advanced collaboration technique that relies on terrestrial radio and GNSS signals communication; which is gathered from a GPS-repeater approach, but changed in a way that "peer users" assist each other for locating function in case of loss of any AGPS-enabled fundamental station. Where, a GPS receiver is supplied with all the peers and end-to-end communication module. Figure 6.13 shows the diagram of the GPS-repeater receiver module. Figure 6.14 shows the design of printed circuit board (PCB), while Figure 6.15 shows the full design with the antenna, repeater, and router.

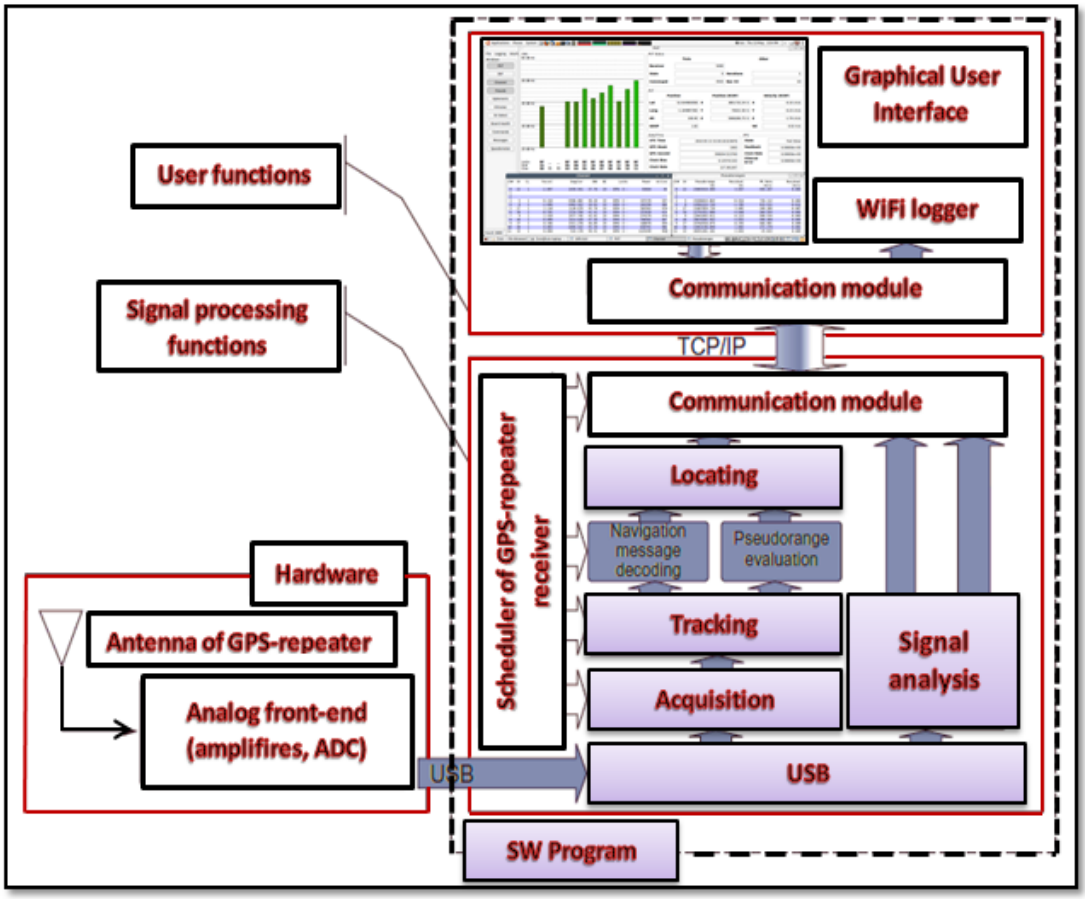

Figure 6.13 Diagram of the receiver module

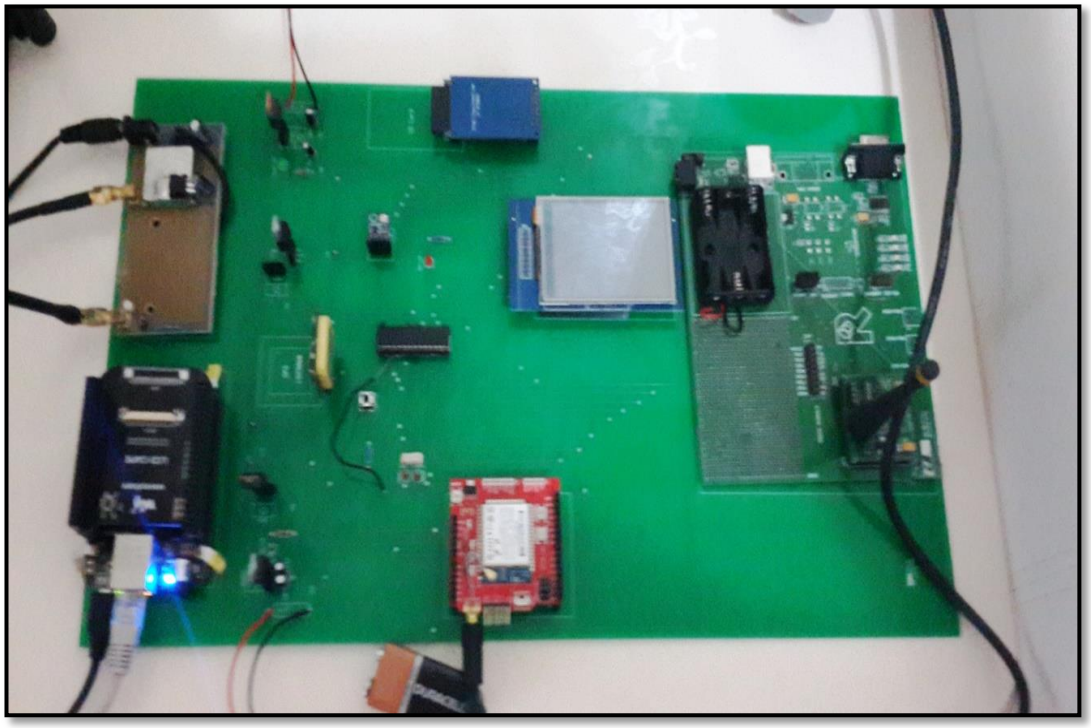

Figure 6.14 PCB design of the GPS-repeater

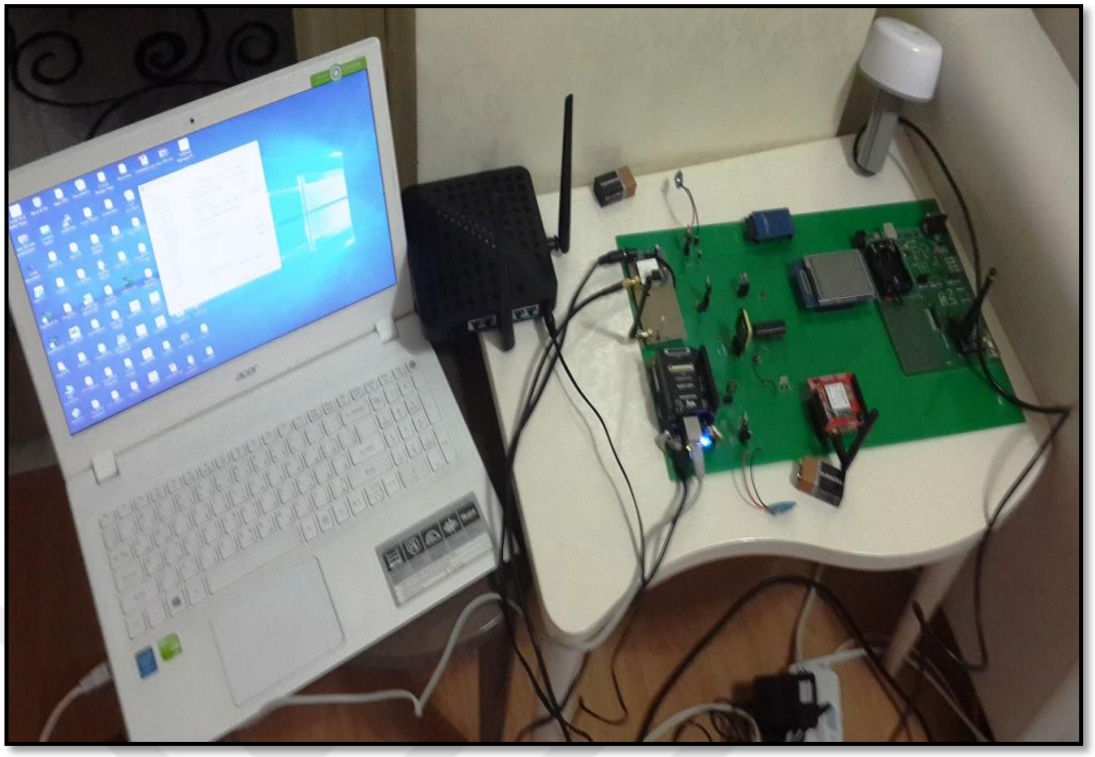

Figure 6.15 The full design with antenna, repeater, and router

The user-related tasks and GNSS-definite signal processing functions are defined by the light and dark shaded blocks respectively. The schedule/control and signal data flows are referred by the white and dark arrows which are used as a communication path between a terminal and open-sky to the satellites for exchanging an appropriate GNSS data.

In this design-model, each terminal works as an Assisted GPS (AGPS) server in an open-sky visibility; where it sends its GPS positioning information to another client named as an aided (assistant) user that processes these data for enhancing the efficacy of its own localization. Where, these data are recognised by the following characteristics: Doppler frequency, properties of the visible satellites, navigation data synchronization, and quality of control signal. The obtained code-phase and Doppler frequency from an assistant user have a high probability; which suitable for acquiring a signal of the satellite at the aided-node that has the capability of minimizing the search space in its acquisition phase; which in turn reduce its Time To First Fix (TTFF) or increase its sensitivity. Needless to say that those assistant-data are correlated to the synchronization data and code phase; which under some supposition can only be efficient such as the shortest distance between users and their accurate

clock synchronization. Where the 1st parameter works well in LAN, while the 2nd one isn't guaranteed for a low cost GPS receiver. A synchronization of a less than 1 m offset is necessary for incurring a well performance with taking into consideration the rate of the open GPS-C/A code.

A novel acquiring technique relies on the beforehand peer-based aiding's concepts; where it includes a computation step for the synchronization error between peers' couples to be utilized as extra aiding information. The overall prototypes of SW receiver were utilized for improving the performance of the mentioned technique using some tests in actual indoor and outdoor circumstances. The overall design test shown in Figure 6.16. The left PC was supplied by the whole software GPS receiver programmed for supporting the assistant user that is linked to rooftop antenna of full visibility of GPS satellites. The right PC was supplied by a wireless receiver on the laboratory corridor.

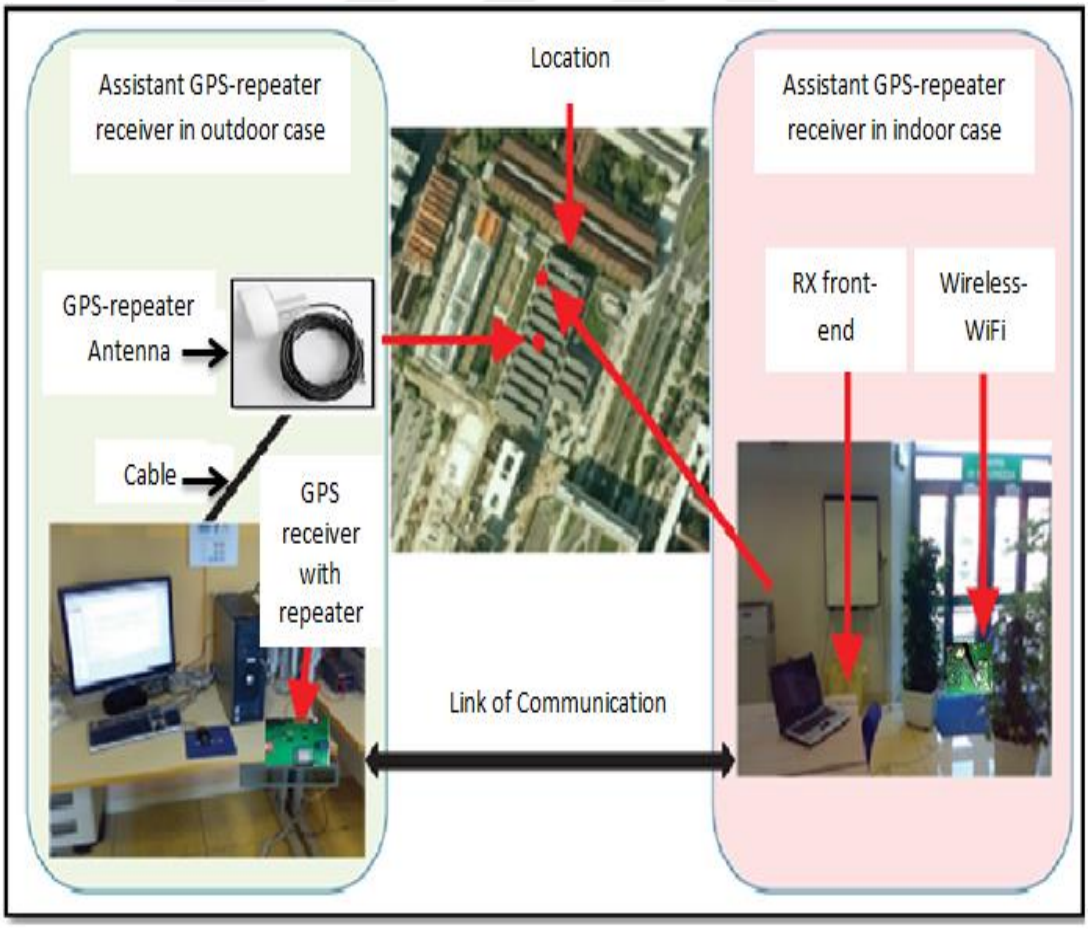

Figure 6.16 Arrangement of the acquiring test

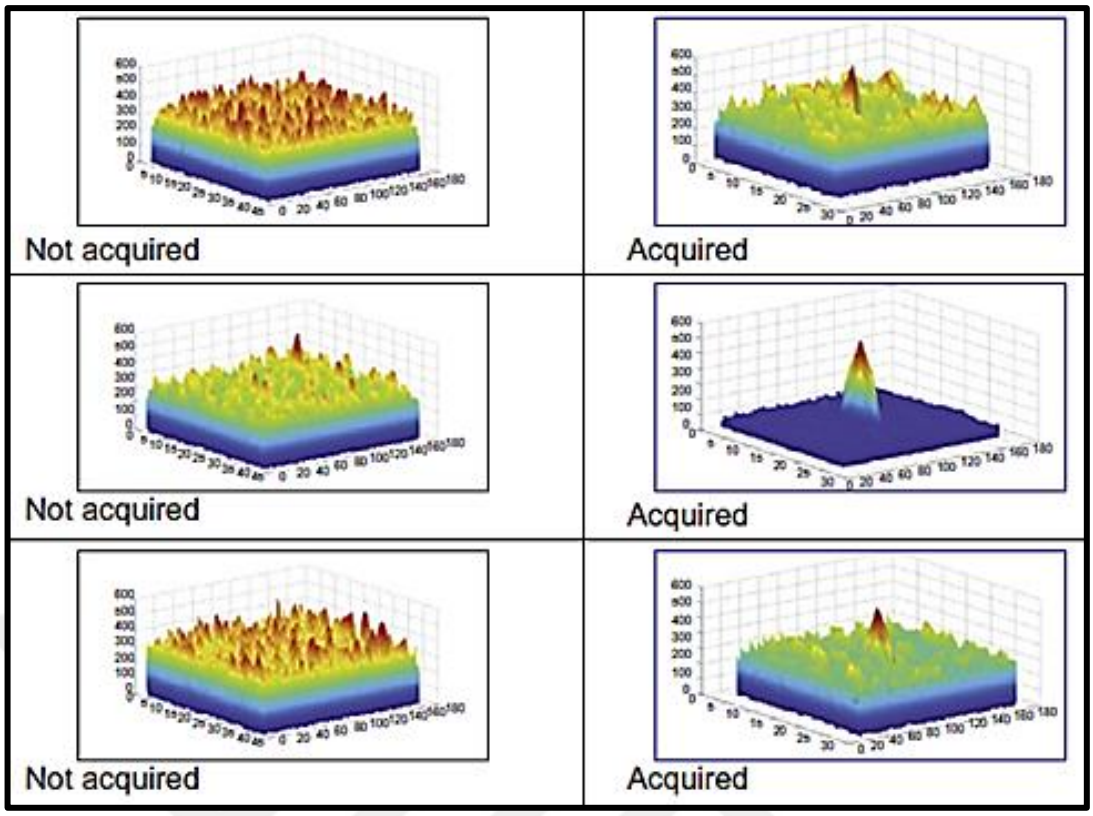

Figure 6.17 The cases of acquiring test: Search spaces determined with peer-based aiding (in the right column) and with no aiding (in the left column)

An Ethernet LAN has been used to make a connection for transferring the synchronized messages. The receiver in the indoor state during the test has the ability of the autonomous tracking of satellite. After many tests, we were able to conclude that an error of less than 40ms resulted for around 90% of the approximations of the transition bit of GPS-repeater, beginning from a synchronization offset of few ms. Therefore, we were able to achieve long coherent integrations, obviating data bit transitions to enhance the sensitivity of signal procuration. Through the utilization of assistant message in the procuration procedure, the other user was able to obtain the position of target sequentially for resolving its position. Figure 6.17 presents the acquiring search spaces, appearing the existence of correlation peaks which were impossible to be computed without aiding. Up to 245Hz was the limit of the frequency range of the search space, spitted to 15 frequency bins, each one of 30 Hz. All the peaks of correlation have raised the noise around the search space's centre, since the estimation of the codec delay and a shift frequency in the assistant message were also moderately perfect for the assistant-node.

6.6. Real-Life Experiment

A reference system of indoor localization has been designed and implemented to evaluate our proposed algorithms. A human was carrying the GPS-repeater model as a moving target along the building of a fixed and variable speed with recording its actual position. Where the error was lower than 40 cm. We have implemented an MPF as a positioning algorithm which was enhanced using the testbed. In addition, a standard PF has been implemented that depends on the exponential, KF, EKF, and MPF within the same platform. The distribution of the range-error of nonlinear filters is drawn from the statistical histogram.

6.6.1. Experiments Test and Results Analysis

The effect of MPF algorithm has been implemented with the use of a high sensitivity GPS-repeater receiver for acquiring data (latitude, longitude, speed and direction angle) inside the building of Electric and Electronic Engineering of the University of Gaziantep playground oval track lap. The GPS initial-position with a direction angle of 164.22^0 and sampling frequency of 4Hz. To ease the computation process, the gathered GPS-data has been entered a preprocessing step. As the data have an alteration only in the decimal part while both integer and degree parts have remained the same, we have eliminated the value before the decimal point with considering the value after the decimal point multiplied by 10^{-3} eliminate with converting the speed to m/s unit. For example, a data of ($123^0 24.15436' long$, $41^0 55.53523' lat$, $1.046/s$ speed & 164.22^0 direction angle) has been converted to ($154.36 \times 10^{-3}\ long$, $535.23 \times 10^{-3}\ lat$, 0.5381 m/s speed & 164.22^0 direction angle).

The comparison results for PF, EKF, AEKF,KF and MPF algorithm of 500 particles are presented in Figure 6.18, where the LAT and LONG's abscissa is 10^{-3}unit. The estimation error of positioning (LAT and LONG) is higher in all filters than that of MPF as presented in Figure 6.19. As a result, the MPF's performance is higher than the other filters; which in turn contributed in developing the reliability of GPS positioning.

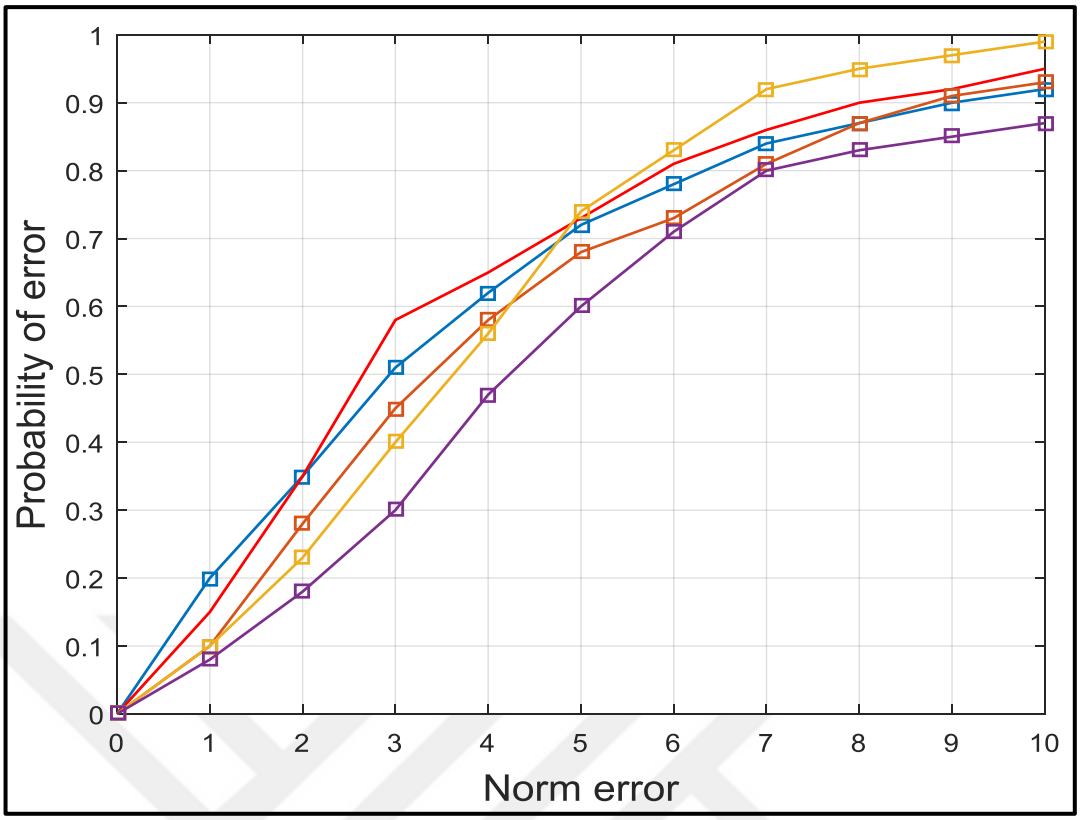

Figure 6.18 Comparison the error probability of filters

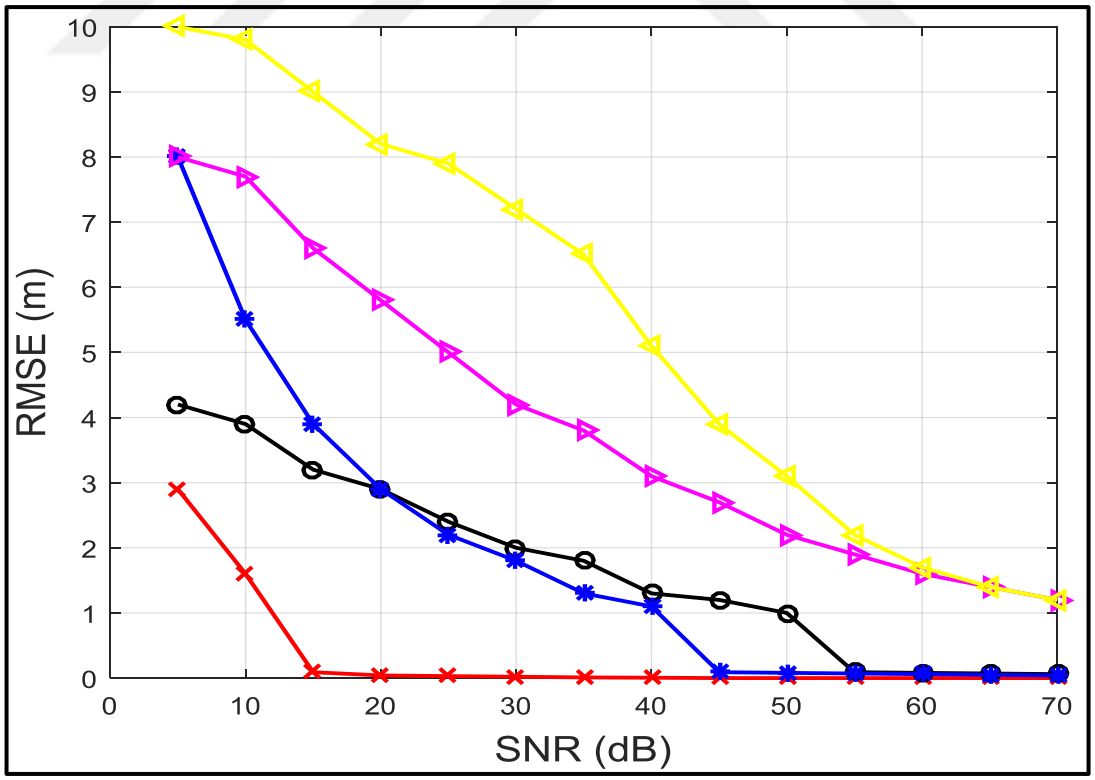

Figure 6.19 Signal to noise ratio vs. RMSE of filters

Figure 6.20 displays the associated speed over time including a signal that has been obtained by the GPS-repeater data. The GPS speed is noise corrupted and thus likely to be higher than how fast the target actually travelled. MPF and PF closely follow the GPS signal-their velocity is overestimated due to noise effects. EKF and KF both provide slower velocity estimates which appear more realistic. The experiments show that the MPF can help resolve ambiguous situation. The filter tends to overestimate the target speed. From a computational point of view, MPF is to be preferred over PF.

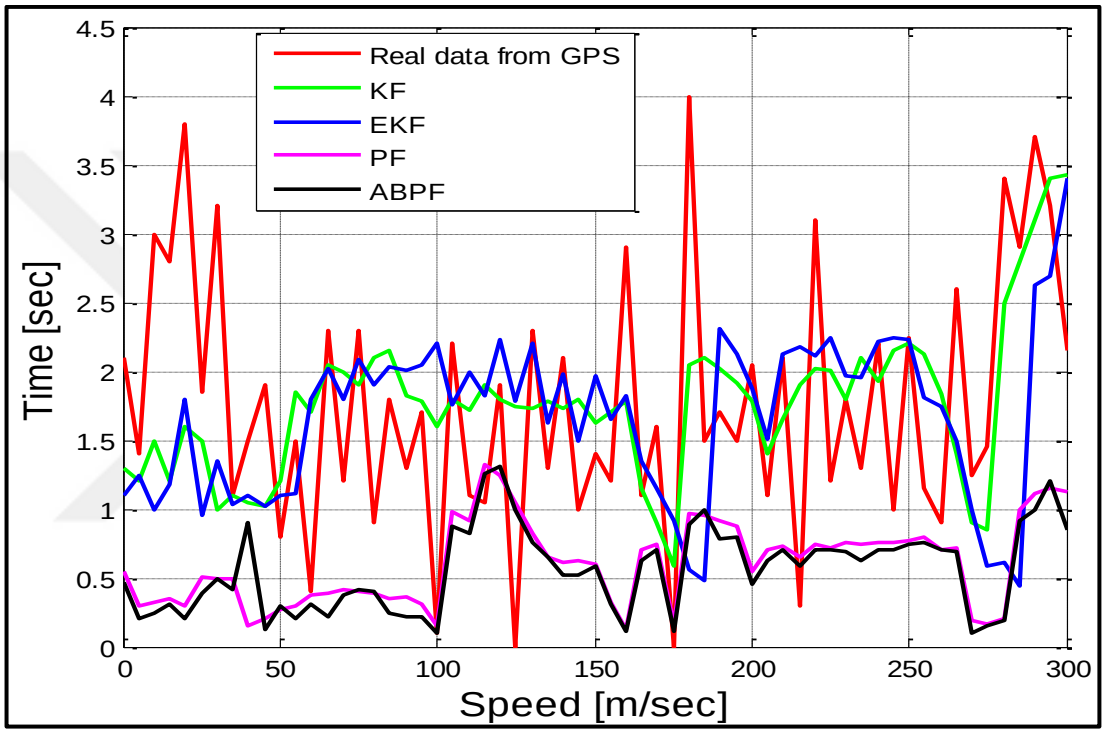

Figure 6.20 Associated speed over time

Thus MPF has enhanced the PF's performance and the approximation accuracy of navigation parameters. So the filter is capable of managing the GPS non-Gaussian noise model with an improved accuracy due to the particles' increment to one limit.

The Particle Filters (PFs) presented previously is applied to the approximation of the relative location by GPS data. In several error samples, the PF algorithm has lower position errors compared to other filters. In our algorithm, a 2.45m is the value that exceeds the GPS solution at best with errors lower than 0.13 m lower on average. Figure 6.21 shows the MPF algorithm's errors in a range of 8 minutes that extended GPS-blackout. The PF described by the indoor navigation under the same

GPS blackout is also outlined for comparison. As anticipated during the blackout, the PF in the indoor navigation has experienced high errors in position, as there were no absolute position computations for correcting errors in the integrations numerically. The PF in this experience has errors that reached to 12 m. The MPF has a higher performance for maintaining precise positions compared to PF. In this thesis, the decision-aided resampling suggested was for speeding up this removal operation, that advancing multipath bias-tracking.

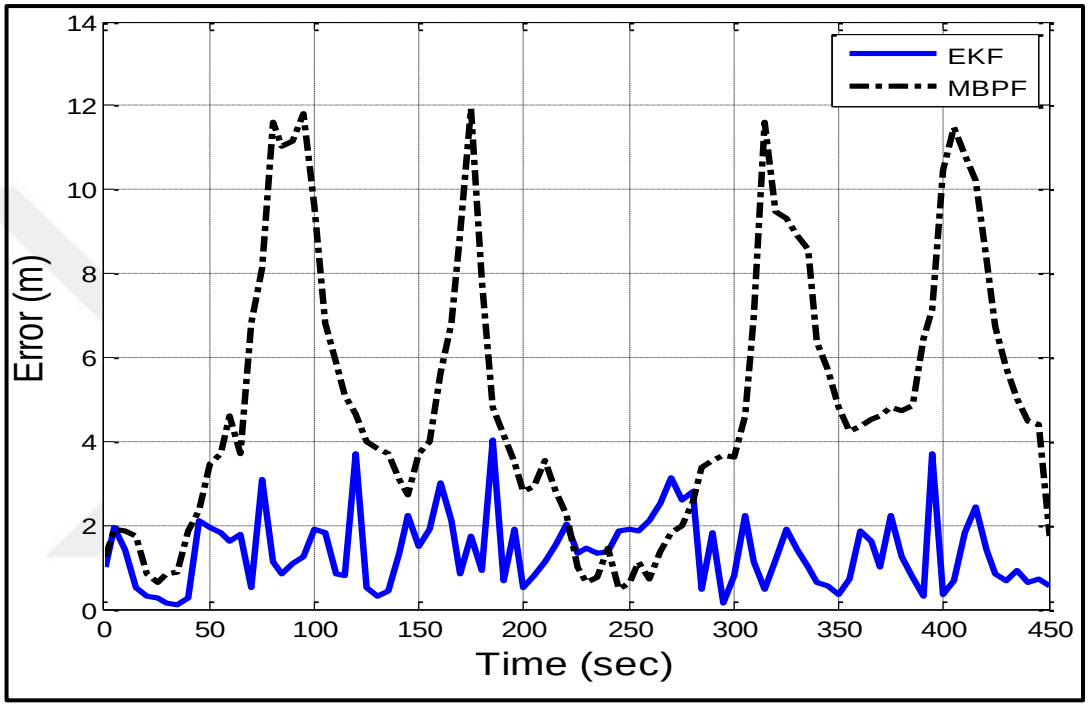

Figure 6.21 MPF algorithm's errors in a range of 8 minutes

The filters (UKF, PF, EKF) have been compared in two experiments. A lower computation time with a superior mean square error of GPS navigation have been obtained using the MPF compared to the others, according to the numerical results shown in Table 6.4 ($\alpha = 0.01$ and particles N=500). It is obvious that the increment resampling weight of N value has led to a better performance of MPF; but in turn the computation time has also increased; which is impractical for real-time applications.

Table 6.4 Comparison of trajectory RMSE of the four approaches

Filter	Error	Time (sec)
EKF	4.0424	2.5162
UKF	3.5185	1.62429
PF	2.5685	1.27931
MBPF	2.3947	1.24725

The final test for the accuracy of the proposed system has been done during GPS-repeater signal blockage within the post processing step. The MPF results were obtained from samples range between 100 and 500 samples that predicted from observation likelihood. As 0.0018 sec is the average duration time taken for a single iteration, so this algorithm is perfect for real-time implementation. The MPF has worked very well even with lower samples. We have observed during our experienced that using the lowest samples' number (10) has led to worst performance for both GPS availability and outages.

We utilized GPS receiver with repeater technology to gather navigational information. According to that, we have obtained position data of the satellites, pseudo-range, and carrier phase measurement noise powers for L1 frequency. Firstly, we have made a comparison between PF, EKF and MBPF for the approximation error of location. In the algorithms, the position and approximation data were similar to single iteration with GPS receiver begins with 6-satellites. Where, there was a loss of locks in the receiver at time ($t=150$) for signals from 3 satellites and 1 satellite is retrieved at $t=500$. Such an issue happens because the received signal cannot be tracked by phase lock loop of the receiver due to many causes such as the low SNR and device fail. So we have figured out that at least 6-satellites are needed in GPS for immediate standalone positioning. Figure 6.21 presents the position error of (EKF, and MBPF); where 500 particles were used in EKF and MBPF. In EKF, the error has increased exponentially when the receiver lost the signal from 3 satellites (beginning at $t=100$). In EKF, the evaluation of its location was corrected at once, when the extra satellite-signal was acquired by the receiver at $t=400$. However, the PF, and MBPF were powerful in doing that with just 3 satellites in sight. The errors' comparison has been depicted precisely between EKF and MBPF, which distinctly clarifies that the MBPF method outperforms the EKF method. It is clear that the MBPF's error is lower than EKF's error. However, both of the 2 methods have a reduction in the approximated error when the particle’s weight has increased at a slow rate. About 25% was the error's reduction in MPF; since PF validates the linear motion model of EKF, while the MPF has a higher reduction with a capability of making the computation despite the crossing walls; which in turn gives a superior client functions.

6.7. Results of Improved BVIRE System Algorithm

As we mentioned in the previous section, the system consists of an object attached to a tag, 4 readers at corners to acquire data from reference tags to be sent to the PC, 16 elements of each actual and virtual reference tags. Our system utilizes a BVIRE algorithm for locating the targets. Our adaptive BVIRE algorithm has been compared to others as shown in Figure 6.22, where the threshold value=2 and positioning error N=30.

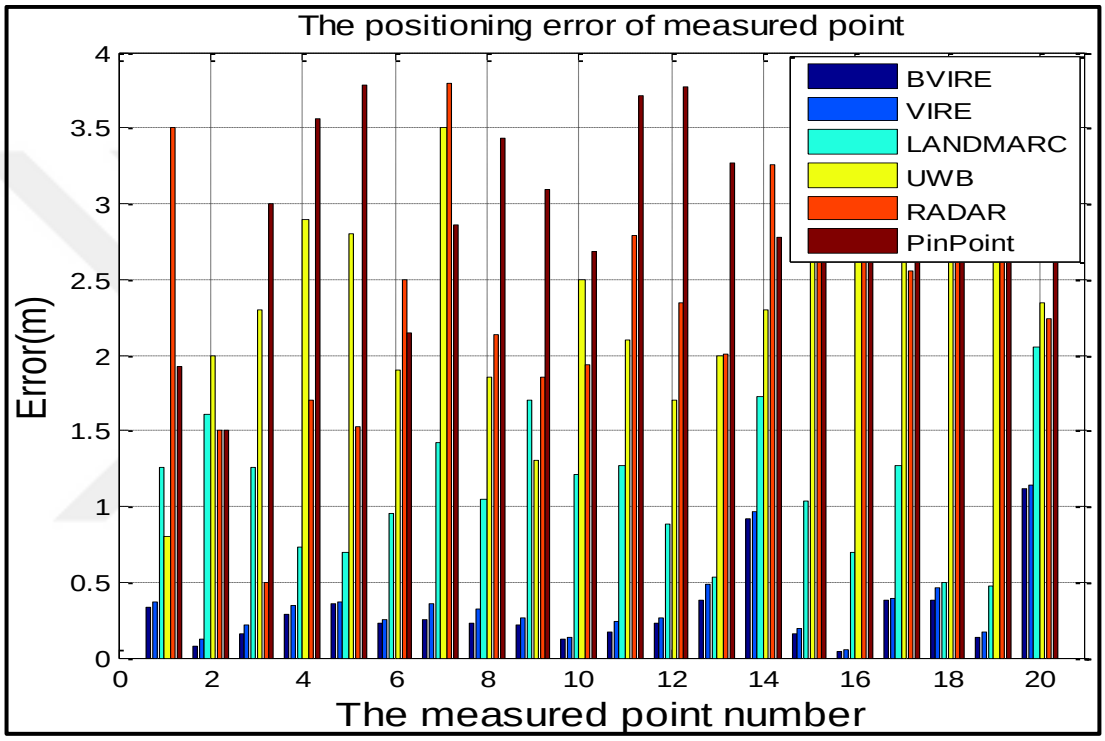

Figure 6.22 Comparison of localization performance using different algorithms

According to the results, our algorithm has minimized the computations overhead by reducing the reference tags and total readers with the support of virtual reference tags at boundaries; which in turn enhanced the locating's accuracy. In addition, our system has been used a linear regression model (LRM) method that utilizes the reference tags efficiently based on the event filtering. As a result, the average error has been reduced in our BVIRE algorithm to 3.12m, 2.47m, 2.36m, 1.12m and 0.35m in regards to PinPoint, RADAR, UWB, LANDMARC and VIRE consecutively. Also, there was an increase in the performance that reaches to 90.25%, 87.5%, 86.49%, 72.3% and 15.14% in comparison to the same mentioned algorithms consecutively. A 0.044 m is an average error in our system of the

estimated difference between minimum and maximum values compared to 1.22m of the PinPoint algorithm. Our BVIRE algorithm has a good adaptability to any change in the system layout such as the label's positions.

Moreover, adding a virtual reference label at the boundaries has considerably enhanced the locating precision. Clearly, the BVIRE algorithm provides a higher degree of accuracy at all locations. For determining the locating efficiency, we have implemented the CDF as shown in Figure 6.23, where the maximum and minimum error values are 0.56m and 0.26m for our algorithm respectively. Thus, we have gained a reduction in the error rang by 78%.

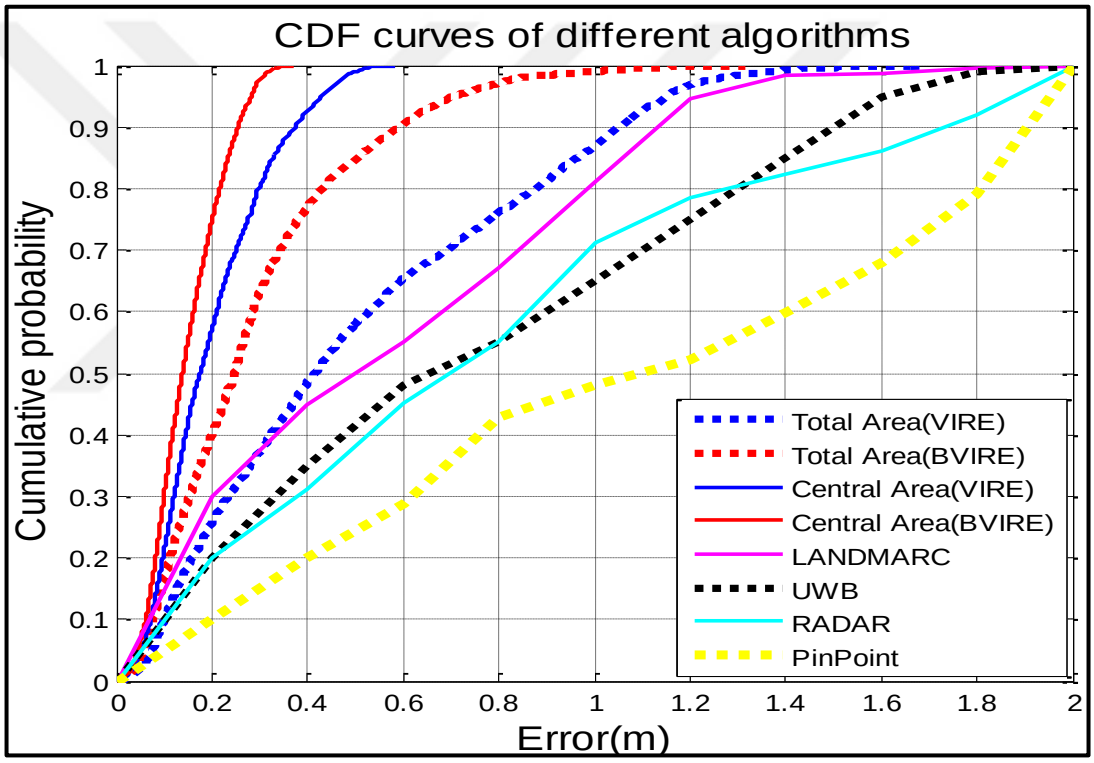

Figure 6.23 The cumulative distribution function of several methods

The range of error values in our algorithm lies within (90-100)cm as shown in Table 6.5, while it is (120-140)cm for VIRE algorithm. Also, there is a high reduction in the percentage error using our algorithm at CDF values of 180, 160, 140 and 120 compared to PinPoint, RADAR, UWB, and LANDMARC consecutively. In summary, our algorithm has a higher performance compared to the others.

Table 6.5 The CDF and percentage error comparison

CDF	BVIRE	VIRE	LAND-MARC	UWB	RADAR	Pin-Point
CDF (20)	40%	30%	30%	20%	19%	10%
CDF (30)	65%	38%	37%	26%	25%	15%
CDF (40)	76%	48%	45%	35%	30%	20%
CDF (50)	86%	58%	50%	42%	37%	24%
CDF (60)	91%	64%	55%	48%	45%	29%
CDF (70)	95%	69%	61%	52%	50%	36%
CDF (80)	98%	75%	67%	55%	55%	42%
CDF (90)	99%	81%	71%	61%	63%	45%
CDF (100)	100%	87%	80%	66%	71%	48%
CDF (120)	100%	98%	93%	75%	78%	53%
CDF (140)	100%	100%	99%	85%	82%	59%
CDF (160)	100%	100%	99%	95%	85%	68%
CDF (180)	100%	100%	100%	99%	90%	79%
CDF (200)	100%	100%	100%	100%	100%	100%

Selecting the right threshold contributes in removing any excessive location data. Omitting many neighbouring labels required in the optimization process is resulted from the too small threshold; while the high value makes a difficulty in getting rid from the noise interference resulted from the virtual references. The threshold's effect is demonstrated in Figure 6.24. We have fixed the threshold value in our system to 2 as the average error reduced to the minimum value, since the error was comparatively large when the threshold reaches 1; because of the channel noise.

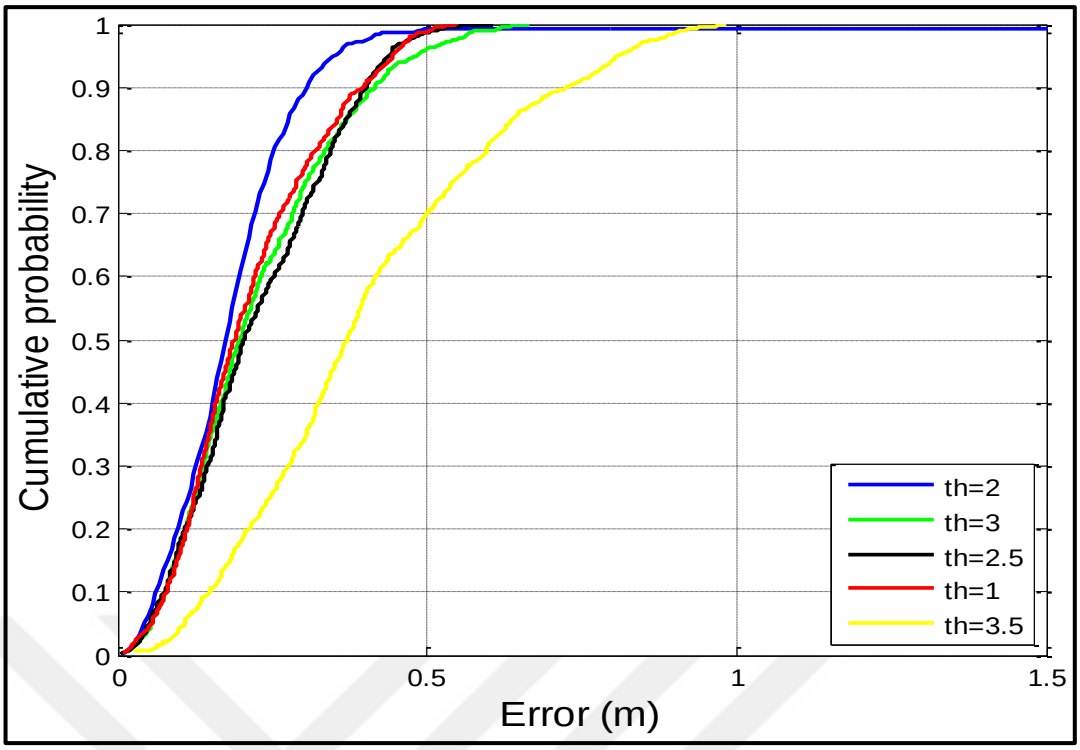

Figure 6.24 Threshold effect on the positioning accuracy

In our algorithm, a 0.446 is the GDOP value; which refers to a reduction by 13.6%, 20% and 40.7% with regards to the VIRE, LANDMARC and PinPoint consecutively. According to the results of Figure 6.25, our approach has the least geometric positional relation that results in a great locating precision.

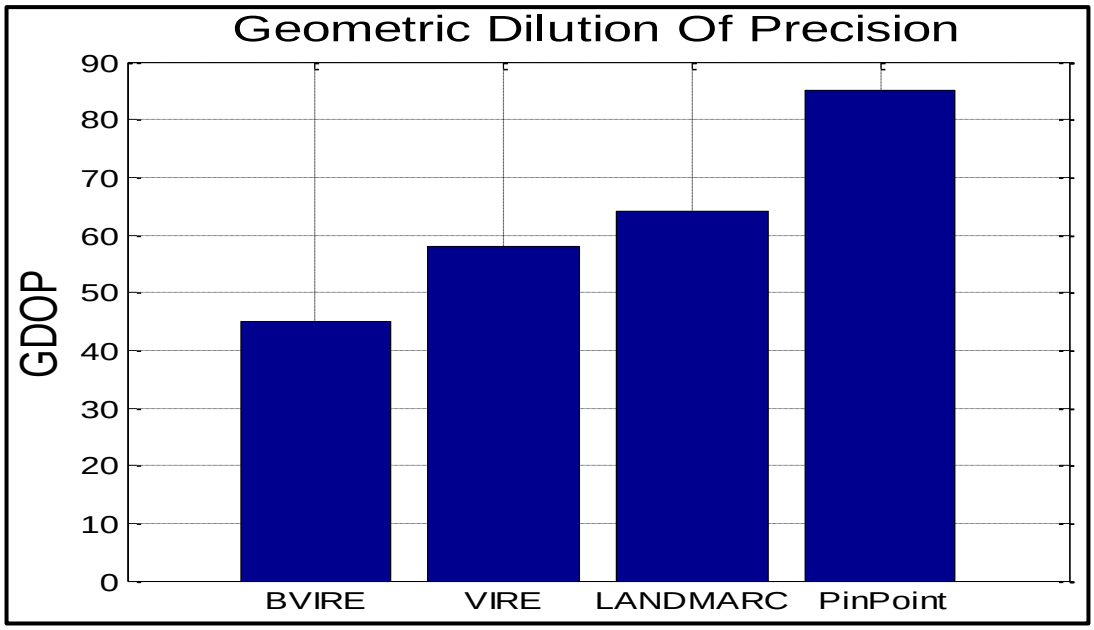

Figure 6.25 Geometric dilution of precision

The results of estimation error are demonstrated in Figure 6.26 and Table 6.6, in which the estimation error at the 5th and 2nd sample tag of our proposed BVIRE algorithm achieved the maximum and minimum values (0.361882m and 0.078961m) respectively. The estimation error's reduction of our proposed BVIRE is 98.75% and 94.34% compared with the PinPoint and UWB respectively, and its Mean Estimation Error (MEE) is 0.240549 m; which means an 8.61% and 54.33% reduction in comparison with the VIRE and LANDMARC respectively. The reduction in the mean positioning error in our algorithm reaches to 0.51m, 0.99m defines the maximum error. In conclusion, our system has a higher efficiency in the locating/tracking services.

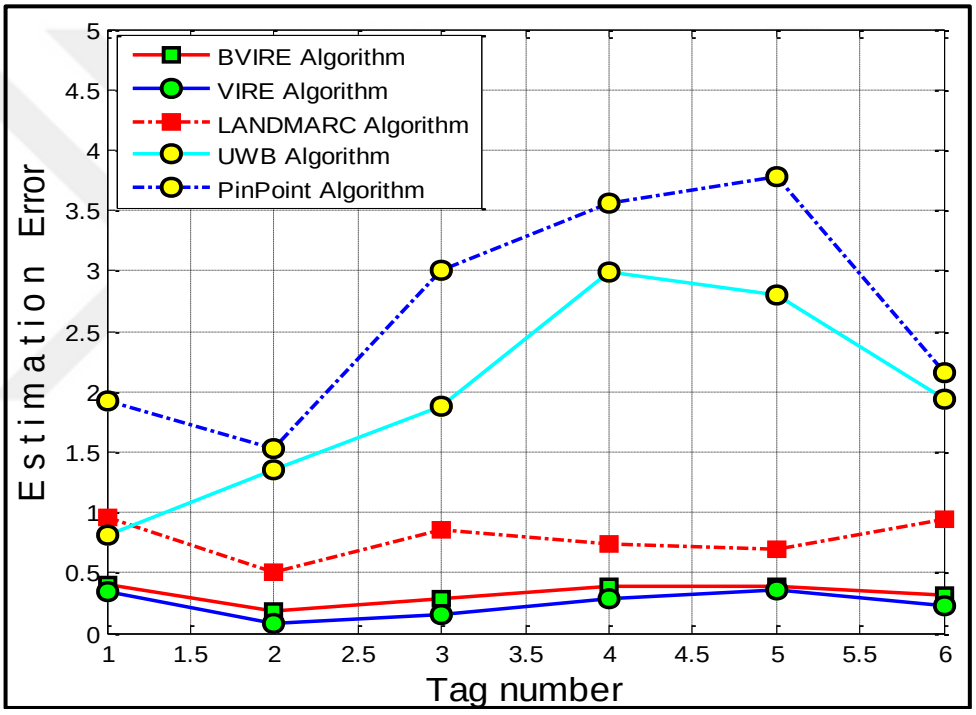

Figure 6.26 Localisation estimation error of tags

The reduction in the estimation errors of each approach is determined as shown in Table 6.6.

Table 6.6 The estimation errors with sample tags

Tag	BVIRE	VIRE	LANDMARC	UWB	Pin-Point
1	0.336402	0.396571	0.956025	0.814251	1.927401
2	0.078961	0.186824	0.506417	1.352281	1.522157
3	0.156341	0.291388	0.857327	1.878113	3.000147
4	0.281015	0.380813	0.734383	2.984160	3.562036
5	0.361882	0.389738	0.699936	2.801103	3.780251
6	0.228693	0.314421	0.949391	1.941072	2.151438

Also, the maximum CEP of PinPoint algorithm is 0.8542, the minimum CEP of BVIRE algorithm is 0.4353. When we compared BVIRE algorithm with PinPoint, LANDMARC, and VIRE algorithms, the CEP value decreased by 40.6%, 20.2%, and 14.6% compared with PinPoint, LANDMARC, and VIRE algorithms. Figure 6.27 shows the CEP results of our improved BVIRE algorithm compared with others.

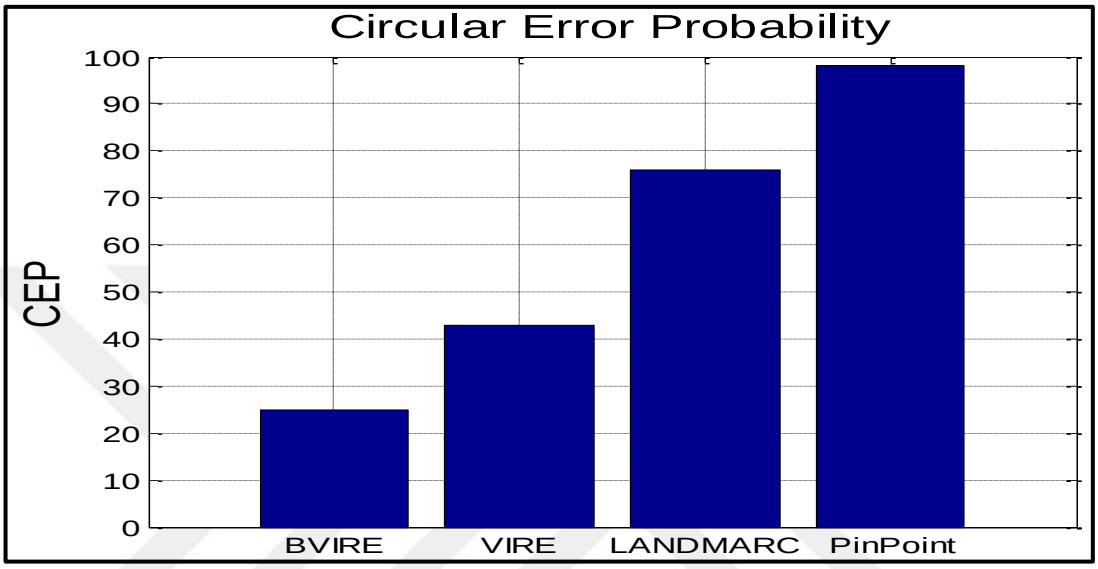

Figure 6.27 Circular Error Probability

The height of the RFID reader has a great impact on the average estimation error; in which they have an inverse correlation as demonstrated in Figure 6.28; so we have fixed the height at 130cm. Our BVIRE approach has the minimum average estimation error compared to the others.

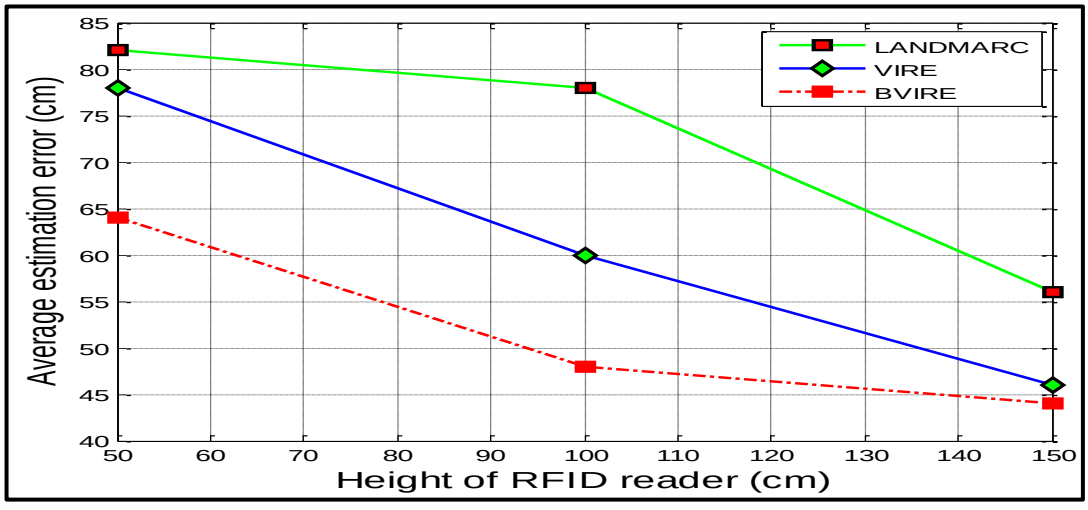

Figure 6.28 The correlation of height vs. estimation error

6.8. Conclusions and Future Plans

Although the classical PF worked well for solving non-Gaussian distribution, it needs a prior knowledge of the real distribution according to the conclusions based on our tests. On the other side, the uncertainty issue of the model distributions was addressed well by the MPF based on the user-defined particles' propagations weight. Where, MPF was the most powerful filter against the noise distribution regarding the others. Also, a good enhancement has been obtained in the tracking application by a few changes in the cost function (in a weight matrix form). The method has been implemented for improving the GPS-repeater positioning precision, as it proved to handle the non-Gaussian and nonlinear issues more effectively based on our experiment, compared with the classical and extended filters. Therefore, it is useful for applications/services that utilize GPS navigation like the vehicles and ships. The most filters eliminate the influence of present observation data, while MPF utilizes the new observation data before evaluating the significant weights and lay out significance density function to develop the performance of conventional particle filter. The real-work of the suggested model was demonstrated by the technique operation on a distinct non-linear localization issue with non-white and non-Gaussian noise. The filter was used to control the nonlinear issue, represented by the estimation uncertainty in GPS-repeater relative position, by the resampling method to reduce the high samples' number that complicates the algorithms based on position-hypotheses. It also has kept a concentrated and accurate position evaluate in an impressive way during the 8 minutes of outspread GPS, while other filters have experienced big errors in the indoor environment. This thesis analysed the PF's method to extenuate multipath influences in GPS navigation. A fundamental technique has been suggested for the navigation system to handle the approximation and detection of multi-path errors. The proceedings multipath were regarded as sudden changes influencing the navigation state space design. We show that the suggested MPF accomplished a great accuracy within a real office case with a reduction in the average RMSE by 2m. The position approximation is advanced from a total accuracy of 4.6 m in the repeater only approach to 2 m within the MPF containing the last wall collision check.

The experiential results have demonstrated the capability of the suggested system in indoor localization and tracking services. Even though the suggested

system accomplished efficient target localization, additional tests and perspective extensions were conceivable. In future work, additional techniques can be mixed to make the system immaculate and resilient, like improving a new algorithm for developing the evaluation precision, achieving absolute studies of defend vector regression for re-weighting samples, suggesting an effective power and low-perplexity techniques to make the system proper for indoor localization.

While for terrestrial locating, the targets within the indoor environments became a significant topic nowadays, since there is an urgent need for a high locating accuracy inside the large buildings. Overall, the current locating system suffers from a low performance and high cost especially at the boundaries due to the circumferential effects and multi-path situation. Thus, in this thesis we have analysed the existing indoor localization methods for having a successful improved BVIRE algorithm. Where, it locates objects of active RFID tags upon the linear-regression model and support of boundary virtual tags in addition to the real reference tags' for enhancing the locating accuracy within a noisy circumference. The system supports multiple tags and multiple readers and is easy to scale up. Designing and implementing an indoor locating system was our main goal for determining the real-time target's location accurately based on the active RFID. Where, the results proved that our system achieved an accurate locating of movable targets within a specific range regarding other algorithms (VIRE, LANDMARC, PinPoint, and UWB). For example, the mean estimation error in our algorithm has been greatly reduced to 98.75 and 94.34% regarding PinPoint and UWB respectively. Our proposed approach arranges the virtual tags strategically; for reducing the amount of used active tags with a higher locating precision. Comparing the localisation algorithms has been addressed and analysed to evaluate their performance precisely and localising moving object position accurately. The values (90.25%) and (13.26%) are the obtained reduction in the average error using our approach with a comparison to PinPoint and VIRE approaches consecutively. The good adaptability to the environment's change is one of the main characteristics in our system. There is a great minimization in the CDF's error using our approach by 38.8% and 68.7% in regards to VIRE and PinPoint approaches consecutively. Also, its CEP has been enhanced by 40.6% and 20.2% compared to PinPoint and LANDMARC algorithms. Moreover, we have minimized the average locating error to 0.21m when setting the

active RFID reader's height at 130 cm. According to the results, our BVIRE algorithm has a better performance, lower cost, and a minimum average error than the others as well as it does not need any additional reference label and does not increase the premise of RF interference with removing the unnecessary tags based on the active RFID.

As a future plan, improving the system delay is our next goal with implementing a 3D positioning. Also, we may focus on combining our algorithm with a variety of location-aware information for an additional enhancement in the locating's precision. Reducing the size of active RFID tags is one of the expected enhancements for easier installation on objects. Active RFID tags are typically larger than passive RFID tags as it contains transceiver and battery. Optimizing the hardware design of RFID system lets the reader capable of providing a signal strength directly instead of level. Therefore, it will give a great enhancement in both efficiency and capacity of real-time signal processing within the indoor positioning system depending on the RSSI value.

REFERENCES

[1] David Gaylor, Glenn Lightsey, and Kevin Key. (2003). Effects of Multipath Signal Blockage on GPS Navigation, *Vicinity of the International Space Station (ISS),* Ion GNSS, Portland, USA.

[2] Istv Manno. (1999). Introdction to the Monto Carlo Method, *Akademiai Kiado*, Budapest, Hungary.

[3] Hernandez Pajares, Juan Zornoza, Jose Miguel, and et al. (2008). GPS Data Processing: Code and Phase, *Algorithms, Techniques and Recipes*. Barcelona.

[4] John Dow, Neilan, and Rizos. (2009). The International GNSS Service in a Changing Landscape of Global Navigation Satellite Systems, *Journal of Geodesy*. **83**. 191-198.

[5] Chansarkar Mangesh, Lionel Garin. (2000). Acquisition of GPS Signals at Very Low Signal to Noise Ration, *Proceedings of ION National Technical Meeting*. US Institute of Navigation, Alexandria VA.

[6] Pratap Misra, Per Enge. (2004). Global Positioning System, *Signal, Measurements, and Performance*. Ganga Jamuna Press.

[7] Yanying Gu, Anthony Lo, and Ignas Niemegeers. (2009). A Survey of Indoor Positioning Systems for Wireless Personal Networks, *IEEE Communications Surveys & Tutorials*. **11**. 13-32.

[8] Grey Welch, and Gray Bishop. (2001). An Introduction to the Kalman Filter, *Technical Report TR*.

[9] Long Kim, Tuan Hong. (2009). Extended Kalman Filter Model for GPS and Indoor Positioning System, *International Forum on Strategic Technlogies*. **2**. 71-75.

[10] Jie Wang. (2012). Toward Robust Indoor Localization Based on Bayesian Filter using Chirp-Spread-Spectrum Ranging, *IEEE Transactions on Industrial Electronics*. **59**. 1622-1629.

[11] Kazuhiro Hotta. (2009). Adaptive Weighting of Local Classifiers by Particle Filters for Robust Tracking, *Pattern Recognition*. **42**. 619-628.

[12] Boon Lee, Young Sook, and Wan Chung. (2008). 3D Navigation Real Time RSSI-Based Indoor Tracking Application, *Journal of Ubiquitous Convergence Technology*. **2**. 67-77.

[13] Olutayo Oyerinde, and Stanley Mneney. (2012). Review of Channel Estimation for Wireless Communication System, *IETE Technical Review*.

[14] James Bao, Yen Tsui. (2005). Fundamentals of Global Positioning System Receivers, *A Software Approach*. John Willey & Sons.

[15] Stefano Burigat, and Luca Chittaro. (2011). Pedestrian Navigation with Degraded GPS Signal, *In Proceedings of ACM Mobile HCI.*

[16] Jaewoo Chung, Matt Donahoe, Chris Schmandt, and et al. (2011). Indoor Location Sensing Using Geo-Magnetism, *In Proceedingd of ACM Mobile Sys.*

[17] Thiele. (1969). Analysis of Yagi-Uda-Type Antennas, *IEEE Transactions on Antennas and Propagation*. **17**. 24-31.

[18] John M, Dow J, Neilan R, and Rizos C. (2009). The International GNSS Service in a Changing Landscape of Global Navigation Satellite Systems, *Jouranl of Geodesy*. **83**. 191-198.
[19] Yanying GU, Anthony Lo, and Ignas Niemegeers.(2009). A Survey of Oindoor Positioning Systems for Wireless Personal Networks, *IEEE Communications Surveys & Tutorials*. **11**. 13-32.
[20] Gaylor D, Lightsey E, and Key K. (2003). Effects of Multipath and Signal Blockage on GPS Navigation in the Vicinity of the International Space Station, *ISS ION GNSS*. Portland, USA.
[21] Dovis R, Lesca D, Margaria G, and Ghinamo G.(2008). An Assisted High Sensitivity Acqisition Technique for GPS Indoor Positioning, *Location and Navigation Symposium*. IEEE/ION.
[22] Sun W, Xue D, Zheng L, and et al. (2008). A study of Real Time Location System in Logistics Management Based on Active RFID, *Proceedings of the 4Th International Conference on Intelligent Logistics Systems*.
[23] Ni L, Yunhao C, Yiu L, Patil A. (2003). LANDMARC: Indoor Location Sensing using Active RFID, *In Pervasive Computing and Communications*.
[24] Norouzi Y, Derakhshani M. (2009). Joint Time Difference of Arrival/Angel of Arrival Position Finding in Passive Radar, *Radar, Sonar & Navigation, IET*. **3**. 167-176.
[25] Bahl P, Padmanabhan V. (2000). RADAR: AN in Building RF Based User Location and Tracking System, *In Proc. IEEE INFOCOM*. **2**. 775-784.
[26] Ni L, Liu Y, Lau Y, Patil A. (2003). LANDMARC: Indoor Location Sensing Using Active RFID, *Proceedings of the First IEEE International Conference Pervasive Computing and Communications*.
[27] Kaplan E, and Hegarty C. (2005). Understanding GPS: Principles and applications, *Artech House*.
[28] Giremus A, Tourneret J, and Calmettes V. (2007). A Particle Filtering Approach for Joint Detection/Estimation of Multipath Effects on GPS Measurements, *Trans on IEEE Signal Processing*. **55**. 1275-1285.
[29] Douc R. (2011). Sequential Monte Carlo Smoothing for General State Space Hidden Markov Models, *The Annals of Applied Probability*. **21**. 2109-2145.
[30] Huerta J, Vidal J, Giremus A, and Tourneret J. (2009). Joint Particle Filter and UKF Position Tracking in Severe Non Line of Sight Situations, *IEEE J. Sel Topics Signal Process*. **3**. 874-888.
[31] Bonnabel S. (2007). Left Invariant Extended Kalman and Attiude Estimation, *IEEE Conference on Decision and Control*.
[32] Martin Ph, Salaun E, and et al. (2010). Generalized Multiplicative Extended Kalman Filter for Aided Attitude and Heading Reference System, *In Proc Control Conf AIAA Guid Navigat*.
[33] Wang X, Chen R, and Guo D. (2002). Delayed Pilot Sampling for Mixture Kalman Filter with Application in Fading Channels, *IEEE Trans Signal Process*. **50**. 241-253.
[34] Long Kam, Tuan Do. (2009). Extended Kalman Filter Model for GPS and Indoor Positioning System, *Proceeding of the International Forum on Strategic Technologies*. **2**. 71-75.
[35] Evennou F, Francois M, and Novakov E. (2005). Map Aided Indoor Mobile Positioning System using Particle Filter, *IEEE Wireless Communications and Networking*. **4**. 2490-2494.

[36] Gustafsson F. (2010). Particle Filter Theory and Particle with Positioning Applications, *IEEE Aerospace and Electronic Systems Magazine*. **25**. 53-82.
[37] Doucet A, Godsill S, and Andrieu C. (2000). On Sequential Monte Carlo Sampling Methods for Bayesian Filtering, *Statist Cimp. **10**. 197-208.*
[38] Thrun S, Fox D, Burgard W, and Dellaert F. (2001). Robust Monte Carlo Localization for Mobile Robots, *Artificial Intelligence*. **128**. 99-141.
[39] Arulampalam M, Maskell S, Gordon N, and Clapp T. (2002). A Tutorial on Particle Filters for Online Nonlinear/Non-Gaussian Bayesian Tracking, *IEEE Transactions on Signal Processing*. **50**. 2.
[40] Subrahmanyam G, and Rajagopalan A. (2007). A New Extension of Kalman Filter to Non-Gaussian Priors, *Springer Berlin/Heidelberg*.
[41] Khalil H. (1996). Nonlinear Systems, *Upper Saddle River: Prentice Hall* (2nd ed).
[42] Seco F, Jimenex A, Prieto C, Roa J, and Koutsou K. (2009). A Survey of Mathematical Methods for Indoor Localization, *IEEE International Symposium in Intelligent Signal Processing*. WISP.
[43] Dieng N, Chaudet C, Charbit M, Toutain L, and Meriem T. (2012). Experiments on the Range Estimator for Indoor Localization, *International Conference on IEEE in New Technologies, Mobility and Security*.
[44] Li T, Bolic M, Djuric P. (2013). Resampling Methods for Particle Filtering, *IEEE Signal Processing Magazine*. **1**. 2-42.
[45] Nicoli M, Morelli C, and Rampa V. (2008). A Jump Markov Particle Filter for Localization of Moving Terminals in Multipath Indoor Scenarios, *IEEE Trans Signal Process*. **56**. 3801-8809.
[46] Hu X, Schon T, and Ljung L. (2008). A Basic Convergence Result for Particle Filtering, *IEEE Trans Signal Process*. **56**. 1337-1348.
[47] Schmitt S, Will H, Aschenbrenner B, Hillebrandt T, Kyas M. (2012). A Reference System for Indoor Localization Testbeds, *Conf in Proc Internet*. 1-4.
[48] Yu K, Guo Y. (2008). Improved Positioning Algorithm for Nonline of Sight Environments, *IEEE Trans Veh Technol*. **57**. 2342-2353.
[49] Gordon N, Salmond D, and Smith A. (1993). Novel Approach to Nonlinear/Non-Gaussian Bayesian State Estimation Radar and Signal Processing, *IEEE Proceedings*. **140**. 107-113.
[50] Wang Jie. (2012). Toward Robust Indoor Localization Based on Bayesian Filter Using Chirp-Spread-Spectrum Ranging, *IEEE Transactions on Industrial Electronics*. **59**. 1622-1629.
[51] Kazuhiro Hotta. (2009). Adaptive Weighting of Local Classifiers by Particle Filters for Robust Tracking, *Pattern Recognition*. **42**. 619-628.
[52] Yao A. (2012). A Compact Association of Particle Filtering and Kernel Based Object Tracking, *Pattern Recognition*. **45**. 2584-2597.
[53] Park S, and Hashimoto S. (2009). Passive RFID in Indoor Environment, *IEEE Transactions on Industrial Electronics*. **56**. 2366-2373.
[54] Ni L, Liu Y, Lau Y, and Patil A. (2004). LANDMARC Indoor Location Sensing Using Active RFID, *Wireless Networks*. **10**. 701-710.
[55] Gezici S, Tian Z, Biannakis G, Kobayashi H, and et al. (2005). Localization Via Ultra Wideband Radios, *IEEE Signal Processing Magazine*. **3**. 70-84.
[56] Hightower J, Want R, Borriello G. (2000). SpotOn: An Indoor 3D Location Sensing Technology Based on RF Signal Strength, *UW CSE University of Washington, Seattle, WA*.

[57] Hazas M, Hopper A. (2006). A Novel Broadband Ultrasonic Location System for Improved Indoor Positioning, *IEEE Transactions on Mobile Computing*. **5**. 1-5.
[58] Kandepu R, Foss B, and Imsland L. (2008). Applying the Unscented Kalman Filter for Nonlinear State Estimation, *Journal of Process Control*. **18**. 753-768.
[59] Rizos C, Grejner D, Toth C, Dempster A, Politi Y, and et al. (2010). A Prototype System for Navigation in GPS Challenged Environments, *GPS World*. **21**. 42-47.
[60] Hui L, Houshang D, Pat B, Jing L. (2007). Survey of Wireless Indoor Positioning Techniques and Systems, *IEEE Transactions on Systems, Man, and Cybernetics-Part C*. **37**. 1067-1080.
[61] Maja S, Mladen R, Dinko B. (2012). RF Localization in Indoor Environment, *Radio Engineering*. **21**. 557-567. Wireless Indoor Positioning System using GPS repeater Technique.
[62] Improved positioning algorithm using modified particle filter of the nonlinear/non-Gaussain GPS state estimation under review
[63] Nonlinear/Non-Gaussian Bayesian State Estimation
[64] Wooyong L, Kyeong H, Taeyoung K, Doodeop E, and et al. (2012). Large Scale Indoor Localization System Based on Wireless Sensor Networks for Ubiquitous Computing, *Wireless Personal Communications*. **63**. 241-260.
[65] Kaplan E, Hegarty C. (2006). Understanding GPS: Principles and Applications, *Artech, House, Norwood, USA*, 2nd edition.
[66] Shao S, Burkholder R. (2013). Item Level RFID Tag Location Sensing Utilizing Reader Antenna Spatial Diversity, *IEEE Sensors*. **13**. 1-2.
[67] Bolic M, Simplot D, and Stoymenovic I. (2010). RFID Systems: Research Trends and Challenges, *Wiley*.
[68] Liu H. (2007). Surver of Wireless Indoor Positioning Techniques and Systems, *IEEE Transactions on System, Man and Cybernetics*. **37**. 1067-1080.
[69] Bhuvanagiri S, Krishna K. (2010). Motion in Ambiguity: Coordinated Active Global Localization for Multiple Robots. *Robotics and Autonomous Systems*. **58**. 399-424.
[70] Kwon T, Song J, and Joo S. (2010). Elevation Moment of Inertia: A New Feature for Monte Carlo Localization in Outdoor Environment with Elevation Map, *Journal of Field Robotics*. **3**. 371-386.
[71] Jardak N, Samama N. (2009). Indoor Positioning Based on GPS-Repeaters: Performance Enhancement using an Open Code Loop Architecture, *Aerospace and Electronic Systems*. **45**. 347-359.
[72] Syrjarinne J, Wirola L. (2006). Setting a New Standard-Assisted GNSS Receivers that Use Wireless Networks. *Inside GNSS*. **1**. 26-31.
[73] Dardari D, Falletti E, Luise M. (2012). Satellite and Terrestrial Radio Positioning Techniques. 1st ed. San Diego, CA, USA: Elsevier Academic Press.
[74] Hui L, Darabi H, Banerjee P, Jing L. (2007). Survey of Wireless Indoor Positioning Techniques and Systems. *Journl of IEEE Transactions on System Man and Cybernetics*. **37**. 1067–1080.
[75] Lionel M, Yunhao L, Yiu CL, Abhishek P. (2003). LANDMARC Indoor Location Sensing using Active RFID. *IEEE 2003 Pervasive Computing and Communications Conference*. Fort Worth, Texas. USA, 407–415.
[76] Jie Y, Qiang Y, Lionel N. (2005). Adaptive Temporal Radio Maps for Indoor Location Estimation. IEEE 2005 Pervasive Computing and Communications Conference. Kauai, Island, 85–94.

[77] Want R. (2006). An Introduction to RFID Technology. *Journal of IEEE Pervasive Computing*. **5**. 25–33.
[78] Yiyang Z, Yunhao L, Lionel M. (2007). VIRE Active RFID-Based Localization using Virtual Reference Elimination. *IEEE 2007 Parallel Processing Conference*. Shaanxi. China, 56–61.
[79] Bolic M, Simplot D, Stojmenovic I. (2010). RFID Systems Research Trends and Challenges. 1st ed. Oxford, OX, UK: Wiley.
[80] Dardari D, Conti A, Lien J, Win M. (2008). The Effect of Cooperation on Localization Systems using UWB Experimental Data. *Journal of EURASIP on Adv Signal Processing*. **1**. 1–11.
[81] Kiran J, Steven H, Sachin K. (2013). PinPoint Localizing Interfering Radios. USENIX 2013 Networked Systems Design and Implementation Conference. Chicago, Linois. USA: USENIX, 241–254.
[82] Attia M, Moussa A, Zhao X, El-Sheimy N. (2011). Assisting Personal Positioning in Indoor Environments using Map Matching. *Journal of Archives of Photogrammetry, Cartography and Remote Sensing*. **22**. 39–49.
[83] Zhang J, Luojun Y, Wang Y. (2009). Improved Wireless Sensor Network Localization Algorithm. *Journal of Computer Engineering*. **35**. 133–135.
[84] Yuan S, Wymeersch H, Win M. (2010). Fundamental Limits of Wideband Localization–Part II. *Journal of IEEE Information Theory Society*. **56**. 4981–5000.
[85] Curran K, Clintock A, Young C, McKeag D, Killeen G. (2013). RFID in the Production Line for Work flow Improvement. *International Journal of Agile Systems and Management*. **6**. 14-22.
[86] Zhang L, Souryal M. RFID-based Localization and Tracking Technologies. (2011). *IEEE Wireless Communications*. **18**. 45–51.
[87] Gressmann B, Klimek H, Turau V. (2010). Towards Ubiquitous Indoor Location Based Services and Indoor Navigation. In: Proc. Workshop on Positioning Navigation and Communication, 107–112.
[88] Zhu F, Wei Z, Chen J, Guo Z. (2009). Analysis of Indoor Positioning Approaches Based on Active RFID. *IEEE Press Piscataway*. **1**.5182−5185.
[89] Boon L, Young L, Wan C. (2008). 3D Navigation Real Time RSSI-based Indoor Tracking Application. *Journal of Ubiquitous Convergence Technology*. **2**. 67-77.
[90] Ahsan K, Shah H, Kingston P. (2010). RFID Applications: An Introductory and Exploratory Study. *International Journal of Computer Science*. **7**. 1-12.
[91] Mironovova M, Havlis H. (2011). Calculation of GDOP Coefficient. *Journal of Society for Technical Communication*. **5**. 978–980
[92] Chawla K, Robins G, Zhang L. Object Localization using RFID. (2010). in Proceedings of the IEEE 5th International Symposium on Wireless Pervasive Computing (ISWPC '10), 301–306.
[93] Boon L, Young L, Wan C. (2008). 3D Navigation Real Time RSSI-based Indoor Tracking Application. *Journal of Ubiquitous Convergence Technology*. **2**. 67-77.

APPENDIX

1. Wireless Communication

In order to have a cheap wireless communication, a Wi.232 serial wireless module that runs at 900MHz is the best tool for such a thing; due to its simple interface (only 4 pins are enough to work) and sufficient data-rate. Where, each module works as a transmitter/receiver at the same time. The following image of the outstretched board gives expediency to the designer with no anxiety for any change in the source-power with a capability of firmware updating. An expansion that reaches up to 1 mile is the range that the antenna can give with its excellent appearance. The antenna looks excellent and expands the communication range to about 1 mile.

However, some steps should be accomplished in order to have the best module utilization for superior efficiency and obviate interferences, such as the UART baud-rate and wireless-signal channel's setting. In the 1st utilization, some random signals were obtained due to other wireless devices that made interference on our default channel. Therefore, to get-rid of this issue, another channel should be used instead of the default one; where it works on DTS mode with 31 channels, so it ultimately remains on Channel 21 with the keeping the baud-rate as it is for the test since it's already quick enough.

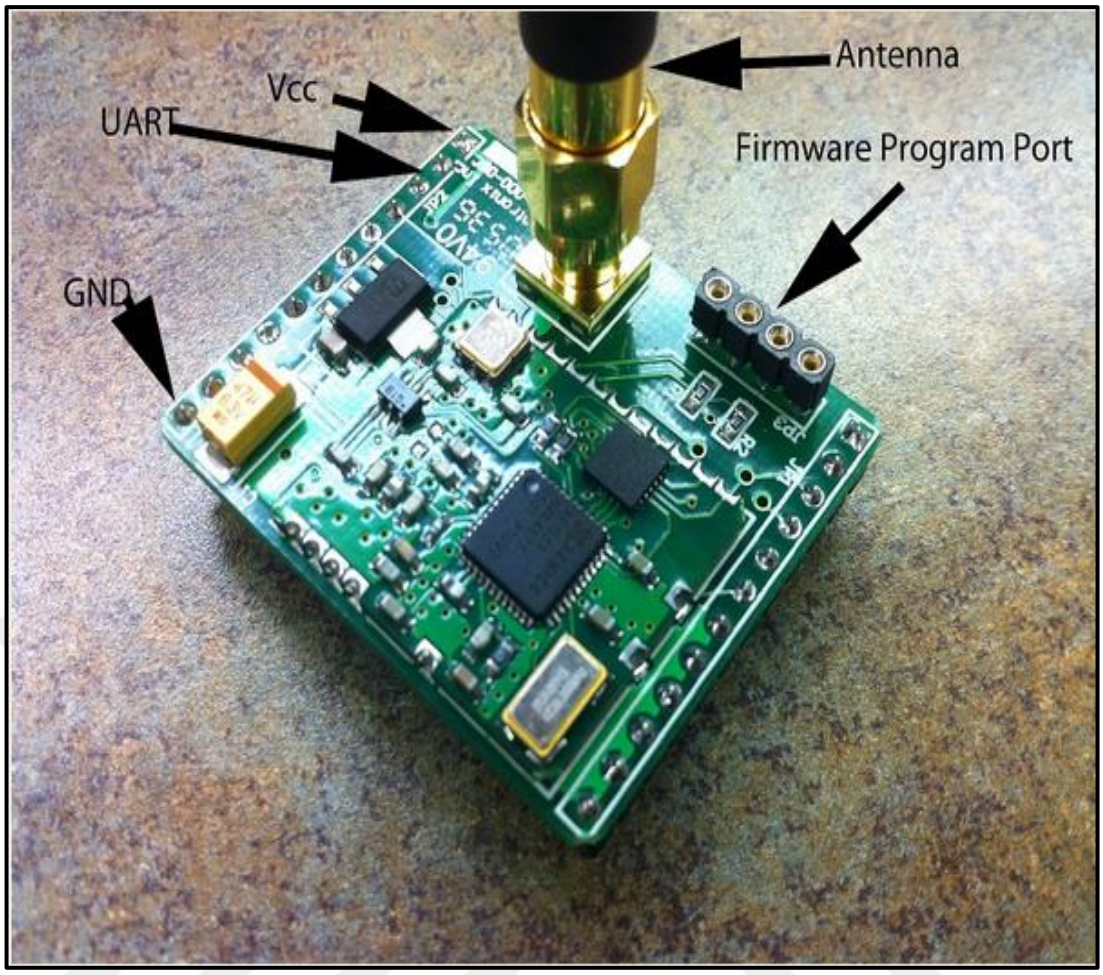

Module of wireless communication

2. Power Source

An independent source of 9v has been utilized; in order to make the system portable and quite enough for each terminal. As the wireless module and MCU require 5v, there was a need for a regulator; to convert the voltage from 9 to 5.

3. Design of GPS-Repeater PCB

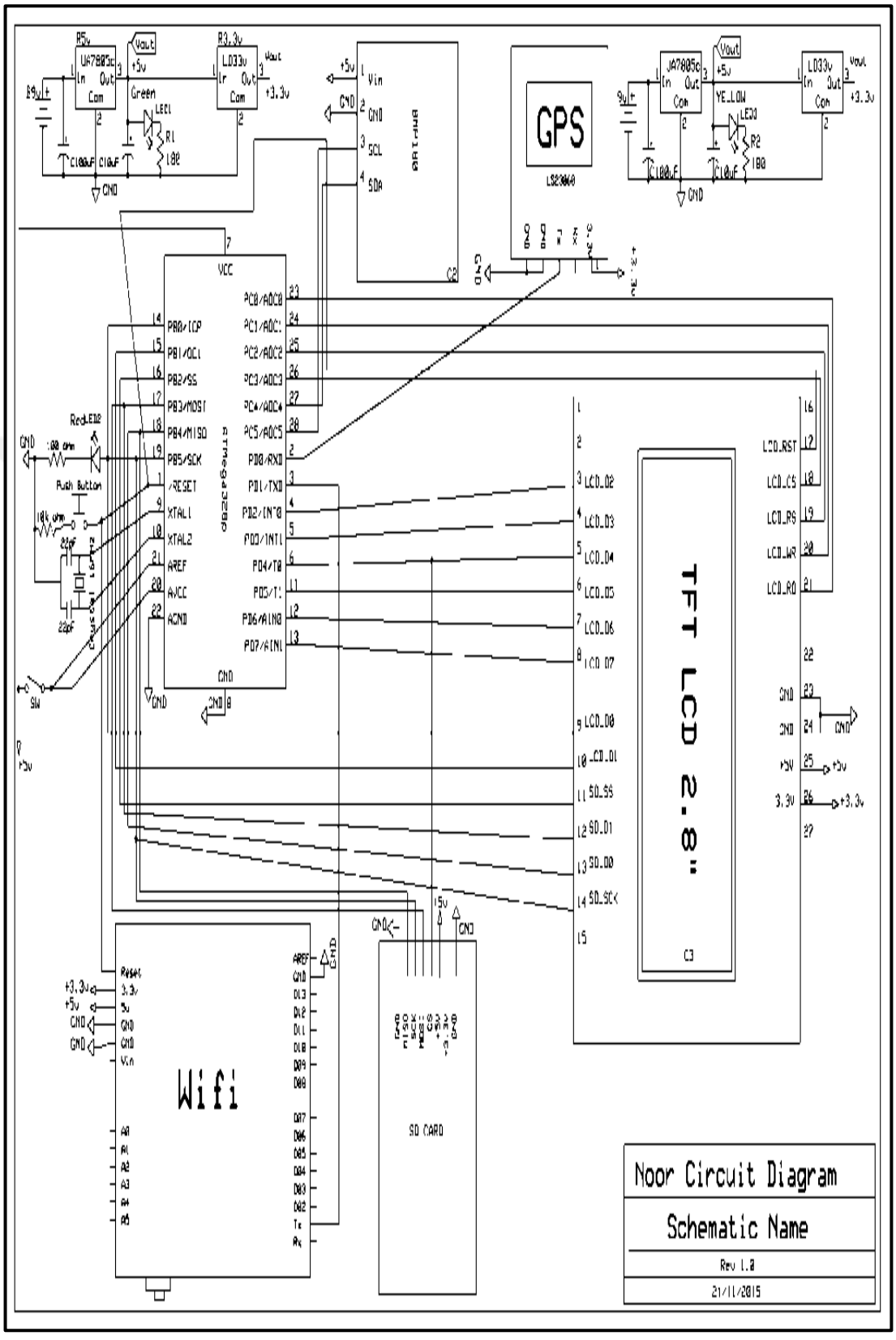

4. Connection Between Components

ATMEGA328p	
Pin Number	Connection Name
1	RESET/(First leg of push button is connected to Pin1 of ATMEGA, second leg is connected to 10k ohm resistor that is connected to GND, third & fourth leg of push button are not connected)
2	RXD (Receive Data)/PD0
3	TXD (Transmit Data)/PD1
4	PD2
5	PD3
6	PD4
7	+5v
8	GND
9	First leg of Crystal 16MHz (XTAL1)
10	Second leg of 16MHz (XTAL2)
11	PD5
12	PD6
13	PD7
14	PB0
15	PB1
16	PB2
17	PB3/MOSI
18	PB4/MISO
19	PB5/SCK
20	+5v
21	+5v
22	GND
23	A0
24	A1
25	A2
26	A3
27	A4/SDA
28	A5/SCL

-First Leg of Crystal 16 MHz is also connected to ceramic capacitor (22pF).
-Second leg of Crystal 16 MHz is also connected to ceramic capacitor (22pF).

Connection between ATMEGA & TFT-LCD		
TFT LCD 2.8"	ATMEGA 328p	
LCD_D2	PD2 (Pin4)	One Side
LCD_D3	PD3 (Pin5)	
LCD_D4	PD4 (Pin6)	
LCD_D5	PD5 (Pin11)	
LCD_D6	PD6 (Pin12)	
LCD_D7	PD7 (Pin13)	
LCD_D0	PB0 (Pin14)	
LCD_D1	PB1 (Pin15)	
SD_SS	PB2 (Pin16)	
SD_D1	PB3/MOSI (Pin17)	
SD_D0	PB4/MISO (Pin18)	
SC_SCK	PB5/SCK (Pin19)	
LCD_RST	RESET (Pin1)	Other Side
LCD_CS	A3 (Pin26)	
LCD_RS	A2 (Pin25)	
LCD_WR	A1 (Pin24)	
LCD_RD	A0 (Pin23)	
GND	GND	
GND	GND	
+5v	+5v	
+3.3v	+3.3v	

Connection between ATMEGA & Wifi	
Wifi	ATMEGA 328p
Tx	TXD/PD1 (Pin3)
GND	GND
GND	GND
GND	GND
+3.3v	+3.3v
+5v	+5v

Connection between ATMEGA & GPS	
GPS	ATMEGA 328p
+3.3v	+3.3v
Tx (Pin3)	RXD/PD0 (Pin2)
GND	GND
GND	GND

Connection between ATMEGA & BMP180	
BMP180	ATMEGA 328p
SDA	A4/SDA (Pin27)
SCL	A5/SCL (Pin28)
GND	GND
+5v	+5v

Connection between ATMEGA & SD-CARD	
SD-CARD	ATMEGA 328p
GND	GND
+5v	+5v
CS	PD4 (Pin6)
MOSI	PB3/MOSI (Pin17)
SCK	PB5/SCK (Pin19)
MISO	PB4/MISO (Pin18)
GND	GND

5. Wi.232 Serial Wireless Module

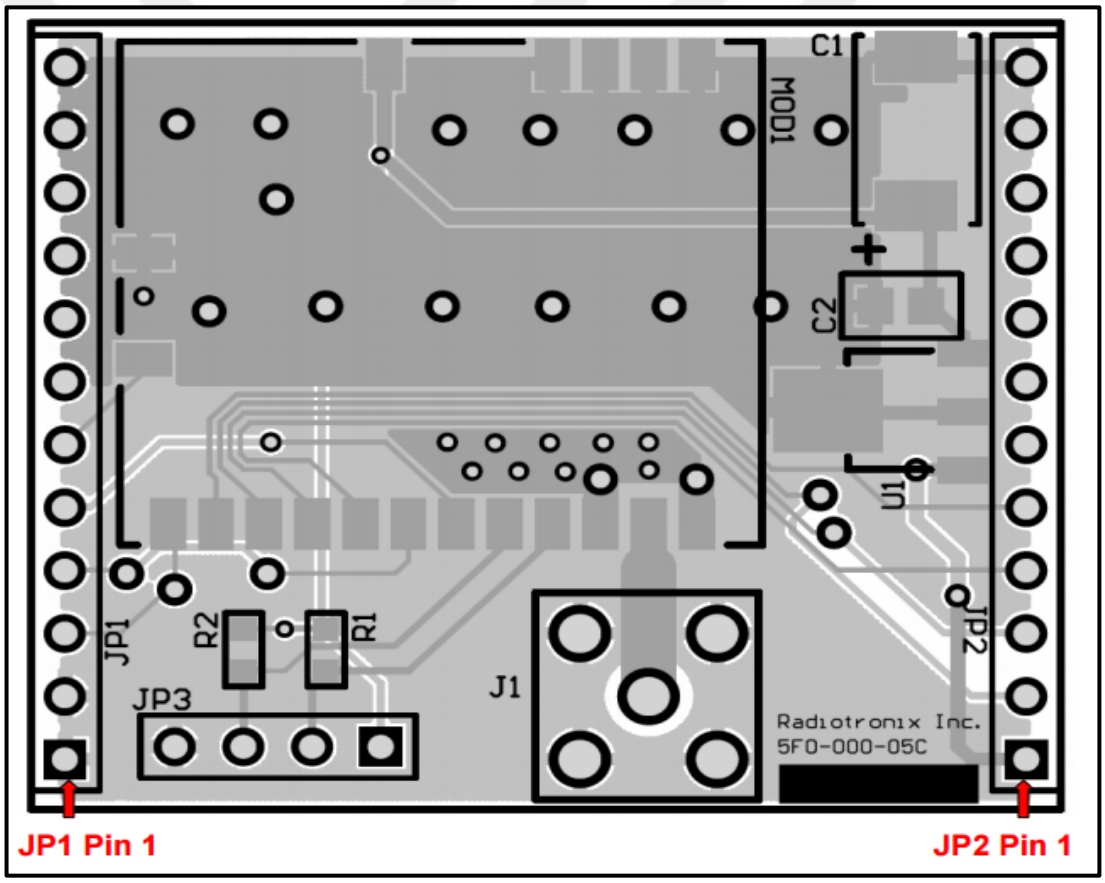

VITA

PERSONAL INFORMATION

Name and Surname: NOOR BAHA ALDIN

Nationality: IRAQ

Email: *nbaha@gantep.edu.tr*

EDUCATION	**Graduate school**	**Year**
Master	Gaziantep University	2012
Bachelor	Technology University	2008
High School	Al-Ma'aly High school	2004

PUBLICATIONS

- **Published a paper on "Error Detection and Correction for ATM Technology" in** International Journal of Advanced Research in Computer and Communication Engineering, Vol. 3, Issue 5, pp.6738-6746-2014).
- **Published a paper on "BVIRE Improved Algorithm for Indoor Localization Based on RFID and a Linear Regression Mode" in** Turkish Journal of Electrical Engineering and Computer Sciences, March, 2016.
- **Published a paper on "Advanced Boundary Virtual Reference Algorithm for an Indoor System Using an Active RFID Interrogator and Transponder" in** Analog Integrated Circuits and Signal Processing, Vol. 88, Issue 3, pp.415-430-2016/DOI:10.1007/s10470-016-0789-y).
- **Published Book on "Error Detection and Correction for ATM Technology" in** Lambert Academic Publishing, Germany, ISBN: 978-3-659-87453-6, May-2016).
- **Published a paper on "ZigBee-Based Indoor Localization System with the Personal Dynamic Positioning Method and Modified Particle Filter Estimation" in** Analog Integrated Circuits and Signal Processing, Vol. 92, Issue 2, pp. 263-279-2017).
- **Published a paper on "An Accurate Indoor RSSI Localization Algorithm Based on Active RFID System with Reference Tags" in** Wireless Personal Communications, 9-August-2017).

FOREIGN LANGUAGE: English

HOBBIES: Reading, Writing